Stochastically excited structures in an infinite fluid domain

Numerical representation of the vibroacoustic behaviour of marine propellers under turbulent excitation

AE5122: Thesis Aerodynamics & Wind Energy

K.T.A. van Gijn

Delft University of Technology

TU Delft

Stochastically excited structures in an infinite fluid domain

Numerical representation of the vibroacoustic behaviour of marine propellers under turbulent excitation

by

K.T.A. van Gijn

to obtain the degree of Master of Science

at the Delft University of Technology,

to be defended publicly on Tuesday June 3, 2025 at 14:00 AM.

Student number:	5415136	
Project duration:	October 14, 2024 – June 3, 2025	
Thesis committee:	Dr.ir. A.H. van Zuijlen,	TU Delft, supervisor
	MSc G.N. Peixoto Dourado,	TNO, supervisor
	Dr. D. Fiscaletti,	TU Delft, examiner
	Dr.ir. M.J.J. Nijhof,	TNO, examiner
	Dr-Ing. R.A.J. Müller,	TNO, examiner

Cover: Cover picture by Karim Iliya

An electronic version of this thesis is available at http://repository.tudelft.nl/.

TU Delft

Preface

This thesis concludes my work at TNO. During my seven-month stay, I have learned more than I could have hoped for. I would like to thank everyone at TNO for giving me the opportunity to do my master thesis here.

The environment created by the colleagues at TNO is truly unique. I have the feeling that I can learn something from every colleague. No matter how busy they were, they always managed to free up some time to explain something. I have the feeling that I can learn a lot more in the TNO environment, which is why I am happy to announce that I will continue working at TNO.

The thesis could not have been what it is now without certain people, whom I would like to thank in particular. First, I would like to thank Gonçalo Peixoto Dourado for his supervision. From the first moment you made me feel at home. You were always around to answer my questions, and made sure to invite me to the football team (which I will join soon, I promise). In addition, you introduced me to many colleagues, also from other departments, making sure that I felt comfortable as soon as possible.

I would also like to thank Alexander van Zuijlen for his supervision. Before I started my masters and had to pick courses, I was looking forward to Fluid-Structure Interaction, which you taught. My expectations were more than met when I took the course. I enjoyed it so much that I wanted to do my thesis on the topic too. It was nice to get to know you better during this period and I am thankful for all your input.

Next, I would like to thank Marten and Roel, who both contributed greatly to my thesis. Both were always available if I needed help and I was happy that I had such knowledgeable people around me. Marten was a great guide during my adventures in COMSOL Multiphysics, a software package that is a source of joy and frustration at the same time. I was really happy when, after many months of going back and forth with COMSOL support, they finally sent us a new function to circumvent a bug. From Roel I learned how to code better, improved my Latex skills a lot, and enjoyed all the cookies he brought during the update meetings. I really look forward to working with you both in the future and I am sure I can learn much more from.

I would also like to thank my mom for her never ending support from the moment I told her that I wanted to do my master's. I would like to thank my dad for everything he taught me and I greatly missed his support during this period.

Finally, I would like to thank Lotte for all her support. I could not have done this without her. I can't wait for us to continue our lives together.

K.T.A. van Gijn
Leiden, May 2025

Summary

Sound plays an important role underwater. Many marine animals rely on sound to navigate or to find pray. In recent years, it is shown that underwater noise effects the marine animals in a negative way. Frequencies produced by shipping overlaps with the dominant frequencies used by fin whales. Humpback whales change their foraging behavior greatly around noisy ships. Therefore, there is a need to reduce underwater noise.

Shipping noise has multiple sources, one of which is the noise produced by the propeller. This study will focus on non-cavitating marine propellers. The propeller is excited by the turbulent flow over the propeller blades. Research on the turbulent flow is outside the scope of this study. Due to the coupling effect of the surrounding water, the model is non-proportionally damped. A modal analysis is used to obtain the eigenfrequencies and eigenmodes of the propeller. Not all eigenfrequencies and eigenmodes are needed to model the response of a marine propeller. Only the frequencies and modes in a specific frequency range are of interest. FEM packages, such as COMSOL Multiphysics, are able to obtain a subset of these eigenfrequencies and eigenmodes efficiently.

The goal of this study is is to develop a method to model the vibroaucoustic response of a marine propeller, excited by a turbulent flow.

The work of De Berg [3] is used as a starting point for this study. In the work, a mathematical model is proposed that is able to compute the response of a non-proportionally damped coupled system excited by a turbulent load. To simplify the analysis, the turbulent load is replaced by a stochastic load. This is a random signal with certain statistical properties.

The response is obtained using different methods. The first method uses only COMSOL Multiphysics to obtain the response power spectral density (PSD). COMSOL Multiphysics is not able to apply a complex distributed load, and can therefore only be used for verification for simple loads. The second method uses the COMSOL Multiphysics eigenmodes and eigenfrequencies, which are imported in Matlab. Here, a stochastic load can be applied. This is the Matlab-COMSOL eigenmode method. Thirdly, the stiffness (K) and mass M matrix are exported from COMSOL Multiphysics and imported in Matlab. From the input matrices, the eigenfrequencies and eigenmodes are obtained. These are used to apply a stochastic load to, resulting in a response PSD. This method is called the KM-method. Finally, the A-matrix method was implemented. This is the model that was proposed by De Berg [3]. The stiffness K, mass M and the damping matrices are exported from COMSOL Multiphysics and imported in Matlab. These input matrices are used to construct the system matrix A. This method can be used to take non-proportional damping into account. Using the system matrix and its transpose, the right and left eigenmodes are obtained, which are used to compute the response PSD.

The methods were used to obtain the response PSD of a two-dimensional beam, surrounded by a fluid domain, excited by a stochastic point load. The COMSOL Multiphysics response PSD was used as a reference. The KM-method performed reasonably well, matching the COMSOL Multiphysics response PSD. The A-matrix method was not able to obtain the same response PSD. It was found that the input matrices were not suitable to construct the system matrix. Finally, the state-space reconstruction method was implemented. From COMSOL Multiphysics, only the displacement part of the eigenmodes can be obtained, but the eigenmodes have to be in state-space. The velocity part of the eigenmodes could be obtained, and thus the eigenmodes could be reconstructed. This method did not match the COMSOL Multiphysics response PSD. However, when a proportionally damped response function was used, the results showed some resemblance.

The KM-method is a reasonable approximation to obtain the response PSD for a two-dimensional beam surrounded by an infinite fluid domain. It is thought that COMSOL Multiphysics writes a part of the damping from the fluid boundary condition in the mass matrix. Therefore, a part of the damping is taken into account in the KM-method.

Contents

List of Figures

List of Tables

Nomenclature

Latin symbols

$\ddot{q}$	Second derivative of q	m/s^2
$\dot{q}$	First derivative of q	m/s
Nullf	Nullspace function	$-$
A	System matrix	$-$
B	State-space mass matrix	$1/kg$
C	Damping matrix	Ns/m
G	Response matrix	$1/Hz$
H	Response function matrix	$1/Hz$
I	Identity matrix	$-$
K	Stiffness matrix	N/m
M	Mass matrix	kg
S	Power spectral density matrix	Hz
X	Right eigenmodes matrix	m
X^T	Transposed right eigenmodes matrix	m
X^{-1}	Inversed right eigenmodes matrix	$1/m$
Y	Left eigenmodes matrix	m
Y^H	Hermitian transpose of left eigenmode matrix	m
$\vec{q}$	Vector notation of q	m/s
A	Constant	$-$
a	Constant, aspect ratio	$-$
b	Constant	$-$
c	Speed of sound	m/s
E	Modulus of elasticity	Pa
F	Force	N
f	Frequency	Hz
f	Sample function, force	$-/N$
h	Modal force vector	N
h	Thickness	m
I	Area moment of inertia	m^4
k	Sample	$-$
k	Stiffness	N/m
k	Wavenumber	$-$

L	Length	m
m	Mass	kg
p	Pressure	Pa
q	Displacement	m
R	Radius	m
R_m	Mechanical resistance	$-$
T	Autocorrelation	$-$
T	Time	sec
t	Time	sec
v	Velocity	m/s
x	Right eigenvector	m
x	sample function	$-$
x	x-coordinate	m
y	Left eigenvector	m
y	y-coordinate	m
z	Deformation function	m
z	z-coordinate	m

Greek symbols

α	Damping factor	$-$
β	Damping factor	$-$
η	Mode contribution	$-$
Λ	Frequency Reduction Factor	$-$
λ	Mass per unit area	kg/m^2
λ	Wavelength	m
μ	Temporal mean value	$-$
ν	Poisson's ratio	$-$
Ω	Eigenfrequencies	Hz
ω	Frequency	Hz
ω_d	Damped frequency	Hz
ω_k	Eigenfrequency k	Hz
ρ	Density	kg/m^3
τ	Change in time	sec
ξ	Damping ratio	$-$
ζ	Damping factor	Hz

Subscripts

A	Acceleration
d	damped
f	Fluid

f	Force
f	Sample function
i	Index
j	Index
k	Index
l	Index
$node$	node
q	Displacement
s	Solid
tbl	Turbulent boundary layer
v	Velocity
x	Index
x	x-direction
y	y-direction
z	z-direction

Abbreviations

CSD	Cross spectral density
CSM	Cross spectral density matrix
FEM	Finite-Element Method
FRF	Frequency Reduction Factor
FSI	Fluid structure interaction
PSD	Power spectral density
TBL	Turbulent boundary layer

1 Introduction

1.1. Background

Sound is continuously present in our daily life. Not only is it used for communication, it is also used as a tool. Under water, where pressure waves are damped much quicker than in air, sound plays a crucial role to navigate, detect objects, or find fish. Sound is also a byproduct of sailing itself.

Underwater noise has been increasing for decades. Since pre-industrial times, underwater noise has increased by $20\,\mathrm{dB}$ in the Northern hemisphere [21]. Between the Second World War and 2008, global ship traffic increased by a factor of 3.5 [17].

The negative effects of underwater noise on marine mammals and fish have been demonstrated in multiple studies. Payne et al. [31] published a study in 1971 that described the overlap of dominant frequencies produced by shipping traffic and frequencies used by fin whales. Blair et al. [5] studied the effect of the impact of ship noise on humpback whales and found significant effects on foraging behavior. Mitson et al. [29] showed avoidance behavior towards noisy vessels from herring schools.

To combat the negative effects of underwater noise, multiple efforts are taken. In 2008 in Hamburg, the International Workshop on Shipping Noise and Marine Mammals agreed to reduce shipping noise in the range of $10\,\mathrm{Hz}$ to $300\,\mathrm{Hz}$ by $3\,\mathrm{dB}$ within 10 years and $10\,\mathrm{dB}$ within 30 years [37]. In that same year, the European Union adopted Descriptor 11 of the Marine Safety Framework Directive, which states that underwater noise must not have an adverse affect on marine ecosystems [28]. Therefore, there is a need to reduce the underwater radiated noise.

1.2. Propeller noise

The noise that a ship produces has multiple sources and can be divided into three main categories: the noise produced from the propeller, from the machinery and from the hull movement through the water [23]. A cavitating propeller produces the most underwater noise. This is a phenomenon where the local pressure of the water flowing over the propeller blade is so low that the water starts to vaporize. When pressure increases again, these vapor pockets collapse violently, generating shock waves and emitting sound. The simplest technique to prevent cavitation is to sail at lower velocities.

The problem of noise generated by propellers consists of multiple topics, including hydroacoustics and structural acoustics. A schematic overview can be found in Figure 1.1. Hydroacoustics research involves analyzing the acoustics as a result of turbulent flows originating from two sources of turbulence. Firstly, the wakefield, including the turbulent boundary layer (TBL), from the hull is known as inflow turbulence. Secondly, the interaction between the surface of the blade and the flow causes the boundary layer over the blade to become turbulent. Both sources cause pressure fluctuations on the blade, which excite the propeller blade, resulting in structural vibrations. This structural response excites the surrounding water, causing pressure waves that are radiated into the far field.

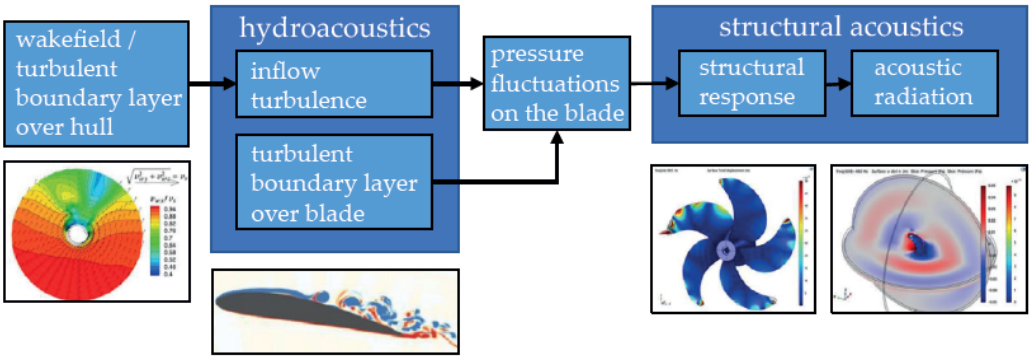

Figure 1.1: Schematic overview of propeller noise production, modified from De Valk [35]

.

1.3. Modeling of non-cavitating propeller noise

To predict the structural response of a propeller blade, the choice is made to use a modal analysis. This is a method where the vibration response of the structure and connected fluid is decomposed into orthogonal modes of deformation. These modes, which are certain shapes of the blade, appear when the blade vibrates at an eigenfrequency. For any excitation, the resulting vibration can be represented by a combination of these modes. Using this modal analysis, it can be shown how much each of these orthogonal modes contributes to the total response. Using the Finite Element Method (FEM), a subset of relatively low-frequent eigenfrequencies and eigenmodes can be obtained efficiently.

Proportional damping is a popular assumption for vibrational systems, because it simplifies the analysis [2]. Submerged structures that radiate sound into their surroundings are non-proportionally damped systems. This means that damping cannot be written as a function of mass and stiffness. Consequentiality, the coupled system is rewritten using a method called state-space. Due to the non-proportional damping, the modes are no longer orthogonal with respect to each other. This is known as bi-orthogonality. Solving the system results in two distinct sets of eigenmodes, typically called left and right eigenmodes, instead of one set for which left and right are identical. For small systems, where the complete set of right eigenmodes is known, the left eigenmodes can be obtained by taking the Hermitian transpose of the inverse of the right eigenmodes. Vice versa, the right eigenmodes can be obtained by taking the inverse of the Hermitian transpose of the left eigenmodes. However, when the system becomes large, which it becomes for typical engineering problems solved in FEM, taking the inverse of a set of modes becomes computationally excessively expensive, since all left or right eigenmodes have to be known.

For the application of marine propellers, not all eigenfrequencies and eigenmodes are of interest. Low frequencies propagate well in water, while higher frequencies are more prone to damping. In addition, underwater mammals are affected by noise in a limited frequency range. Therefore, a method has to be found to obtain the left and right eigenmodes corresponding to frequencies in the range of interest only.

1.4. Research objective and research questions

The goal of this study is to develop a method to model the vibroaucoustic response of a marine propeller, excited by a turbulent flow. Research on turbulent flow over the blade is outside the scope of this study. The statistical properties of the turbulence are needed to model the structural response. The model should accommodate the excitation in the form of a so-called cross-spectral matrix.

Now that the goal of the study is defined, the research questions can be formulated.

1. What sound radiation model best describes a cantilever beam (and a plate) under distributed deterministic and stochastic bending load, surrounded by water?
   (a) How can the model take into account sound radiation?

   (b) How can the radiation model be verified?

2. What method describes the vibratory response to, and radiated noise caused by a stochastic distributed excitation on a ship propeller surrounded by an infinite heavy fluid domain ?
   (a) How can the model take into account sound radiation?
   (b) How can the radiation model be verified?
3. What are the effects of high damping, multi-layering and anisotropical material variations on vibration and the radiation of noise?

1.5. Thesis outline

First, the theoretical background will be discussed in chapter 2. Some statistical principles are shown, followed by a literature review. From the literature, the most suitable method to model the response of a marine propeller excited by a stochastic distributed load will be used. This method will form the foundation of the study.

Due to the complexity of the problem, incremental complexity steps will be taken in the methodology discussed in chapter 3. First, the general approach of the problem is described. Next, a small one-dimensional test case is demonstrated to gain a better understanding of the fundamentals of the problem. After that, the first step towards a marine propeller is taken with a cantilever plate in vacuum, excited by different stochastic loads. COMSOL Multiphysics will be used to validate simple loading cases. Next, the methodology to take into account the surrounding water is described. Three different methods are discussed.

The results of the three different methods to incorporate water in the model are described in chapter 4. Based on the results, a conclusion can be made in chapter 5. In addition, multiple recommendations are given.

2

Theoretical Background

In this chapter, the theoretical foundation of this study is presented. First, the characterization of random signals will be described. Literature relevant to this assignment is discussed next. Finally, a summary of the work on the most suitable response method is given since this study builds upon this.

2.1. Random signals

This section on random signals is based on the work of Meirovitch [27].

Before starting to describe some properties of random signals, a *deterministic* signal is introduced. This is a function where for any time t, their value can be obtained. If a system is loaded with a deterministic load, the response is also deterministic. Deterministic is the opposite of random.

In real life, there are many phenomena that cannot be described in a deterministic way. Examples are waves in the ocean or the velocity fluctuations in the wind. This means that it is not possible to determine the value of these phenomena for some future t. There are simply far too many factors at play to capture the response in a function. These processes are *non-deterministic*, or more commonly referred to as *random*. The pressure fluctuation in a turbulent boundary layer can also be considered as random [30].

Given a certain sample function $x_k(t)$ that is taken from a random and stationary (explained later) and process, the temporal mean value is defined as:

$$\mu_x(k) = \lim_{T\to\infty} \frac{1}{T} \int_{-T/2}^{T/2} x_k(t)dt \tag{2.1}$$

Even in systems with random behavior there is often structure. For example, in a turbulent flow there are coherent structures, i.e. the state of the fluid at different points are different moments in time can be correlated. One of the tools to asses coherence is the autocorrelation, which is a method to determine how fast a signal loses coherence with itself. The autocorrelation is defined as

$$R_x(k,\tau) = \lim_{T\to\infty} \frac{1}{T} \int_{-T/2}^{T/2} x_k(t)x_k(t+\tau)dt, \tag{2.2}$$

or in discrete form:

$$R_x(k,\tau) = \lim_{T\to\infty} \frac{1}{T} \sum_{k=1}^{n} x_k(t)x_k(t+\tau)dt. \tag{2.3}$$

If the mean and the autocorrelation function depend on the time that the sample was taken, the process is said to be *non-stationary*. Conversely, if the sample does not depend on the time that it is taken, it is *stationary*. The process is called *ergodic* when the temporal mean and autocorrelation function are the same, regardless of which part of the time history from the total process was taken to compute these averages. Therefore, it follows that:

$$\mu_x(k) = \mu_x = constant, \quad R_x(k,\tau) = R_x(\tau) \tag{2.4}$$

The assumption is made that the turbulence over a marine propeller is ergodic. This implies that the statistical properties of the incoming turbulent flow are not a function of time. The effect of the rotation of the propeller is left outside of the scope of this study. Typically this assumption is made for the wake field left by a ships hull. For a rotating propeller the blades travel through different parts of the wake field which may have different stochastic properties making the signal non-ergodic. However, in the scope of this study the effect of rotation of the propeller is neglected

The autocorrelation function is used to obtain information regarding the random signal in time. In certain scenarios, it is more useful to use the *power spectral density function*. This provides information in the frequency domain rather than the time domain. In essence, the power spectral density function does not provide more information about the signal, but it is represented differently. For example, take a sample function $x(t)$. This signal is ergodic random. The autocorrelation can be obtained as:

$$R_f(\tau) = \lim_{t\to\infty} \frac{1}{T} \int_{-T/2}^{-T/2} x(t)x(t+\tau)dt \tag{2.5}$$

By taking the Fourier transform of $R_f(\tau)$, the power spectral density function $S_f(\omega)$ can be obtained as:

$$S_f(\omega) = \int_{-\infty}^{\infty} R_f(\tau)e^{-i\omega\tau}d\tau \tag{2.6}$$

Using the same logic as the inverse Fourier transform, the autocorrelation function can be obtained from the power spectral density function as:

$$R_f(\tau) = \frac{1}{2\pi} \int_{-\infty}^{\infty} S_f(\omega)e^{i\omega\tau}d\omega \tag{2.7}$$

The correlation of two signals can also be quantified. This is called the *cross-correlation function*. This is defined as

$$R_{x_1,x_2}(\tau) = \lim_{T\to\infty} \frac{1}{T} \int_{-T/2}^{T/2} x_1(t)x_2(t+\tau)dt \tag{2.8}$$

And in similar fashion as Equation 2.6, by taking the Fourier transform of Equation 2.8 the *cross-spectral density (CSD)* $S_{x_1,x_2}(\omega)$ can be obtained as:

$$S_{x_1,x_2}(\omega) = \int_{-\infty}^{\infty} R_{x_1,x_2}(\tau)e^{-i\omega\tau}d\tau \tag{2.9}$$

For complex values of the CSD the absolute value describes the magnitude of the correlation between the two signals while the phase of the CSD describes the phase difference between the two signals. The cross spectral density is of great importance to this study, since working towards this form of the excitation is the goal of the research.

When analyzing a system with many signals, each signal can be correlated with another. This results in the cross spectral density matrix (CSM). For a system with three signals (1, 2 and 3), the CSM matrix is defined as

$$S_f(\omega) = \begin{bmatrix} S_{11} & S_{12} & S_{13} \\ S_{21} & S_{22} & S_{23} \\ S_{31} & S_{32} & S_{33} \end{bmatrix} \tag{2.10}$$

Where the autocorrelation function is found on the diagonal, and the cross-correlation can be found on the off-diagonal.

2.2. Vibration modes of propellers

Obtaining the eigenmodes of a complex geometry, such as a propeller, can be considered challenging. Carlton [9] describes the challenges as follows: 'the blade is non-symmetrical, both radially and chordwise. The change in radial pitch angle results in twist, causing a more complex shape in the radial direction. Furthermore, the propeller is immersed in water, resulting in a reduction of the modal frequency and an eigenmode shape modification compared to a propeller in vacuum.' First, the study of Burrill et al. [8] is used to gain a general understanding of propeller eigenmodes and the understand the effect of air and water on the eigenfrequency and the mode shapes. From De Rosa et al. [15] onward, studies will be discussed that obtained the eigenfrequencies and eigenmodes of marine propellers (or related to) numerically.

To eliminate some of the difficulties, it is easier to look at the vibration of a flat symmetrical plate that resembles the shape of a propeller. The shape of the plate can be seen in Figure 2.1. In addition, taking measurements in air is easier than in water. Experiments on such a plate were conducted by Burrill et al. [8]. This plate was elliptical and had a constant thickness both in chordal and radial directions. Relative to propellers, the size of the Burrill plate was small; the plate had a span of $131.32\,\mathrm{mm}$, a maximum chord length of $86.11\,\mathrm{mm}$, and a uniform thickness of $1.4\,\mathrm{mm}$. Due to the dimensions, the eigenfrequencies were found at relatively high frequencies, ranging from $73\,\mathrm{Hz}$ for the fundamental mode, to $3009\,\mathrm{Hz}$ for the 10th mode.

The first 10 modal forms are shown in Figure 2.1. The lines represent flexural nodal lines, which is where the plate bends. The fundamental mode is omitted, which has no flexural nodal lines, since the whole plate moves in the same direction. The fundamental mode has no Overall, it can be seen that the number of flexural nodal lines increases with frequency.

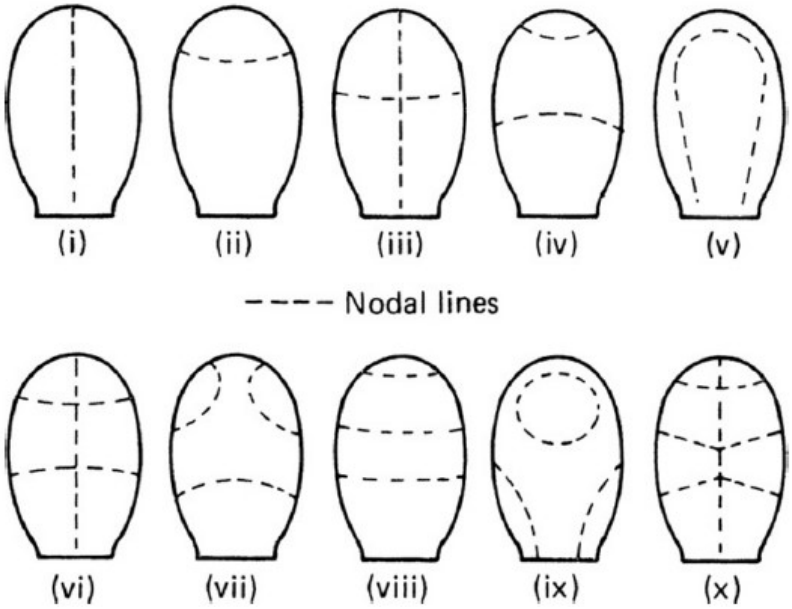

Figure 2.1: Eigenmode shapes of a Burrill plate [8].

Next, experiments were conducted on full-scale propellers in air and water. The modes of the Burrill-plates could be recognized in the full-scale propeller. The most notable effect water on the eigenmodes of a submerged propeller is the reduction of the eigenfrequency at which modes occur. However, the reduction factor is not constant for all modes and changes for each eigenfrequency. Burrill defined the frequency reduction factor (FRF) as:

$$\Lambda = \frac{\text{frequency of mode in water}}{\text{frequency of mode in air}} \tag{2.11}$$

The ratio increases with eigenfrequency. Burrill researched two different types of propellers. On the first propeller, FRF ranged from 0.625 on the first mode to 0.980 on the fourth mode. On the second propeller, the FRF ranged from 0.645 for the first mode to 0.795 for the tenth.

The shape of the mode was generally preserved in air and water, although some shifts in the model line position can be seen. This is demonstrated in Figure 2.2.

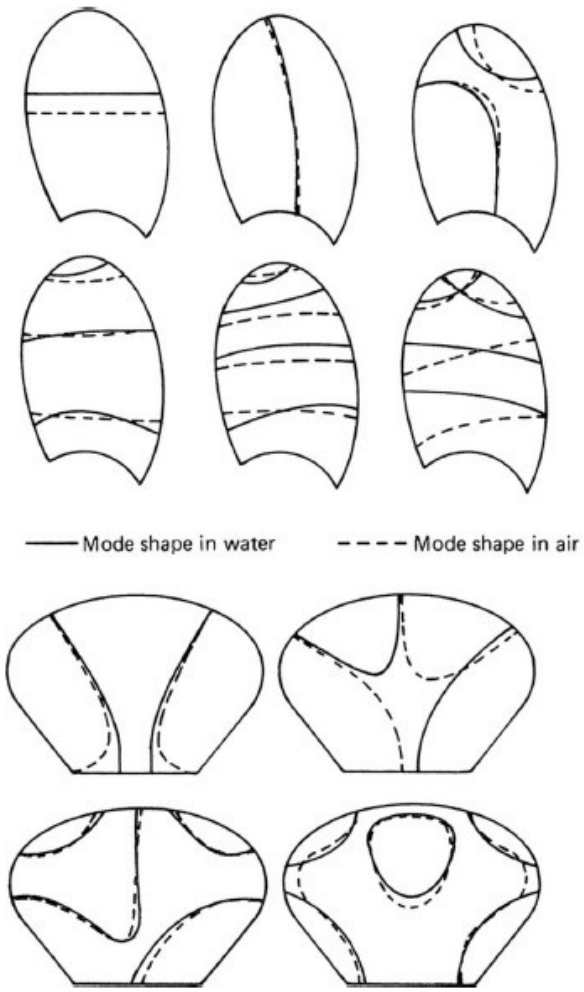

Figure 2.2: Eigenmode comparison of a propeller in air and water of two different propellers [8].

De Rosa et al. [15] conducted a study where an analytical and numerical response model of a simply supported plate excited by a turbulent boundary layer was developed. In their study, they chose a relatively small fluid domain, which was attached to one side of the plate. The pressure distribution on the plate due to the turbulent boundary layer was expressed analytically with the model developed by Corcos [13] [14]. Model constants are chosen based on the work of Blake [6] in the pressure distribution model. Furthermore, the fluid loading effect on the dynamic response of the structure is assumed to be negligible. It is verified that the air does not significantly change the natural frequency or modify the mode shapes. The details of this verification are not shown in the paper. The analytical response of the plate is derived in closed form. In addition, a numerical scheme was created, where care was taken to discretize random distributed loads correctly. This numerical model is based on the work of Elishakoff [16] and is defined as:

$$S_q(\omega) = XG(\omega)X^T S_f(\omega) XG(\omega)^* X^T \tag{2.12}$$

Where X is the matrix from the finite element modal approach containing the mode shape. S_f is the discretized random load matrix. The elements of the diagonal response function are defined as:

$$G_j(\omega) = \frac{1}{\omega_j^2 - \omega^2 + i\zeta\omega_j^2} \tag{2.13}$$

Where ω is the angular frequency, ω_j is the natural frequency of mode j, and ζ is the damping factor.

The analytical and numerical models showed good agreement. De Rosa et al. [15] used eigenvectors with an orthogonal base, which means that the system was proportionally damped.

Ciappi et al. [11] published a study of a plate of a scaled ship hull excited by a turbulent boundary layer. The experimental data allowed the authors to tune the Corcos [13] and the Chase [10] pressure distribution models to construct a numerical equivalent . It was shown that both could be fitted to the data with good agreement. The wet and dry natural frequencies were identified with hammer impact tests. By obtaining the first 16 eigenfrequencies, a relation for the added mass of the fluid could be identified with work from Blevins et al. [7]. This was then fed into a finite element model to estimate higher eigenfrequencies. Fahy [19] stated that the shape of the eigenmodes remains almost unchanged. A validation of this statement is not presented in the work, and an orthogonal base of the eigenmodes is assumed. Again, the Chase and Corcos models were used, but now as input for the acceleration response of the plate. The numerical model was based on the work of Elishakoff [16].

Magionesi [26] published a study on the structural noise of a sonar dome of a ship induced by a turbulent flow. The pressure fluctuations due to the turbulent boundary layer was obtained by a measurement on a scaled ship. Multiple pressure distribution models were tested with the experimental data. Also, the noise in the dome was measured. In order to model the noise in the dome, first the natural eigenfrequencies and modal damping coefficient were obtained by performing a hammer impact test, both for a dry and a wet plate. COMSOL was used to obtain higher eigenfrequencies. The excitation of the dome due to the TBL was modeled with the numerical model based on the work of Elishakoff [16]. Good agreements were found for lower frequencies. The response above $1200\,\mathrm{Hz}$ was not obtained, since the numerical resolution of the panel was too coarse. In order to obtain the noise produced by these vibrations, the Helmholtz equation was used. Again, good agreements were found.

Abbas et al. [1] developed a new method where a laser Doppler vibrometer (LDV) was used for a vibratory analysis of a rotating propeller in both air and water. The method allowed for a Lagrangian analysis by tracking a point fixed on the blade. In order to validate the technique, wireless accelerometers were attached to the propeller in air. Since it was not possible to validate the LDV while the propeller was submerged in water with this method, a COMSOL numerical model was used. The LDV method showed good agreement with both the accelerometers and the COMSOL model. Therefore, the method can be used to obtain the eigenfrequencies of propellers underwater. The focus of this paper was on finding the eigenfrequencies, not the eigenmodes. Furthermore, although the LDV results showed good agreement with the COMSOL model for a propeller underwater, the propeller was placed in a water basin, which could influence the measurement since it had limited dimensions. It does not become clear from the paper how they accounted for this in the COMSOL model.

Tsigklifis et al. [34] developed a structural response model of an elastic aerofoil. This was excited by a homogeneous isotropic turbulent flow. First, an analytical model was derived by combining two models. The Sears [32] model for unsteady hydrodynamic gusts and the Theodorsen [33] model for the lift and moment as a result of a heaving and pitching airfoil strip were superimposed, and strip theory was used to derive the response of the airfoil. As an input, the turbulence intensity and integral length-scale were needed. The equations of motion from the Euler-Bernoulli beam and torsional equations were used. In order to validate the model, measurements of a NACA0015 hydrofoil were collected in a water channel, where a honeycomb was used to generate turbulence. Also, a finite element and finite boundary model was constructed in COMSOL to further validate the analytical model. Consistent agreement was found between the eigenfrequencies in still air and water. Under flow, the frequency of higher eigenfrequencies were over-predicted, with the differences attributed to multiple reasons. First, material and geometrical uncertainties are important sources of discrepancies. More importantly, the flow was confined in the experiment, and a boundary layer adjacent to the tip of the hydrofoil started to develop. This was not taken into consideration by the analytical and numerical models.

Magionesi et al. [25] published a study on the Fluid-Structure-Interaction (FSI) of a propeller wake and a rudder. This study was not validated with experimental data. However, since the authors used COMSOL Multiphysics to simulate the interaction, it provides a reference to set up a complex numerical model, similar to the one in this stu. In order to research the wake of the propeller, a Detached Eddy Simulation (DES) was developed. This pressure field was then used as input for the structural domain. The FSI methodology was one-way, which means that there was no feedback from the structural domain to the fluid domain. In order to account for an infinite fluid domain, non-reflection boundary conditions

were used. The authors performed preliminary simulations to prevent the influence of the fluid domain size on the vibrations of the propeller. Also, a mesh study was carried out to ensure that the mesh size did not have an effect on the solution. Details of these preliminary studies are not shown. A modal analysis was performed to obtain the first eigenmodes. This allowed the authors to obtain the magnitude of the mean deformation and the vibratory response.

De Berg [3] wrote a thesis where a mathematical model was proposed to calculate the response of both non-proportional and proportionally damped systems with an arbitrary geometry surrounded by a fluid. The stiffness, damping and mass matrix were exported from COMSOL Multiphysics, from which the eigenmodes and eigenfrequencies were computed. The response of cantilever beams and simply supported plates in vacuum excited by a stochastic point and body load could be verified with COMSOL Multiphysics. Next, a simply supported plate with a fluid box attached on one side was excited by a stochastic body load. Discrepancies were found in the response spectral density, in both magnitude and response shape. The source of the discrepancies was not found, but was believed to be caused by scaling in the fluid part of the mass matrix or a general lack of understanding how the stiffness, damping and mass matrix were constructed in COMSOL Multiphysics.

Summarizing, multiple papers were studied where structures, surrounded by a fluid, were excited by a stochastic load. However, only De Berg [3] took into account non-proportional damping. Therefore, this model will be used as a foundation of this study.

2.3. Framework by De Berg

The work of De Berg [3] will be used as a starting point for the current research and therefore his work will be discussed in more detail. The foundation of De Berg's work can be found in Meirovitch [27].

The coupled equation of a system with motion of n degrees of freedom can be written as:

$$M\vec{\ddot{q}}(t) + C\vec{\dot{q}}(t) + K\vec{q}(t) = \vec{f}(t), \tag{2.14}$$

where M is the mass matrix, C is the damping matrix, and K is the stiffness matrix. The vector $\vec{q}$, which has a length of n, contains the displacement of all the degrees of freedom. The displacement is relative to their original position, so without a force f acting on the system. Vector f is also of length n, and contains the force that is acting on each mass. The mass matrix M only contains non-zero values on the diagonal for simple systems. A linear relation between force and displacement is assumed.

De Berg [3] used a modal approach, which assumes that the solution can be written as:

$$\vec{q}(t) = \sum_{k=1}^{n} \eta_k(t)\vec{x_k} = X\vec{\eta}(t) \tag{2.15}$$

The matrix X contains the eigenvectors $\vec{x}$, which describe the eigenmodes. The vector $\vec{\eta}$, with length n, is the contribution of each node. This means that each displacement is a linear combination of shapes, and $\vec{\eta}$ tells how much of each shape contributes to the total displacement. This concept is of great importance for the stu and will be the foundation of the work.

When a system with n degrees of freedom is discretized, there will be n modes. For finite element methods, this number can grow rapidly when a fine mesh is used. The assumption is made that the first modes are dominant. In general a mode will only contribute significantly around its eigen frequency. Little damping implies the mode only contributes significantly in a small frequency range around the eigenfrequency. This frequency range increases with increased damping. For the response of a mechanical system the location of the modes are generally spread out at low frequency and the modal density (i.e. number of modes found in a frequency range of fixed size) will increase with frequency. If it is assumed that the frequency range of interest starts at zero and is in a the region of low modal density and damping is not very strong it is save to assume that the first few modes will dominant the response of the system. For continuous systems, there will be an infinite amount of modes.

2.3.1. Response in the case of proportional damping

When a system is proportionally damped, the damping matrix C can be written as a linear combination of the mass matrix M and the stiffness matrix K:

$$C = \alpha M + \beta K \tag{2.16}$$

Where α and β are arbitrary constants that for instance represent system properties of a modeled system. Equation 2.14 reduces to:

$$(1 + i\alpha)M\ddot{\vec{q}}(t) + (1 + i\beta)K\vec{q}(t) = \vec{f}(t) \tag{2.17}$$

Using the stiffness and mass matrix, the eigenmodes X can be obtained, using the following eigenfrequency equation:

$$KX = \Omega MX \tag{2.18}$$

Where Ω contains the squared eigenfrequencies on the diagonal as diag$[\omega_1^2, \omega_2^2, .., \omega_n^2]$. It is useful to normalize the eigenmodes, since eigenmodes can be scaled and still be eigenmodes. Therefore, the eigenmodes are scaled with the mass and stiffness matrix, and is equated as:

$$X^T MX = I, \quad X^T KX = \Omega \tag{2.19}$$

where the eigenmodes are scaled such they form the identity matrix I with the mass matrix and the squared eigenfrequencies with the stiffness matrix. Using Equation 2.15 and Equation 2.19, Equation 2.17 can be rewritten in modal space to:

$$\ddot{\vec{\eta}}(t) + \Omega\vec{\eta}(t) = \vec{h}(t) \tag{2.20}$$

where $\vec{h}(t)$ is modal forces vector, defined as:

$$\vec{h}(t) = X^T\vec{f}(t) \tag{2.21}$$

The information described in this subsection so far describes the fundaments to obtain the displacement in power spectral density $S_q(\omega)$. The full derivation can be found in De Berg [3]. The displacement power spectral density can be obtained with:

$$S_q(\omega) = X\bar{G}(\omega)X^T S_f(\omega)XG(\omega)X^T \tag{2.22}$$

In this equation, $S_f(\omega)$ is the excitation spectral density. G is the frequency response function. For a proportionally damped system, the response function is defined as:

$$G_k(\omega) = \frac{1}{-\omega^2 + 2i\zeta_k\omega\omega_k + \omega_k^2} \tag{2.23}$$

In the equation, the dimensionless damping factor is defined as:

$$\zeta_k = \frac{\alpha + \beta\omega_k^2}{2\omega_k} \tag{2.24}$$

Furthermore, the spectra of the velocity can be obtained as:

$$S_v(\omega) = \omega^2 S_q(\omega) \tag{2.25}$$

Which is a useful property to calculate the radiated noise. The acceleration spectra can be obtained with:

$$S_a(\omega) = \omega^4 S_q(\omega) \tag{2.26}$$

2.3.2. Response in the case of non-proportional damping

The equations described in subsection 2.3.1 only apply to proportionally damped systems. Real world systems are generally not proportionally damped, which means that the damping matrix can not be described using the mass and stiffness matrix.

To incorporate non-proportional damping, the same modal approach is used. The state-space description is applied, where the vector $\vec{x}(t)$ contains information about the displacement and the velocity of the degrees of freedom, which is defined as:

$$\vec{x}(t) = \begin{bmatrix} \vec{q}(t) \\ \dot{\vec{q}}(t) \end{bmatrix} \tag{2.27}$$

Equation 2.14 can be rewritten as:

$$\dot{\vec{x}}(t) = A\vec{x}(t) + B\vec{f}(t) \tag{2.28}$$

where $f(t)$ is a force. Matrices A and B are defined as

$$A = \begin{bmatrix} 0 & I \\ -M^{-1}K & -M^{-1}C \end{bmatrix} \qquad B = \begin{bmatrix} 0 \\ M^{-1} \end{bmatrix} \tag{2.29}$$

A is no longer symmetric. As a consequence, the eigenmodes are no longer orthogonal, which is a property that is desirable since it allows to decouple the system. This means that the system can no longer be diagonalized with one set of eigenmodes, which is a direct result of non-proportional damping.

Another consequence is that the system now has two sets of eigenmodes: The right eigenmodes, which are a solution to Equation 2.28 and the left eigenmodes, which are a solution to the same system of equations after replacing A with its Hermitian transpose. Note that since A is real valued the eigenvalues associated with both sets of eigenmodes are identical, i.e. only the mode shapes differ. The left eigenmodes are needed to map the excitation force to the model space, where as the right eigenmodes are used to map the displacement to modal space. The right and left eigenmodes can be described respectively by:

$$AX = \Omega X \tag{2.30}$$

$$Y^T A = \Omega Y^T \tag{2.31}$$

Where X contains the right eigenmodes, Y contains the left eigenmodes and Ω are the eigenfrequencies, where the left and right eigenfrequencies are the same. This is the first method to obtain both sets of eigenmodes.

The left and right eigenmodes have certain properties, which can be found in De Berg [3] and Meirovitch [27]. One of the properties is called *bi-orthogonality*. This property can be used to decouple the equations of motion. The bi-orthogonality is defined as:

$$\vec{y}_l A \vec{x}_k = 0 \quad \text{for} \quad k \neq l \tag{2.32}$$

Furthermore, the following relation between the left and right eigenmodes is given:

$$Y^H = X^{-1} \tag{2.33}$$

This states that the Hermitian transpose of the left eigenmodes is equal to the inverse of the right eigenmodes. This provides a method to calculate left eigenmodes. In order to calculate the inverse of X, all right eigenmodes need to be known. This is not feasible except for small systems, since there will be as many eigenmodes as degrees of freedom. Although it provides a method to compute the left eigenmodes, the computational expense makes the method unusable for realistic systems. The assumption is made that the most relevant modes are those with relatively low eigenfrequencies, so there is no need to obtain all eigenmodes. In addition, FEM packages are able to provide the first n modes in a computationally efficient manner, reducing the computational cost significantly [12].

The following spectral density response function is derived for a non-proportionally damped system with stochastic loading, using the state-space approach:

$$S_q(\omega) = X\bar{G}(\omega)Y^H BS_f(\omega)B^H YG(\omega)X^H \tag{2.34}$$

Where the diagonal response function G is defined as:

$$G_k(\omega) = \text{diag}\left[\frac{1}{i\omega - \omega_k}\right] \tag{2.35}$$

Where the excitation power spectral density is defined as:

$$S_f(\omega) = \begin{bmatrix} S_{xx} & S_{xy} & S_{xz} \\ S_{yx} & S_{yy} & S_{yz} \\ S_{zx} & S_{zy} & S_{zz} \end{bmatrix} \tag{2.36}$$

Where the diagonal terms represent autocorrelation and the off-diagonal terms present cross-correlation between excitation forces.

To better understand the structure of the loading matrix S_f an example is given using a rod in the x-direction, using hexahedral mesh elements. A schematic representation of the rod can be found in Figure 2.3.

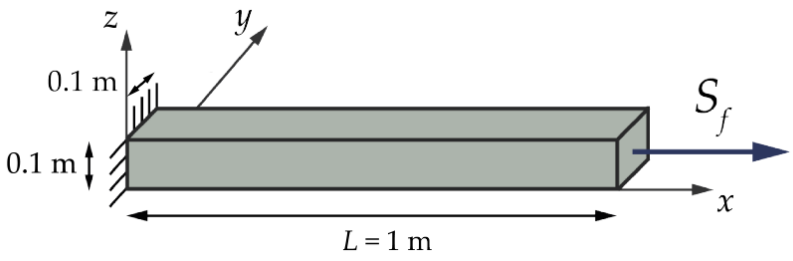

Figure 2.3: Schematic of a rod in x-direction used in the example of De Berg [3].

This rod is divided into 100 elements, and each element contains 4 nodes. This means that the system contains 404 nodes. Since there are 3 spatial dimensions there are 1212 degrees of freedom. The matrix S_f will have 1212x1212 elements. A boundary load is placed at the end of the rod in the x-direction. All the elements of S_f will be zero, except for S_{xx}. Since there the load is only on the boundary, S_{xx} will contain only zeros, except for the last element:

$$S_{xx} = \begin{bmatrix} 0 & \dots & 0 \\ \vdots & \ddots & \vdots \\ 0 & \dots & S_{\text{node}}{}^{4\times4} \end{bmatrix} \tag{2.37}$$

2.3.3. Response of a solid surrounded by an infinite fluid

Although the mathematical model stated in Equation 2.34 can compute the response power spectral density of an arbitrary non-proportionally damped solid excited by an arbitrary stochastic load, fluid is not incorporated explicitly. Since this study is about marine propellers, fluid has to be taken into account. Using the same approach as subsection 2.3.2, the mass, damping and stiffness matrices can be redefined to incorporate the effect of the surrounding fluid. This resulting set of equations is called a coupled system and can be expressed as:

$$\begin{bmatrix} M_{ss} & 0 \\ M_{fs} & M_{ff} \end{bmatrix} \begin{bmatrix} \ddot{\vec{q}} \\ \ddot{\vec{p}} \end{bmatrix} + \begin{bmatrix} C_{ss} & 0 \\ 0 & C_{ff} \end{bmatrix} \begin{bmatrix} \dot{\vec{q}} \\ \dot{\vec{p}} \end{bmatrix} + \begin{bmatrix} K_{ss} & K_{sf} \\ 0 & K_{ff} \end{bmatrix} \begin{bmatrix} \vec{q} \\ \vec{p} \end{bmatrix} = \begin{bmatrix} \vec{f_{tbl}} \\ \vec{0} \end{bmatrix} \tag{2.38}$$

The mass, damping and stiffness matrices are composed of different smaller matrices. Note that even though the names mass, damping and stiffness are used to identify the matrices M, C and K the parts associated with the fluid in these matrices do not represent mass, damping and stiffness directly. The subscript s is used for the structural domain, f is used for the fluid domain and the coupling of the fluid and solid domains is described by fs.

The nodal displacements of the structural domain are contained in the vector $\vec{q}$, the nodal pressure in the fluid domain is contained in the vector $\vec{p}$. The pressure fluctuations in the turbulent boundary layer cause a nodal loading, described by $\vec{f_{tbl}}$. Substituting Equation 2.38 in Equation 2.29, A is rewritten as:

$$A = \begin{bmatrix} 0 & I \\ -\begin{bmatrix} M_{ss} & 0 \\ M_{fs} & M_{ff} \end{bmatrix}^{-1} \begin{bmatrix} K_{ss} & K_{sf} \\ 0 & K_{ff} \end{bmatrix} & -\begin{bmatrix} M_{ss} & 0 \\ M_{fs} & M_{ff} \end{bmatrix}^{-1} \begin{bmatrix} C_{ss} & 0 \\ 0 & C_{ff} \end{bmatrix} \end{bmatrix} \tag{2.39}$$

And B as:

$$B = \begin{bmatrix} 0 \\ \begin{bmatrix} M_{ss} & 0 \\ M_{fs} & M_{ff} \end{bmatrix}^{-1} \end{bmatrix} \tag{2.40}$$

Using the right eigenvectors obtained from Equation 2.39 and the left eigenvectors from the transpose of Equation 2.39, Equation 2.34 can now be evaluated for a coupled system.

The matrix S_q now contains 4 submatrices and is defined as:

$$S_q = \begin{bmatrix} S_q^{ss} & S_q^{fs} \\ S_q^{sf} & S_q^{ff} \end{bmatrix} \tag{2.41}$$

The response of the structure is given by S_q^{ss} . In the fluid domain, the pressure response is described by S_q^{ff} . Furthermore, S_q^{fs} describes the pressure times the complex conjugate of the displacement on the interface. For degrees of freedom on the surface, S_q^{fs} can be used to evaluate the sound intensity I, which is defined as:

$$I(\vec{r}, \omega) = \frac{1}{2} Re\{p(\omega)\bar{v}_{\perp}(\vec{r}, \omega)\} \tag{2.42}$$

Here, $\bar{v}_{\perp}(\vec{r}, \omega)$ is the complex conjugate of the perpendicular velocity to the surface at some location indicated by $\vec{r}$. It relates to the pressure-velocity spectrum as:

$$S_{fv} = i\omega S_{fs} \tag{2.43}$$

Taking the velocity normal to the surface, $S_{fv\perp}$ is defined as the cross-spectra pressure and the velocity. When this quantity is integrated over the surface, the acoustic power can be computed:

$$P_{\text{rad}} = \frac{1}{2}\int_{\Gamma} Re\{S_{fv_\perp}(\vec{r},\omega)\}d\Gamma \tag{2.44}$$

2.4. Discussion

First, some theoretical fundamentals were shown. Next, a literature study was performed. The study performed by Burrill et al. [8] was used to get a general idea of the modal shapes of a marine propeller. Multiple studies were found that constructed a numerical model to obtain a response of a stochastically excited structure. These modes assumed an orthogonal mode base, which means that proportional damping was assumed.

Only one study managed to incorporate non-proportional damping, which was presented in De Berg [3]. This method was verified on simple cases using COMSOL Multiphysics. Although De Berg [3] did not manage to obtain the same response PSD as COMSOL Multiphysics, his model is deemed most suitable to implement in the current study. The model is able to incorporate non-proportional damping, which a coupled system of water and a marine propeller has too. The model requires five inputs:

1. X, the right eigenmodes (Equation 2.30)
2. Y, the left eigenmodes (Equation 2.31)
3. G, the response function (Equation 2.35)
4. B, which is a function of the mass matrix (Equation 2.40)
5. S_f, the power spectral density of the loading (Equation 2.41)

In principle, if one were to obtain all the inputs of the model, the response of any solid surrounded by any fluid, excited by any stochastic load could be obtained. In the work of De Berg [3], B and G are defined. The loading S_f, as a result of the turbulent flow is outside the scope of this study. To account for a load, a stochastic excitation is used.

The problem arises when trying to find the left and right eigenmodes. A method is to take the Hermitian of the right eigenmodes, which will give the left eigenmodes. Although it sounds promising, this requires that all right eigenmodes are known, which is infeasible. Another more feasible approach is to solve the eigenfrequency problem twice, once for the system matrix A and one for the transposed system matrix. A FEM package could be used to obtain a subset of the eigenmodes efficiently. The model of De Berg [3] will be implemented in this study. Next, the methodology is discussed in chapter 3, where multiple approaches are discussed to obtain the response PSD of a stochastically excited structure.

3

Methodology

This chapter will discuss the methodology to model the vibratory response of a propeller excited by stochastic load. To verify the model, it is useful to build the model with steps of incremental complexity. By doing so, it becomes easier to identify obstacles. In Table 3.1, an overview of the steps in incremental complexity can be found. There are three types of challenges. First, the solid geometry is discussed.

The most simple geometry in this case would be a cantilever beam. The next step in incremental complexity is a cantilever plate, where the challenge lies in an extra spatial dimension. However, since the simulations are often performed in three dimensions, the added complexity of taking the third dimension into account is small. Therefore, the cantilever plate will be used as the starting point. Finally, a complex solid geometry can be analyzed. For example, a cantilever Burrill plate can be used. Ideally, this last step would be used to approximate a propeller blade.

The next challenge lies in the load type. All of the loads that are being taken into account are bending loads. The most simple case is a static point load. Next, point load will be used. The term 'stochastic point load' is used to describe a PSD applied to a certain point. Although the term 'stochastic' can also be used to describe cross-spectra, the term is still used for a point load throughout the study. Finally, the solid is excited with a distributed stochastic load (CSM), defined in Equation 2.10. Note that this type of loading condition is unavailable in COMSOL Multiphysics. Stochastic distributed loads require a method that does not rely on COMSOL Multiphysics to apply the loading. The workflow to obtain solutions for the different loading types is described in the next sections.

The final challenge lies in the environment of the solid. The most simple environment is vacuum. In general there will be negligible material damping in the solid. Next, the solid will be surrounded by an infinite fluid domain, to resemble a marine propeller. Therefore, a proper boundary condition of the fluid domain should be selected to account for this. This introduces non-negligible damping, since the pressure waves can leave the domain.

Increasing complexity →			
Geometry	Cantilever beam	Cantilever plate	Cantilever complex
Loading	Static load	Point load PSD	Distributed stochastic (CSM)
Environment	Vacuum	Water	

Table 3.1: Steps of incremental complexity.

Taking a step in each increasing complexity domain results in a new study case. As an example, a cantilever beam in a vacuum is taken. A study case would be to apply a deterministic point load. A next study case would be to apply a stochastic point load. As such, 18 different study cases can be defined. To reduce the number of studies performed, an effort is made to skip steps of incremental complexity. Therefore, section 3.3 starts with a cantilever plate, excited by different stochastic loads, surrounded by a vacuum.

To verify the steps of incremental complexity, COMSOL Multiphysics will be used, a commercially available software package. In COMSOL Multiphysics Multiphysics, a stochastic body load and a stochasic point load can be applied. However, the ability to prescribe a cross-spectral density is too limited to accurately describe a marine propeller. Therefore, the model of De Berg [3] will be implemented in Matlab. For more simple cases, such as a stochastic point load, COMSOL Multiphysics can still be used to verify the Matlab model.

3.1. General approach

Regardless of geometry, loading or environment, the response of a stochastically excited structure can be obtained using different methods. A flowchart of the problem is shown in Figure 3.1. First, the geometry of the solid is defined, and if required, the fluid is defined. For simple systems, such as a one-dimensional system in a vacuum, the geometry can be defined in Matlab. For more complex solids and fluids, it is easier to model the geometry in COMSOL Multiphysics. In general, five different paths can be used.

3.1.1. COMSOL method

The first path uses only COMSOL Multiphysics. First, the geometry is defined, after which COMSOL Multiphysics computes the system matrices. This is matrix A in Equation 2.29 for a solid in vacuum, or Equation 2.39 for a solid in a fluid. From the system matrix, the eigenmodes and eigenfrequencies can be obtained. Using a reduced model study, a stochastic point or body load can be applied to the solid, from which the response can be computed.

3.1.2. Matlab - COMSOL eigenmodes method

The second path is to let COMSOL Multiphysics obtain the eigenmodes and eigenfrequencies, and import them to Matlab. Since the loading is applied in Matlab, the user has full control over the loading matrix, and this is one of the large advantages of making a numerical model not in COMSOL Multiphysics. If a stochastic point or a body load is applied, the response can be compared with COMSOL Multiphysics. However, the loads have to coherent, which is another drawback from COMSOL Multiphysics. If a distributed stochastic load is applied, the results cannot be compared with COMSOL Multiphysics.

3.1.3. KM-method

The third method exports the stiffness and mass matrix from COMSOL Multipysics and imports them in Matlab. Using Equation 2.18, the eigenfrequencies and eigenmodes can be obtained. This method is not able to take into account non-proportional damping. In Matlab, a loading can be applied. Using the *eigs* function in Matlab, the first eigenfrequencies and eigenmodes can be obtained efficiently.

3.1.4. A-matrix method

The fourth method uses the mass, stiffness and damping matrices from COMSOL Multiphysics and imorts them in Matlab. These input matrices are used to construct A, defined in Equation 2.39. From A, the right eigenmodes can be obtained. Using A^T, the left eigenmodes can be obtained. Using the *eigs* function in Matlab, the first eigenfrequencies and eigenmodes can be obtained efficiently. On these eigenmodes, a loading can be applied, resulting in a response PSD.

3.1.5. Matlab only method

The last path only uses Matlab. Two methods can be used to obtain the eigenmodes and eigenfrequencies. First, an analytical expression can be found. This is possible for a rectangular plate that is simply supported on all sides, since the modes are functions of integer half-waves. Most of the times, finding an analytical expression for the mode shapes is not possible. For a cantilever plate, the eigenfrequencies can be obtained analytically. However, there is no function that describes the eigenmodes fully. Secondly, the system matrix can be defined, from which the eigenmodes and eigenfrequencies can be obtained. This usually only possible for very simple models, such as the the three degree-of-freedom system of section 3.2. Next, the loading is applied, resulting in a response PSD.

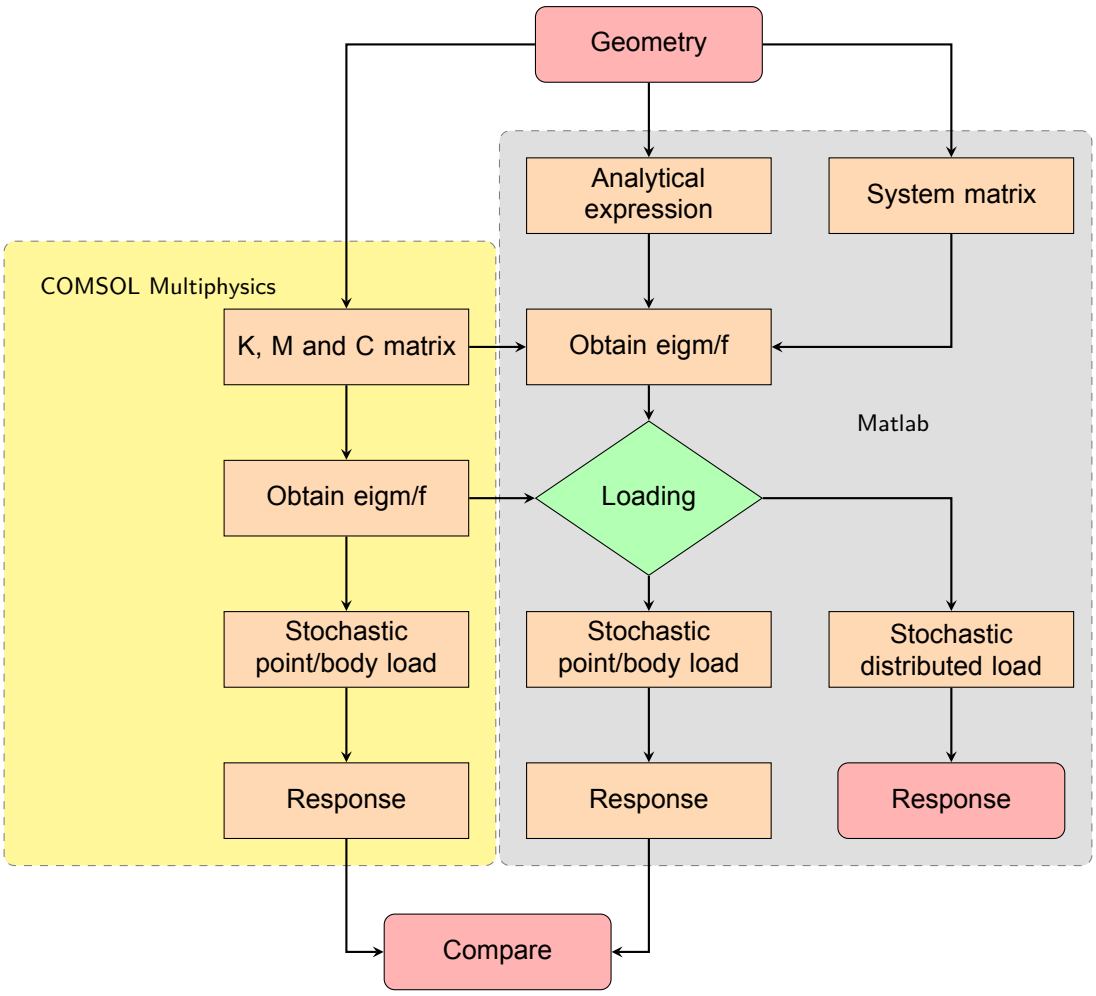

Figure 3.1: General approach to model the response of a stochastically excited structure.

3.2. One-dimensional test case

Since the problem of non-proportionally damped systems is quite complex, it would be useful to develop a better understanding of the foundation of the problem. This will also allow for a more thorough analysis of the results. Equation 3.1 to Equation 3.12 are taken from Kinsler et al. [22]. The linear motion of a single spring-mass oscillator is described as:

$$\frac{\mathrm{d}^2x}{\mathrm{dt}} + \frac{k}{m}x = 0 \tag{3.1}$$

where x is the displacement, m is the mass and k is the stiffness constant of the spring. A method to solve the differential equation is to make the assumption that the solution has a form of:

$$x = Ae^{\gamma t} \tag{3.2}$$

This substitution will provide a solution to the equation if $\gamma^2 = -\omega_0^2$. Taking the root results in $\gamma = \pm i\omega_0$, where $i = \sqrt{-1}$, means that the solution consists of two parts. This can be equated as:

$$x = A_1e^{i\omega_0 t} + A_2e^{-i\omega_0 t} \tag{3.3}$$

Where constants A_1 and A_2 are determined using the initial conditions. Using the following two trigonometric quantities:

$$e^{i\omega_0 t} = \cos(\omega t) + i\sin(\omega_0 t) \tag{3.4}$$

$$e^{-i\omega_0 t} = \cos(\omega t) - i\sin(\omega_0 t) \tag{3.5}$$

Equation 3.3 can be rewritten as:

$$x = (A_1 + A_2)\cos(\omega_0 t) + i(A_1 - A_2)\sin(\omega_0 t) \tag{3.6}$$

Although this is a solution to Equation 3.1, from a physical point of view the displacement must be completely real and should not contain an imaginary part. It is required that the constants are equal, such that the imaginary term equates to zero. However, this implies that $A_1 + A_2 = 2A_1$, and only a single constant is left, leaving the solution incomplete. To keep two constants to obtain the complete solution, the assumption is made that A_1 and A_2 are complex, which results in:

$$A_1 = a_1 + ib_1 \tag{3.7}$$

$$A_2 = a_2 + ib_1 \tag{3.8}$$

Substituting in Equation 3.3 results in:

$$x = (a_1 + a_2)\cos(\omega_0 t) - (b_1 - b_2)\sin(\omega_0 t) + i[(b_1 + b_2)\cos(\omega_0 t) + (a_1 - a_2)\sin(\omega_0 t)] \tag{3.9}$$

Where a_1, a_2, b_1 and b_2 are real constants. If the coefficients in the imaginary term equate to zero, the displacement is real at all t, which means that A_1 and A_2 are complex conjugates. Equation 3.9 becomes:

$$x = 2a_1\cos(\omega_0 t) - 2b_1\sin(\omega_0 t). \tag{3.10}$$

Usually, the mathematical steps to get rid of the imaginary term is unnecessary, and the convention is that the "*real part of the complex solution is by itself a complete general solution*"(Kinsler et al. [22]), although this implies only looking the positive frequencies. In the real world, systems are often damped. This can be accounted for in Equation 3.3 as:

$$m\frac{\mathrm{d}^2x}{\mathrm{dt}^2} + R_m\frac{\mathrm{d}x}{\mathrm{dt}} + kx = 0, \tag{3.11}$$

where R_m is a constant known as the mechanical resistance. Again, Equation 3.2 can be used to obtain a solution, where the complex notation of the solution is used in a similar fashion as the case without damping. The full derivation is left out, but results in the complete solution as:

$$\tilde{x} = e^{-\alpha t}(A_1 e^{i\omega_d t} + A_2 e^{-i\omega_d t}), \tag{3.12}$$

where the tilde notation is used again to indicate that terms can become complex. α is a positive damping constant, such that the vibration decays exponentially in time. ω_d is damped angular frequency of the vibration. Again, the complex conjugate is required to obtain a real displacement.

Next, a system with three degrees of freedom can be researched. An illustration can be found in Figure 3.2.

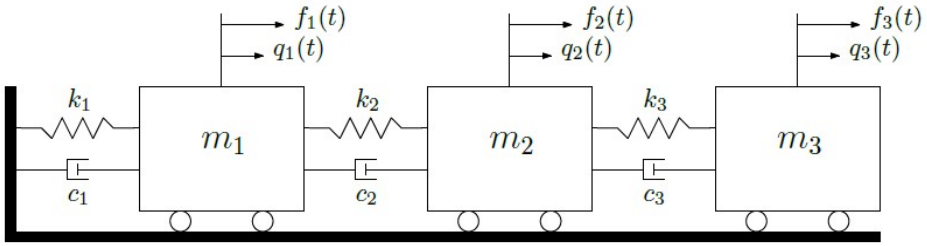

Figure 3.2: System with three degrees of freedom [3].

Three carts are connected to each other, and the left most kart is connected to a solid wall. The carts are connected with each other through a spring and damper. On each kart, which represents a degree of freedom, a force can be applied, resulting in a displacement. Here, k is the spring stiffness, c is the damping and m is the mass of each kart. This system can be expanded to a system with n degrees of freedom, the multi-degree-of-freedom system.

Equation 2.29 is used to construct the system matrix, from which the eigenvalues and eigenvectors are taken. The mass of each element is $1.0\,\mathrm{kg}$ and the stiffness of each element is $1.0\,\mathrm{N\,m^{-1}}$. To research the effect of non-proportional damping, three different damping values are taken: 0, 1.0 and $2.0\,\mathrm{N\,s\,m^{-1}}$. Using a damping of $1.0\,\mathrm{N\,s\,m^{-1}}$, the system matrix A is constructed as:

$$A = \begin{bmatrix} 0 & 0 & 0 & 1 & 0 & 0 \\ 0 & 0 & 0 & 0 & 1 & 0 \\ 0 & 0 & 0 & 0 & 0 & 1 \\ -2 & 1 & 0 & -2 & 1 & 0 \\ 1 & -2 & 1 & 1 & -2 & 1 \\ 0 & 1 & -1 & 0 & 1 & -1 \end{bmatrix}. \tag{3.13}$$

3.2.1. Effect of damping on the eigenvalues

For each damping value, the eigenvalues are computed and can be found in Figure 3.3. The real part of the eigenvalues describes the exponential damping, the imaginary part describes the oscillation. If there is no damping, the eigenvalues are completely imaginary, since they describe an undamped osculation. The effect of damping on the eigenvalues can be found in Figure 3.3. Furthermore, as expected, each complex conjugate of the eigenfrequency is obtained.

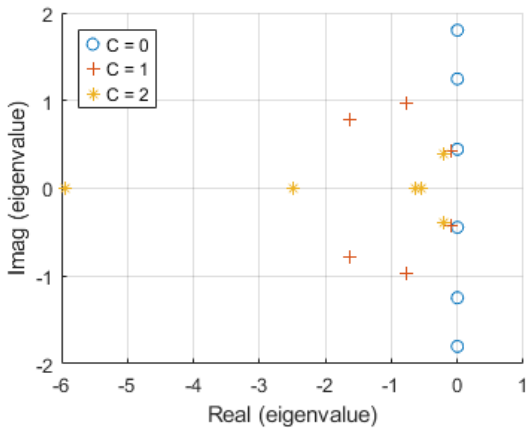

Figure 3.3: Eigenvalues of simple 1D system, using $C_i = 0, 1, 2$.

This example has been a very simple case of FEM for a system without fluid. A more generalized example of FEM, including acoustics (Appendix C) can be found in Appendix B.

Now that the fundamentals of the problem are better understood, a step in geometry complexity can be made. To start, a cantilever plate in vacuum, excited by a stochastic load, is researched.

3.3. Cantilever plate in vacuum

The next step is to increase the complexity of the solid. Therefore, a cantilever plate is chosen, since it has a resemblance with the blade of a propeller. First, the eigenmodes have to be obtained, after which a load can be applied.

3.3.1. Eigenmode analysis

As described in chapter 2, there are three different paths that can be taken to obtain the eigenmodes. All three different paths will be taken for a cantilever plate in a vacuum. This will help to decide the most suitable method to solve a system where a cantilever plate is surrounded by a fluid and excited by a stochastic load.

COMSOL Multiphysics simulation

In section 2.4, it was established that the required input of the excitation model are the left and right eigenmodes. To start, an eigenmode analysis is performed on a simple cantilever steel plate in a vacuum in COMSOL Multiphysics. This path requires the least amount of steps from the user, since COMSOL Multiphysics is a high-level software where many steps required for the eigenmode analysis are performed by the software. Due to the vacuum and the undamped material, the right and left eigenmodes will be the same, so finding the right eigenmodes suffices. The plate dimensions are $1\,\mathrm{m} \times 0.5\,\mathrm{m} \times 0.01\,\mathrm{m}$and is made from steel with a density of $7850\,\mathrm{kg/m^3}$, a Young's modulus of $205\,\mathrm{GPa}$ and a Poisson's ratio of 0.28. The first six eigenmode shapes of a cantilever plate can be found in Figure 3.4.

It is important to remember that the eigenmodes (in COMSOL Multiphysics the eigenvectors) after solving may have an arbitrary scaling. The eigenmodes need to be normalized as was described in De Berg [3] to obtain a response spectra using. Therefore, proper normalization is needed. COMSOL Multiphysics is able to normalize the eigenmodes with the root mean square (RMS) of the deformation amplitude, the maximum deformation or with the mass matrix. Looking at De Berg [3]'s model, the eigenmodes are normalized with the mass matrix, which is defined as

$$X^T M X = I \tag{3.14}$$

Later on when the plate is surrounded by a fluid and the left eigenmodes start to become significantly different from the right ones, the left eigenmodes need to be scaled using Equation 3.33, which will be

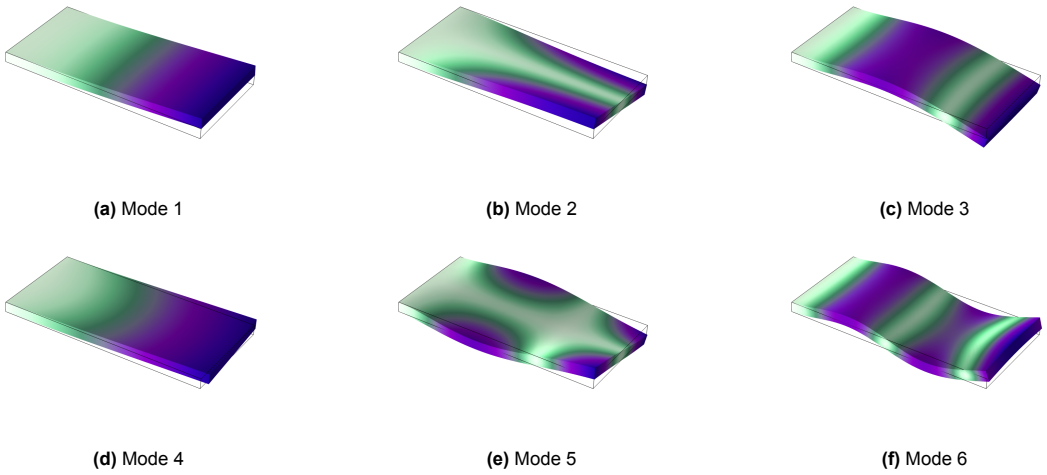

(a) Mode 1 **(b)** Mode 2 **(c)** Mode 3

(d) Mode 4 **(e)** Mode 5 **(f)** Mode 6

Figure 3.4: Eigenmodes of a cantilever plate, with properties described above.

discussed later. It is important to verify that the right eigenmodes extracted from COMSOL Multiphysics are indeed correctly scaled with the mass matrix. This can be confirmed by computing the Gram matrix of $X^T M X$ as was performed by Heilmann [20]. The results can be found in Figure 3.5.

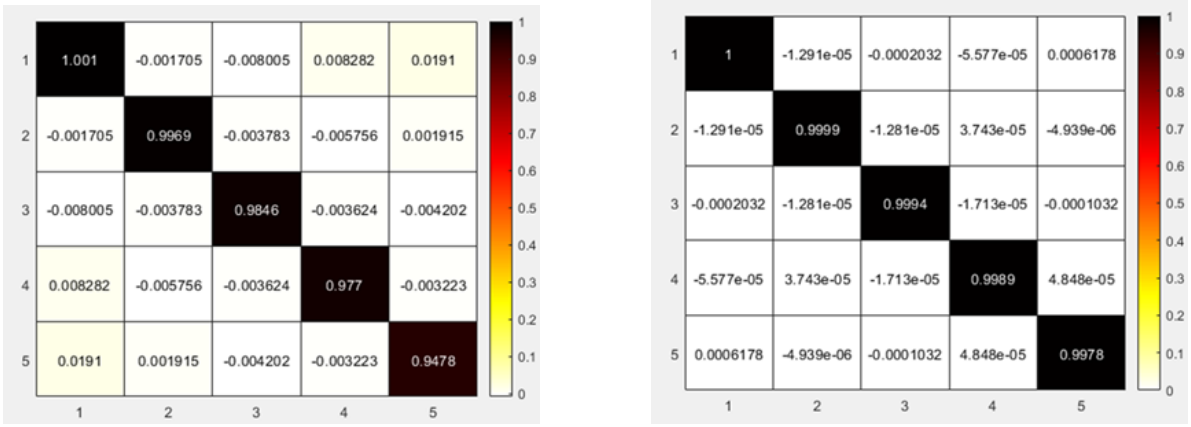

(a) Coarse mesh **(b)** Fine mesh

Figure 3.5: Gram matrices of mass-scaled eigenmodes of a cantilever plate in vacuum.

The Gram matrix has been computed for a course and a fine mesh. Two conclusions can be drawn from Figure 3.5. First, it can be seen that the Gram matrices approach 1 on the diagonal, and 0 on the off-diagonal. This confirms that the eigenmodes are approximately orthogonal. This was also expected since the plate is not damped and placed in vacuum. Another interesting finding is that when Figure 3.5a is compared to Figure 3.5b, it can be seen that the diagonal converges to 1 and the off-diagonal converges to 0. This can also be expected, since an increasingly fine mesh should approach the solution to the continuous problem.

KM-method simulation

The COMSOL Multiphysics model is of a steel cantilever plate without material damping surrounded by a vacuum. Therefore the damping matrix only contains zeros. Since there is no damping in the system, there is no need to use a state-space domain to construct the system matrix A, defined in Equation 2.29. Therefore, the following eigenvalue problem can be obtained from the equations of motion describing the system:

$$KX = \Omega M X, \tag{2.18}$$

where Ω contains the squared eigenfrequencies on the diagonal. The stiffness matrix K and mass matrix M are required from COMSOL Multiphysics. The nodes that are fixed because of boundary conditions are removed from the matrices. This can be achieved as follows

$$M = \mathrm{Nullf}^T M_c \mathrm{Nullf} \tag{3.15}$$

Where Nullf is the nullspace function supplied by the COMSOL Multiphysics model [4]. The nullspace function removes the constrained nodes. In this case, the mass matrix M was taken, and the same method is used to remove the constrained nodes from the stiffness and loading matrix. It is verified that using $X^T M X$ produces the identity matrix which means that the eigenmodes are scaled correctly to be used further.

Analytical solution

Because this is a simple case, an analytical solution is available and can be used as a reference solution to verify the results produced by the numerical methods. The equation for the eigenfrequencies of a cantilever plate in a vacuum can be found in Blevins et al. [7], and is formulated as

$$f_{ij} = \frac{\lambda_{ij}^2}{2\pi a^2} \left[\frac{Eh^3}{12\gamma(1-\nu^2)} \right]^{1/2} \tag{3.16}$$

Where a is the aspect ratio, which in this case is 2.5. E is the modulus of elasticity, h is the thickness of the plate. The mass per unit area is indicated with γ and the Poisson's ratio with ν. The eigenfrequencies of a steel cantilever plate for all three paths can be found in Table 3.2.

	Analytical (Hz)	COMSOL Multiphysics (Hz)	KM Matrices (Hz)
Mode 1	8.36	8.43	8.43
Mode 2	43.53	44.45	44.45
Mode 3	52.17	52.72	52.72
Mode 4	139.05	141.62	141.62
Mode 5	146.61	148.31	148.31
Mode 6	257.74	262.32	262.32

Table 3.2: Comparison of analytical and COMSOL Multiphysics eigenfrequencies.

The results from the numerical methods are found to be close to the analytical solution. The differences are well within an acceptable range.

3.3.2. Stochastic point load

Now that the eigenmodes can be obtained using multiple methods, a loading can be applied to the cantilever plate. Depending on whether the COMSOL Multiphysics eigenmodes are imported in Matlab or the eigenmodes are computed based on the system matrices from COMSOL Multiphysics, the loading should be applied in a slightly different way. The cantilever plate can be found in Figure 3.6 and has a dimension of $1\,\mathrm{m} \times 0.5\,\mathrm{m} \times 0.05\,\mathrm{m}$. The plate is made from steel with a density of $7850\,\mathrm{kg/m^3}$, a Young's modulus of $205\,\mathrm{GPa}$ and a Poisson's ratio of 0.28. The stochastic point load will be applied at $[1, 0.4, 0.05]\,\mathrm{m}$. The response will be measured at the same coordinate.

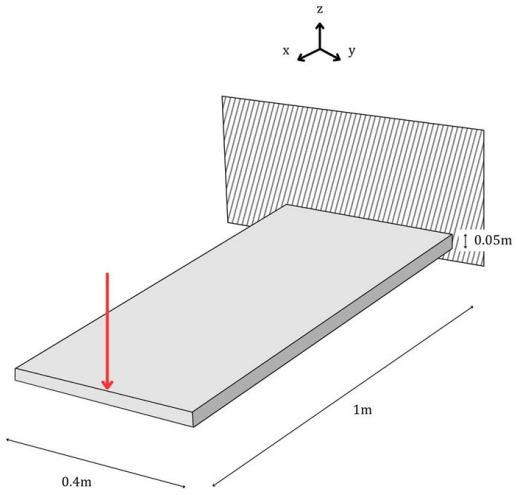

Figure 3.6: Schematic geometry of a cantilever plate in vacuum, excited by a stochastic point load.

First, the loading based on the COMSOL Multiphysics eigenmodes is discussed. A unit loading of $1\,\mathrm{N}^2/\mathrm{Hz}$ is used throughout the simulations, since research into the load is outside of the scope of the study.

The function used to obtain the eigenmodes is shown in section A.1. However, this does not evaluate the deformation at all mesh points. Nevertheless, the eigenmodes contain enough detail to continue the computation. The eigenmodes are stacked as

$$X = \begin{bmatrix} \mathrm{eigm}_x \\ \mathrm{eigm}_y \\ \mathrm{eigm}_z \end{bmatrix} \tag{3.17}$$

Depending on the number of eigenfrequencies that are evaluated, the eigenmode matrix will contain more columns. The loading matrix should be the the same length and width as the length of the stacked eigenmode matrix, which becomes obvious from checking Equation 2.22 where $X^T S_f X$. The coordinates on where the eigenmode deformation is evaluated can be extracted from COMSOL Multiphysics. Depending on where the load should be applied and in which direction, that specific loading matrix element will become 1. Since the eigenmodes are stacked based on for which direction the equation is solved, the loading matrix is structured as:

$$S_f = \begin{bmatrix} S_{xx} & 0 & 0 \\ 0 & S_{yy} & 0 \\ 0 & 0 & S_{zz} \end{bmatrix} \tag{3.18}$$

Using the system matrix approach, the method changes slightly. However, when done improperly, the simulations will produce incorrect results, and therefore emphasis is put on the correct construction of the loading matrix. Although the loading described in Equation 2.36 is correct, it is more convenient to use a different ordering. Using the same ordering as the mass, damping and stiffness matrix the loading is defined as:

$$S_f = \begin{bmatrix} S^1_{xx} & 0 & 0 & 0 & 0 \\ 0 & S^1_{yy} & 0 & 0 & 0 \\ 0 & 0 & S^1_{zz} & 0 & 0 \\ 0 & 0 & 0 & S^2_{xx} & 0 \\ 0 & 0 & 0 & 0 & \dots \end{bmatrix} \tag{3.19}$$

Where the off-diagonal terms are left zero, since only pressure forces are taken into account. Also, each mode is used three times, to solve for the deformation in x, y and z respectively. In principle, the matrices can be reordered to group the nodes based on which direction the respective equations solves for. This would result in a loading matrix equivalent to the method based on the COMSOL Multiphysics eigenmodes, described above. To reduce the amount of steps in the method that can possibly lead to mistakes, the choice is made to use the original ordering.

It is good practice to place points in the geometry where a point load need to be placed and where the response has to be measured, since this point will then be taken into account by the COMSOL Multiphysics mesh.

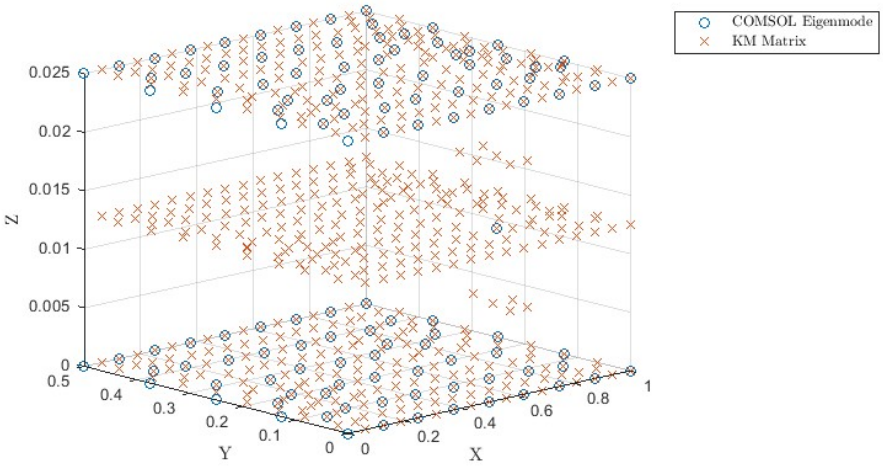

Figure 3.7: Coordinate difference between the COMSOL Multiphysics eigenmode and the matrices.

The response of the cantilever plate can be found in Figure 3.8, where three different methods are used. The force is applied at $[1.0, 0.25, 0.05]$ m. In principle, the response can be measured at any coordinate. For now, the response has been measured at the same coordinate where the force is applied, since this will produce a response spectral density with the most distinct peaks. The response is evaluated up to $1000\,\mathrm{Hz}$. In principle, the response can be obtained up to the highest eigenfrequency that can be represented on the discretized domain. After that point, the response will decrease since the response function will no longer increase. To reduce numerical costs, the decision is made to evaluate the response up to a $1000\,\mathrm{Hz}$.

First, the response is computed using COMSOL Multiphysics only. Next, the COMSOL Multiphysics eigenmodes are imported in Matlab, where a stochastic point load is applied. Finally, the stiffness and mass matrices from COMSOL Multiphysics are imported in Matlab, from which the eigenmodes and eigenvalues are computed. The results coincides, which means that the methods are verified, although differences in the amplitude of the peaks can be found. This is caused by the resolution of the frequency array over which this the methods are computed. If the resolution increases, the peaks will become higher. This is a direct result of the response function, where the distance is measured between the respective eigenfrequency and the frequency for which the model is evaluated. The response function is defined as:

$$G_k(\omega) = \frac{1}{-\omega^2 + 2i\zeta_k\omega\omega_k + \omega_k^2} \tag{2.23}$$

When $\omega = \omega_k$ and $\zeta = 0$, the response function will become infinite if the evaluated frequency and the respective eigenfrequency are identical. Also, it should be noted that the valleys of the KM-method are slightly shifted to the left, which is likely caused by some numerical noise. Using the KM-method, purely real eigenfrequencies are computed. On first glance, COMSOL Multiphysics also seems to return only real eigenfrequencies. However, using the damping ratio, defined as:

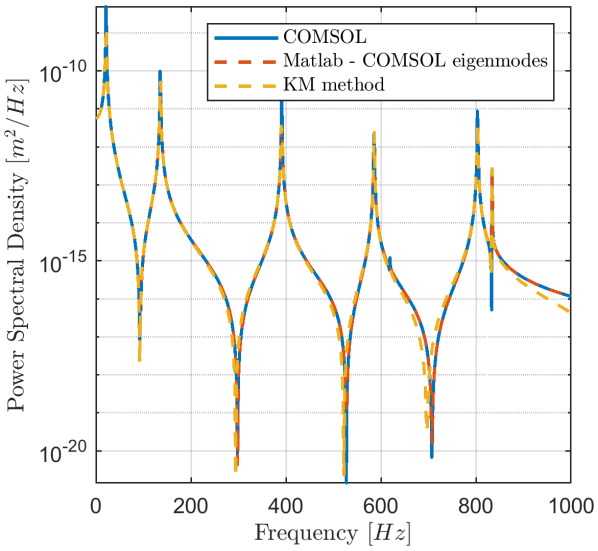

Figure 3.8: Power spectral density of a cantilever plate excited by a stochastic point load.

$$\xi_k = \frac{\text{imag}(\omega_k)}{\text{real}(\omega_k)} \tag{3.20}$$

results in values of the order 10^{-10} to 10^{-15}, which means that there is a small imaginary component in the eigenfrequencies. This means that there is still some damping in the system, which can be caused by numerical noise. A source of the noise could be round-off errors. Since the results are so close together, it is decided to continue with the research. In order to verify the results, a simple check was performed at $0\,\text{Hz}$, where the stiffness was checked by checking the ratio between the response and the applied force. First, the COMSOL Multiphysics eigenmodes method was checked. The stiffness was calculated as follows:

$$\sqrt{\frac{\text{Response PSD}}{\text{Input PSD}}} = 3.75 \times 10^{-5} \tag{3.21}$$

Furthermore, a simple beam deflection formula was used to check the response of a beam to a unit force. The following formula was used:

$$\delta = \frac{FL^3}{3EI} \tag{3.22}$$

Where the stiffness was checked by looking at the ratio between the deflection and the unit force, which is computed as:

$$\frac{\text{Response}}{\text{Force}} = 3.90 \times 10^{-5} \tag{3.23}$$

Furthermore, a simple simulation was performed in COMSOL Multiphysics, where a deterministic point load of $1\,\text{N}$ was applied on the same cantilever plate that was discussed previously. Using Equation 3.23, the stiffness is 3.78×10^{-5}. Since all three values are well within an acceptable range, the solutions are deemed verified.

3.3.3. Two stochastic point loads

Now that the results for a single stochastic point load are verified, the next step can be taken, and a stochastic distributed load can be applied to a cantilever plate. The forces are placed at $[1, 0.1, 0.05]$ m and $[1, 0.3, 0.05]$ m, and the response is measured at $(1, 0.2, 0.05)$ m. First, two point loads are placed on the cantilever plate, shown in Figure 3.9. This allows for a step between a single point load and a distributed load. Also, this is the most complex load COMSOL Multiphysics can model. Therefore, the self-developed method can still be validated with the COMSOL Multiphysics results. Both stochastic forces are unit forces, meaning that both loads are $1\,\mathrm{N}^2/\mathrm{Hz}$.

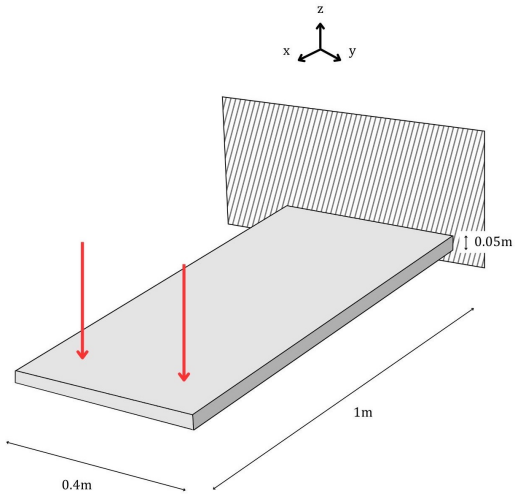

Figure 3.9: Schematic representation of a cantilever plate excited by two stochastic point loads.

The response of the cantilever plate can be found in Figure 3.10. All three methods produces identical results, although the resolution of the frequency over which the response was evaluated causes amplitude differences. Clear peaks are visible at the eigenfrequencies of the plate. The lowest mode is the most dominant, containing the most power. In general, a downwards slope can be seen across the peaks. This also agrees with the ideas developed earlier, where the most dominant modes were the lower ones.

Since there are multiple loads, it is important to discuss the correlation between them. The autocorrelation function was defined as

$$R_{x_1,x_2}(\tau) = \lim_{T\to\infty} \frac{1}{T} \int_{-T/2}^{T/2} x_1(t)x_2(t+\tau)dt \tag{2.8}$$

In the results of Figure 3.10, there was no correlation between the two stochastic point loads.

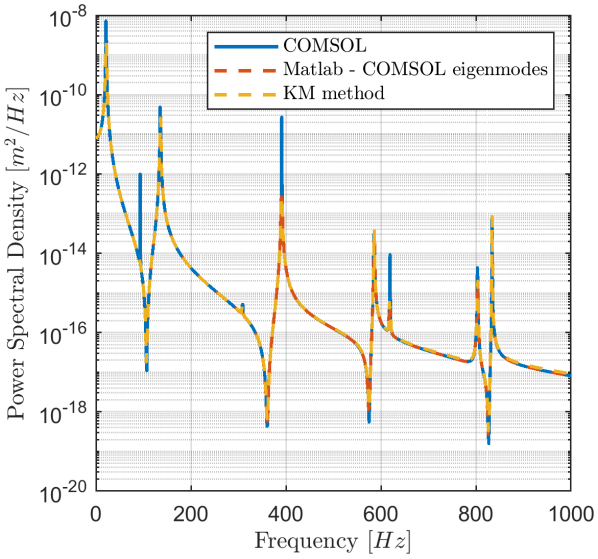

Figure 3.10: Power spectral density of a cantilever plate excited by two stochastic point loads, without correlation.

It would also be interesting to see the effect of correlation between the two point loads. Therefore, a simulation was made where there was a full correlation between the points, which results in a correlation value of 1. The results can be found in Figure 3.11.

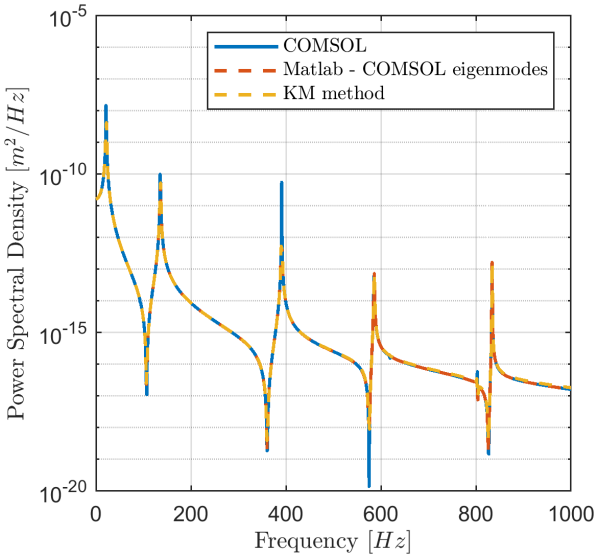

Figure 3.11: Power spectral density of a cantilever plate excited by fully correlated stochastic two point loads.

Overall, the response is shifted up slightly, which makes sense due to the fact that the two point loads are in phase. Furthermore, there is a large difference around $800\,\mathrm{Hz}$. Without correlation, there is a large peak. However, if there is a full correlation, this peak disappears, something all 3 methods were able to capture. In general, the shape of the response remains the same. Also, it would be interesting to research the effect of a correlation of -1. This means that the loads are in opposite phase, because if one signal is positive, the other is negative. The results can be found in Figure 3.12.

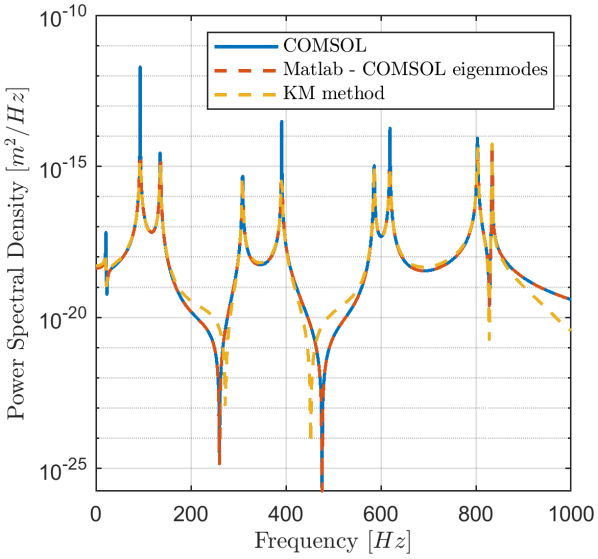

Figure 3.12: Power spectral density of a cantilever plate excited by two stochastic point loads, with a correlation of -1.

The effect is more profound than the effect of the loads working in phase. The slope of the power over the frequencies reduces, while the whole response spectrum shifts downwards. This can be explained by the fact that the loads are out of phase, where as if they are in phase, they are working simultaneously in the same direction. Using the KM-method, two of the three valleys are shifted. The valley around $270\,\mathrm{Hz}$ is shifted to the right, and the valley around $460\,\mathrm{Hz}$ is shifted to the left. At this moment, it is unclear where this discrepancy comes from. Interestingly, the KM-methods peaks agree with the COMSOL Multiphysics and Matlab-COMSOL Multiphysics method.

3.3.4. Distributed load

Now that the COMSOL-Matlab eigenmodes method and the KM-method are verified with the COMSOL method, the next step can be taken and a distributed load can be applied. COMSOL Multiphysics is not able to apply a distributed load, and thus the other methods were developed.

At this stage, the fourth method is implemented, the A-matrix method. The system matrix A is constructed from the stiffness, mass and damping matrices from which the right and left eigenmodes are taken. For convenience, the structure of the system matrix shown in Equation 2.29 is given again, and is written as:

$$A = \begin{bmatrix} 0 & I \\ -M^{-1}K & -M^{-1}C \end{bmatrix} \tag{2.29}$$

A load is applied of $1\,\mathrm{N}^2/\mathrm{Hz}$ to the cantilever plate and the response is measured at the same location used for the point stochastic loading. The choice is made for a fully uncorrelated load, which means that there are no off-diagonal elements in the loading matrix S_f. In reality, the load induced by turbulence has cross-correlation terms, but for the demonstration of the method, this is not taken into account. The schematic geometry can be found in Figure 3.13. The response PSD can be found in Figure 3.14.

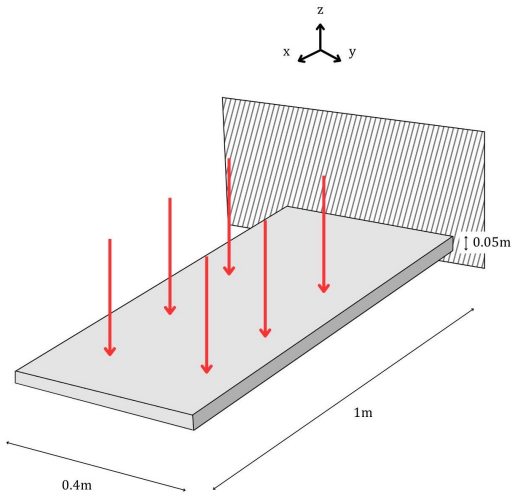

Figure 3.13: Schematic representation of a cantilever plate excited by a distributed stochastic load without coherence.

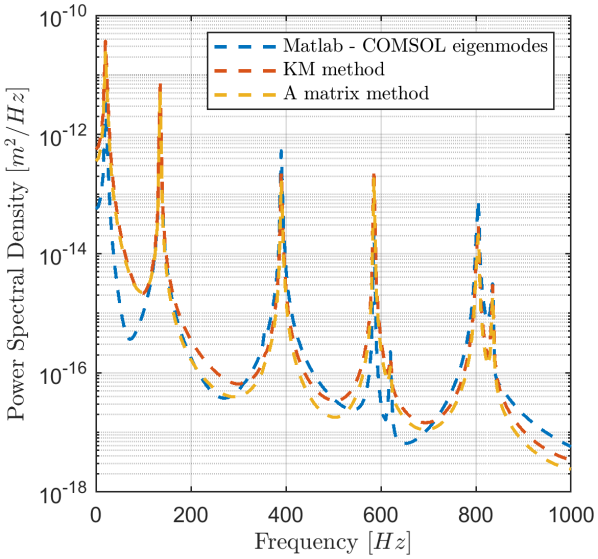

Figure 3.14: Power spectral density of a cantilever plate exited by a distributed stochastic load.

The results are interesting in multiple ways. First, it was validated that the A-matrix method is able to construct the response with a cantilever plate without damping in vacuum. This is is a promising results, since the A-matrix method has to be used for a coupled system. All three methods were able to produce the same PSD peaks, but there are some discrepancies in the valleys. The MATLAB-COMSOL method under predicts the response PSD around $100\,\mathrm{Hz}$. In the next valley, the COMSOL-Matlab method and the A-matrix method find the same valley, but the KM-method produces a larger response. This behavior of one method producing a slightly larger valley than the others can be found across all valleys. Although the methods produce slightly different valleys, finding the same peaks is most important for the application of radiated noise.

3.4. Coupled system

So far, four different paths have been used to obtain a response PSD of a cantilever plate. First, the response PSD was obtained using COMSOL Multiphysics only. Since COMSOL Multiphysics is only able to apply relatively simple loads, this method could not be used for a distributed load. Secondly, COMSOL-Matlab eigenmodes method was implemented. The eigenmodes computed by COMSOL Multiphysics were imported in Matlab. In Matlab, the loading was applied, which resulted in a response PSD. Thirdly, the KM-method was implemented. The stiffness K and mass M matrix were exported from COMSOL Multiphysics and imported in Matlab. From the stiffness and mass matrix, the eigenmodes and eigenfrequencies were obtained by solving Equation 2.18. On these eigenmodes, a stochastic load was applied, resulting in a response PSD. Finally, the A-matrix method was implemented. Using the stiffness, mass and damping matrices from COMSOL Multiphysics, the system matrix A was constructed. From the system matrix, the eigenfrequencies and the left and right eigenmodes were obtained. Using these modes, a stochastic load was applied. All the methods were verified with each other.

Now that the methods are verified for a cantilever plate in vacuum, the most difficult step can be taken were the plate is surrounded by a fluid. This step is deemed most difficult since De Berg [3] was not able to implement the fluid to match the COMSOL Multiphysics results. At the time it was believed that the differences were caused by scaling in the mass matrix. Since his data is available, the most straightforward method is to change the scaling in the data from De Berg [3].

3.4.1. De Berg [3] reference study

The results of the analysis performed by De Berg [3] are shown in Figure 3.15. As was described in his work, there was an order difference of 10^{24} between the results produced by COMSOL Multiphysics and his own work. The COMSOL Multiphysics response is shown in blue, the response of the A-matrix method implemented in Python is shown in orange. The peaks and valleys do not match, meaning something more complex than eigenmode scaling is causing the differences. The geometry of the COMSOL Multiphysics model is shown in Figure 3.16.

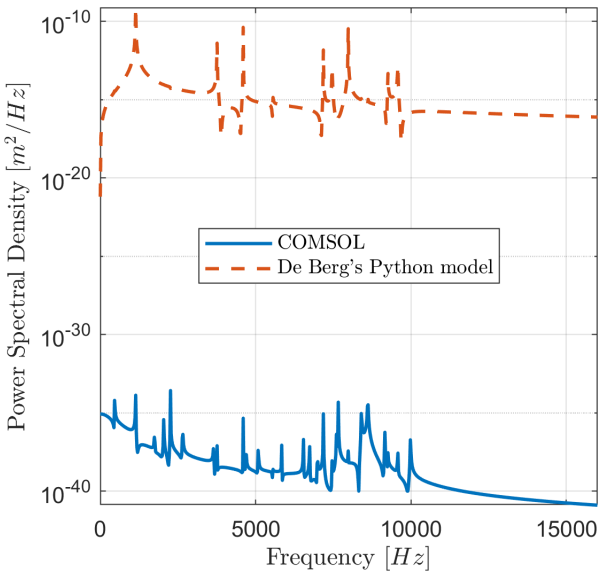

Figure 3.15: Power spectral density of the response of a cantilever plate, attached on one side to a fluid domain, excited by a body load.

3.4.2. Initial method: Mass matrix scaling

Since the work of De Berg [3] pointed to scaling in the mass matrix, it is worth checking what the mass matrix looks like.

The first 10 columns and rows of the obtained mass matrix are presented in Figure 3.17. Here, some

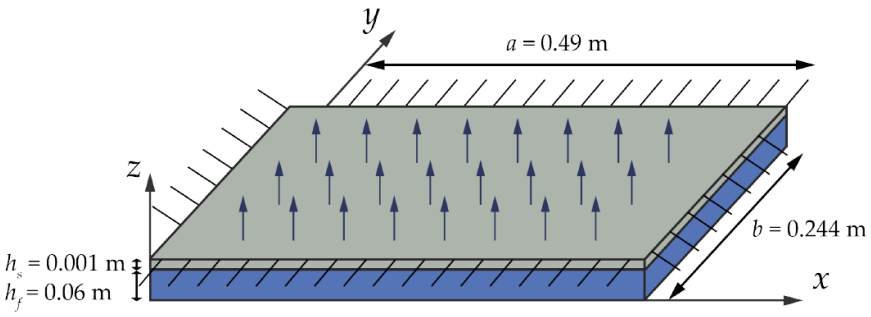

Figure 3.16: Schematic overview of a fixed plate with a fluid domain attached to one side. The plate is excited by a stochastic body load [3].

interesting findings were done. First, the mass matrix is no longer symmetric, and contains nonzero elements on the off-diagonal. This is in contrast to the mass matrix obtained from a cantilever plate in a vacuum, where the matrix only contained values on the diagonal. Secondly, the mass matrix contains imaginary values and thirdly, the mass matrix contains negative masses. Both these findings could be caused by COMSOL Multiphysics attempting to take some proportional damping caused by the fluid domain into account in the mass matrix. However, this is not verified, and cannot be stated with absolute certainty. Lastly, the order difference of the elements is large. This is interesting, since the density of the water surrounding the plate is $997\,\mathrm{kg/m^3}$, and the density of the steel plate is $7900\,\mathrm{kg/m^3}$, which is roughly a ratio of 7.9. However, looking at the first elements in the mass matrix, the smallest element has a value in the order of 10^{-17} and the largest value is in the order of 10^{-3}. Also, there is a large order difference on the diagonal, where element $[1, 1]$ is much smaller than element $[6, 6]$. This could result in numerical instabilities when the inverse of the mass has to be computed, that is needed for the system matrix A and to compute B.

	1	2	3	4	5	6	7	8	9	10
1	6.3701e-16	0	1.8588e-05	3.0280e-05	-7.6839e-17	0	0	8.3009e-20	1.9210e-17	0
2	0	5.1522e-04	0	0	0	-3.4348e-04	0	0	0	8.5869e-05
3	0	0	5.1522e-04	0	0	0	-3.4348e-04	0	0	0
4	0	0	0	5.1522e-04	0	0	0	-3.4348e-04	0	0
5	-7.6839e-17	0	0	7.1151e-20	6.1472e-16	0	0	1.6149e-04	-7.6839e-17	0
6	0	-3.4348e-04	0	0	0	0.0027	0	0	0	-3.4348e-04
7	0	0	-3.4348e-04	0	0	0	0.0027	0	0	0
8	0	0	0	-3.4348e-04	0	0	0	0.0027	0	0
9	1.9210e-17	0	0	-5.0467e-06	-7.6839e-17	0	0	8.4703e-20	4.9722e-16	0
10	0	8.5869e-05	0	0	0	-3.4348e-04	0	0	0	0.0028

Figure 3.17: Mass matrix extracted from COMSOL Multiphysics.

When a cantilever plate in a vacuum is evaluated, the mass matrix sums to three times the mass of the solid, because the system solves for u, v and w, the deformation in x, y and z respectively. The sum of the fluid part of the mass matrix does not equate to the mass of the fluid. After reordering, the mass matrix looks as:

$$M = \begin{bmatrix} M_u & & & \\ & M_v & & \\ & & M_w & \\ & & & M_f \end{bmatrix} \tag{3.24}$$

Where the subscript u, v and w indicate for which spatial direction the subsystem is solved. Since the subsystems of the plate sum to the analytical mass of the plate, it is worth checking if the fluid subsystem should be scaled such that is sums to the analytical mass.

3.4.3. Mass matrix scaling results

Three different scaling factors are computed. First, the fluid part of the mass matrix is multiplied with 10^{-10}. The results can be found in Figure 3.18.

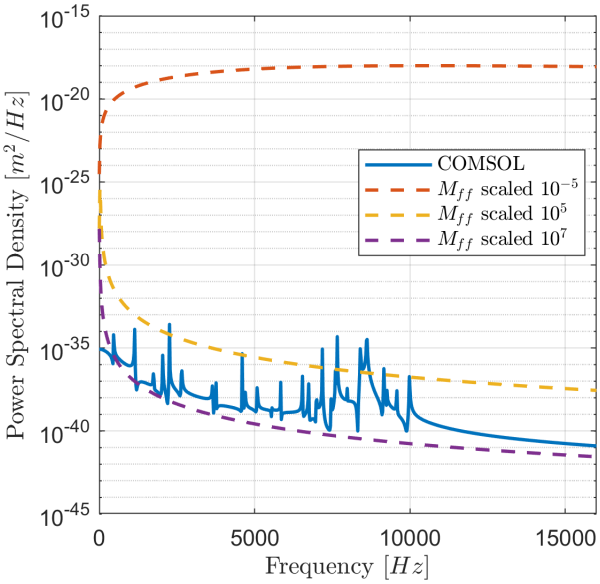

Figure 3.18: PSD of the results of scaling the fluid part of the mass matrix.

When the mass is reduced, the amplitude of the response increases. This can be explained by the fact that a light object has a lower inertia than a heavy object. Also, many more peaks start to form at frequencies where COMSOL Multiphysics did not find a response, up to $16\,\mathrm{kHz}$. Next, the results of scaling the fluid part of the mass matrix with 10^{10} can be found in Figure 3.18. There are no longer any peaks visible, which can also explained with the same intuition before. The response of the system is now far below the COMSOL Multiphysics response.

Finally, the fluid part of the mass matrix is multiplied with 10^{5}. The response of the system now lies above the COMSOL Multiphysics response, and there are still no peaks visible. From this, it can be concluded that scaling the fluid part of the mass matrix with any constant will never match the COMSOL Multiphysics response.

3.4.4. De Berg [3] COMSOL Multiphysics and Python model analysis

Taking a closer look at the mesh used in the COMSOL Multiphysics model raises the question of validity. In order to reduce computational costs, a very coarse mesh was used, which can be seen in Figure 3.19. The mesh has around 200 elements.

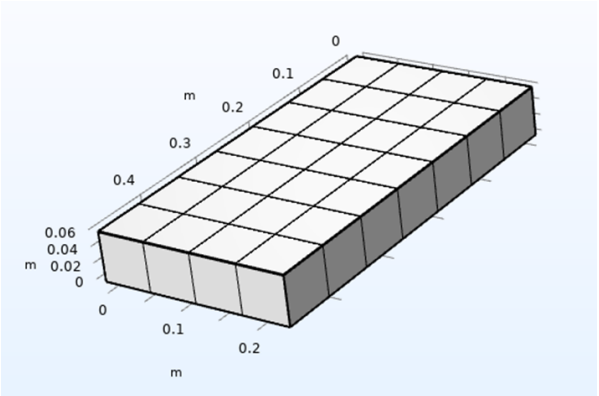

Figure 3.19: Mesh used by De Berg [3] to discretize a cantilever plate attached to a fluid domain on one side.

However, the COMSOL Multiphysics model was still able to obtain eigenfrequencies up to $10\,\mathrm{kHz}$, which should not be possible with such a coarse mesh.

Therefore, it would be interesting to see how the original coupled equation was derived. This can be found in the work of De Rosa et al. [15], where a study is performed of a plate fixed on all edges, and exposed to turbulent air on one side. The fluid part of the mass matrix is defined as:

$$M_{ff} = diag\left(\frac{1}{c_0^2}\right), \tag{3.25}$$

Where c_0 is the speed of sound of the air. The submatrix only contains values on the diagonal, which is different from the COMSOL Multiphysics mass matrix. Therefore, it should be better understood what COMSOL Multiphysics is producing.

It was found that the elements of the fluid part of the mass matrix are:

$$m_f = \frac{1}{\rho_f c_0^2}, \tag{3.26}$$

where m_f is a fluid mass element. Interestingly, the only difference between what COMSOL Multiphysics is producing and what the fluid mass submatrix should be is the inverse of the fluid density, although it was found that multiplying the fluid mass matrix with any constant does not match the COMSOL Multiphysics results.

Taking a closer look in the Python code of De Berg [3], it was found that first all the right eigenmodes were obtained from the system matrix A. Rather than solving the transposed of the system matrix to obtain the left eigenmodes, the inverse of the right eigenmodes was taken. This is only feasible for very small systems. However, it was found that not all right eigenmodes were used to compute the left eigenmodes.

To continue, a new COMSOL Multiphysics model will be created to better account for an infinite fluid domain. Also, the mesh element size will be based on the maximum eigenfrequency, set by a threshold.

3.5. Setting up the simulation

The COMSOL Multiphysics model is recreated, from which the mass, damping, and stiffness matrices are extracted, from which the system matrix A is constructed.

In order to simulate a cantilever plate surrounded by an infinite fluid domain, the fluid boundary condition and domain size should be discussed first. To reduce computation costs and to allow for easier verification of the model during the development of the method, the COMSOL Multiphysics model is converted to 2D. A beam of $1\,\mathrm{m} \times 0.05\,\mathrm{m}$ will be used throughout the method development. The beam is made from steel with a density of $7850\,\mathrm{kg/m^3}$, a Young's modulus of $205\,\mathrm{GPa}$ and a Poisson's ratio of 0.28. The surrounding fluid is water, and has a density of $997\,\mathrm{kg/m^3}$ and a speed of sound of $1500\,\mathrm{m\,s^{-1}}$.

3.5.1. Boundary conditions

This section is based on the documentation provided by COMSOL [12]. Common boundary conditions for the wave and Helmholtz equation are:

1. Sound-hard boundaries
2. Sound-soft boundaries
3. Impedance boundary conditions
4. Nonreflecting boundary conditions

To research the eigenmodes of a propeller, the boundary of the fluid should mimic an infinite domain. These boundary conditions are known as nonreflecting boundary conditions. In COMSOL Multiphysics, three non-reflecting boundary conditions are available:

1. Port conditions

2. Matched boundary conditions
3. Radiation boundary conditions

The port condition is used to model exciting and absorbing waves in waveguide structures, which can be ducts or channels.

Matched boundary conditions include the *perfectly matched layer (PML)* or the *absorbing layer*. These are two different techniques used to damp the outgoing waves such that there are no or very little reflections.

The solution of the simulation using a PML will only be correct close to that frequency. Care has to be taken when a PML is used to perform an eigenfrequency analysis, because the frequency for which the PML should tuned is not known beforehand, since it is not known what the eigenfrequencies are before the analysis is done. The scaling of the PML will be defined with the typical wavelength set equal to the PML layer thickness, and therefore it is required to known the wavelength beforehand. To circumvent this, the typical wavelength should be defined by the user, based on the expected eigenfrequency. It should also be noted that the PML is a purely mathematical concept. Often, the reflection is a complex-valued, where the physical damping mechanism cannot be linked to the magnitude of the complex part. Furthermore, nonphysical modes can be present inside the PML. The PML should always be inspected to prevent this. COMSOL Multiphysics advises to use a radiation boundary condition in open problems when performing eigenfrequency studies [12].

The radiation boundary condition is divided into three categories: plane wave radiation, spherical wave radiation and cylindrical wave radiation. This boundary condition allows the pressure waves to leave the domain with minimal reflection. When using the radiation boundary condition, the incident pressure field node can be activated to calculate the total and reflected acoustic field intensity variables at the boundary. This node should not be used with the PML, since this is an absorption layer.

3.5.2. Fluid domain size

The radiation boundary conditions are only accurate in the far-field region [12]. In this region, the waves are locally planar, and the pressure and velocity are in phase. To obtain a first estimate where the far-field regions begins, the following equation can be used:

$$R > \frac{8a^2}{\lambda} = \frac{8}{2\pi} k a^2 \tag{3.27}$$

Where a is the radius of the sphere that contains all objects and sources. The wavelength is annotated with λ, and the wavenumber is k. The wavelength is defined as:

$$\lambda = \frac{c}{f}. \tag{3.28}$$

Where c is the speed of sound and f the frequency in Hertz. The wavenumber k is defined as:

$$k = \frac{1}{\lambda} \tag{3.29}$$

Applying this to a cantilever plate of $1\,\mathrm{m} \times 0.05\,\mathrm{m}$, evaluated up to $1000\,\mathrm{Hz}$, surrounded by water with a speed of sound of $1500\,\mathrm{m\,s^{-1}}$, this equates to:

$$R > \frac{8(\sqrt{0.5^2 + 0.025^2})^2 1000}{1500}, \quad R > 1.34m \tag{3.30}$$

A schematic representation of the model can be found in Figure 3.20. The stochastic point load will be applied at $(0.9, 0.025)$, and the results will be discussed in subsection 3.5.4.

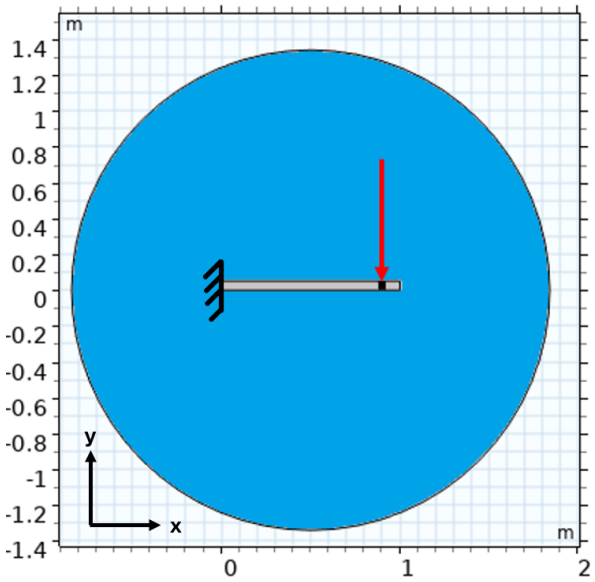

Figure 3.20: Schematic of the cantilever beam surrounded by a fluid domain.

3.5.3. Mesh sensitivity

In this section, the mesh sensitivity study is discussed. Such a study is performed to research the effect of the mesh on the outcome of the study.

When the coupled system discretized with a mesh, the mesh element size should be defined such that the elements are much smaller than the wavelengths of the waves traveling through the system. The wavelength is defined in Equation 3.28. If the mesh elements are too large, the study would be unable to compute all desired frequencies correctly. Therefore, a rule of thumb of 12 elements per wavelength in the propagation direction is applied. This can give a first estimate of how fine the mesh needs to be [12].

Since the domain covers two spatial dimensions, the mesh size grows with the power two of the number of elements per unit length. Reducing the mesh element size becomes computationally expensive to solve. The amount of mesh elements can be reduced by using second order Lagrange or serendipity elements. The maximum mesh element size can be set to one fifth of the wavelength, while still being able to capture the behavior of the waves. Furthermore, an unstructured mesh will be used, as it is not clear beforehand how the waves travel. If a structured mesh was used, the angle between the wave and the element surface could becomes large, decreasing the accuracy of the solution.

A mesh sensitivity study is performed, where the effect of the mesh resolution on the eigenfrequencies is plotted against the number of mesh elements. The results can be found in Figure 3.21. The relative change of the eigenfrequencies of the first eight modes with respect to the finest mesh is provided. The assumption is made that if the mesh resolution is increased, the eigenfrequencies converge to their true frequency. This can also be seen in the figure, where an increase of the mesh resolution decreases the change of the eigenfrequencies with respect to the eigenfrequencies on a coarser mesh. As a baseline, a fine mesh was taken with 4723 elements, and the changes are relative to the outcome of the study on that mesh. Since the mesh is constructed to capture the eigenfrequencies up to a $1000\,\mathrm{Hz}$, the relative change of the eigenfrequencies is small when the mesh element size is reduced. Therefore, the coarsest mesh is used to reduce computational effort. The mesh can be seen in Figure 3.22.

3.5.4. COMSOL Multiphysics reference study

Now that a proper mesh is constructed, the eigenfrequencies and eigenmodes can be found accurately. On the modes, a stochastic load can be projected.

The eigenmodes found of the cantilever beam surrounded by water domain can be found in Figure 3.23. Similarities can be found to the eigenmodes of a cantilever plate in vacuum of Figure 3.4, although the

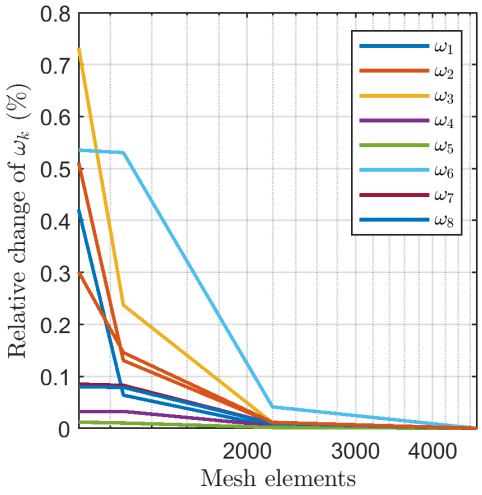

Figure 3.21: Relative change of eigenfrequencies found on meshes with an increasing amount of mesh elements. The assumption is made that the most fine mesh resembles the true eigenfrequencies most accurately.

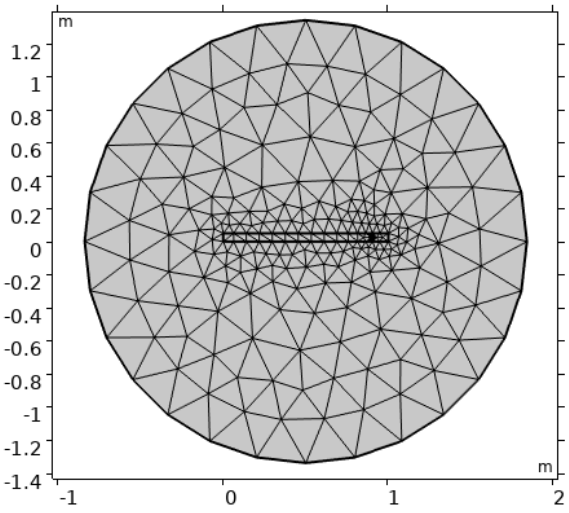

Figure 3.22: Mesh of a 2D cantilever plate surrounded by an infinite fluid domain.

torsional behavior is not captured.

A reference study is made in COMSOL Multiphysics of a cantilever plate surrounded by water, excited by a stochastic point load. The power spectral density of the response can be found in Figure 3.24. It becomes clear that the fluid has a large effect compared to the power spectral density of the same plate in vacuum, shown in Figure 3.8. The peaks are much lower, and the integrated power over all frequencies is much less, which is a direct effect of the damping effect of the water. To reduce computational costs, the simulation is run up to $1000\,\mathrm{Hz}$.

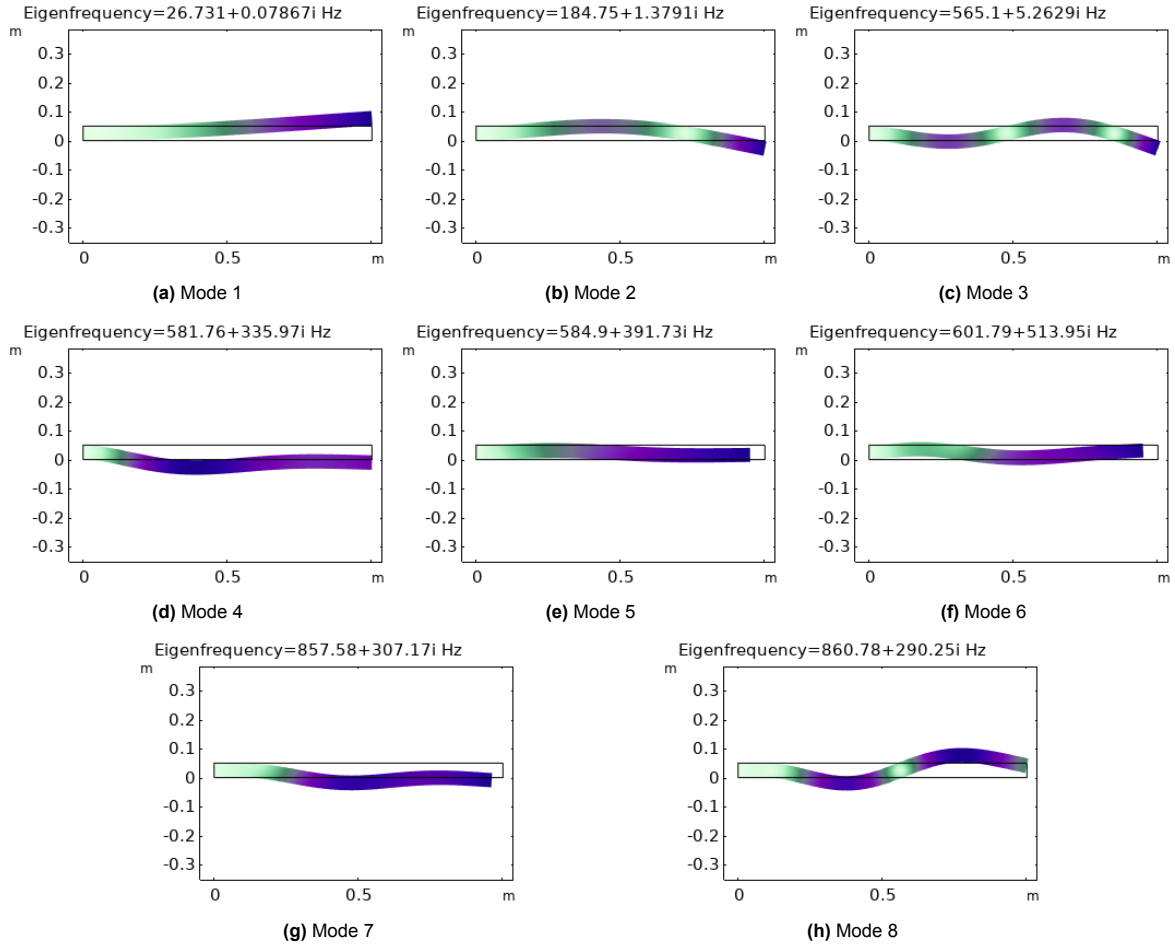

(a) Mode 1 **(b)** Mode 2 **(c)** Mode 3

(d) Mode 4 **(e)** Mode 5 **(f)** Mode 6

(g) Mode 7 **(h)** Mode 8

Figure 3.23: Eigenmodes of a 2D cantilever beam up to $1000\,\mathrm{Hz}$.

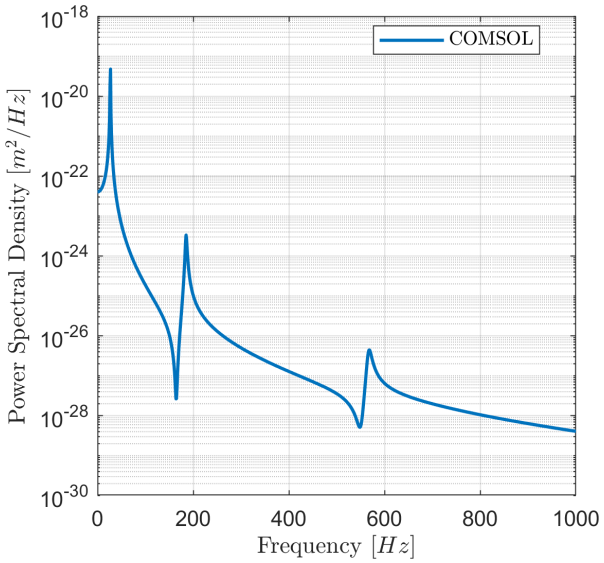

Figure 3.24: Power spectral density of the response of a cantilever plate surrounded by an infinite fluid domain excited by a stochastic point load.

Now that a reference is made, two methods can be implemented to obtain the response of a stochastically excited structure in an infinite fluid domain, where the user has full control over the loading matrix.

The first method is discussed in section 3.6, the second method is discussed in section 3.7.

3.6. Method 1: System matrix eigenmodes

The first method implements two models. First, the model proposed by De Berg [3] is implemented. From the COMSOL Multiphysics model of section 3.5, the stiffness, damping and mass matrix are extracted. These are used to build the system matrix A of Equation 2.29. From the system matrix, the eigenmodes up to a $1000\,\mathrm{Hz}$ are computed. Next, the system matrix is transposed and the first eigenmodes up to a $1000\,\mathrm{Hz}$ are computed. These will be used as input for Equation 2.34. This method is referred to as the A-matrix method.

$$A = \begin{bmatrix} 0 & I \\ -M^{-1}K & -M^{-1}C \end{bmatrix} \tag{2.29}$$

$$S_q(\omega) = X\bar{G}(\omega)Y^H BS_f(\omega)B^H YG(\omega)X^H \tag{2.34}$$

The second method that is implemented is the KM-method. Here, the eigenmodes are computed using only the stiffness and mass matrix. The eigenmodes are computed using Equation 2.18. The eigenmodes are used in Equation 2.22 to compute the response. Although this method does not take into account the damping matrix, it can still be used as a reference to see the influence of the damping matrix.

$$KX = \Omega MX \tag{2.18}$$

$$S_q(\omega) = X\bar{G}(\omega)X^T S_f(\omega)XG(\omega)X^T \tag{2.22}$$

Both these methods require the mass matrix from COMSOL Multiphysics. When using a spherical wave radiation boundary condition on the fluid domain, the mass matrix can no longer be obtained in a straightforward way due to a bug in COMSOL Multiphysics. A method to still obtain the mass matrix is described in section A.2.

3.7. Method 2: State-space eigenmodes reconstruction

The response of a non-proportionally damped system can be evaluated with Equation 2.34, which is repeated above. The equation requires the left eigenmodes Y and right eigenmodes X. Since COMSOL Multiphysics version 6.2, the user is able to obtain both the left and right displacement eigenmodes from COMSOL Multiphysics. Before version 6.2, users were only able to obtain the right displacement eigenmodes. However, the eigenmodes for Equation 2.34 are in state-space. This means that the top part of eigenmodes should describe the displacement, and the bottom half should describe the velocity. Since only the displacement part of the eigenmodes is given by COMSOL Multiphysics, the state-space eigenmodes have to be reconstructed. This method is called the 'state-space reconstruction' method, or SSR for short.

When the eigenmode displacement is multiplied with the eigenfrequency, the eigenmode velocity is obtained. To demonstrate this relation between the eigenmode displacement and the eigenmode velocity, the three degree-of-freedom system of section 3.2 is used. The first state-space eigenmode of the three degree-of-freedom model is shown in Equation 3.31.

$$\vec{x}_1 = \begin{bmatrix} q_1 \\ \dot{q}_1 \end{bmatrix} = \begin{bmatrix} 0.00338 + 0.287i \\ -0.00421 - 0.357i \\ 0.00187 + 0.159i \\ -0.516 \\ 0.644 \\ -0.287 \end{bmatrix} \tag{3.31}$$

Where the top part represents displacement and the bottom half represents velocity. Multiplying the displacement with the eigenfrequency results in:

$$\omega_1 q_1 = -0.0212 + 1.801i \begin{bmatrix} 0.00338 + 0.287i \\ -0.00421 - 0.357i \\ 0.00187 + 0.159i \end{bmatrix} = \begin{bmatrix} -0.516 \\ 0.644 \\ -0.287 \end{bmatrix} = \dot{q} \tag{3.32}$$

The same relation can be used to obtain the eigenmode velocity from the COMSOL Multiphysics eigenmode displacement. Care has to be taken with the scaling of the eigenmodes. Using Equation 2.33, the following relation can be obtained:

$$Y^T X = I \tag{3.33}$$

When the left eigenmodes are obtained from COMSOL Multiphysics, the left eigenmodes should be scaled such that this relation holds.

3.8. Discussion

In this chapter, the methodology was discussed that is needed to model the response of a cantilever plate surrounded by an infinite fluid domain excited by a stochastic load. First, the steps of incremental complexity were discussed, followed by a general approach of the problem. Next, a simple one-dimensional test case was constructed, to understand the effect of non-proportional damping on a system.

Next, a cantilever plate in vacuum was discussed, where four methods were shown to obtain the eigenmodes. It was checked that these eigenmodes were normalized correctly using the mass matrix. After the eigenmodes were computed, a stochastic point load was applied. The loading was discussed, since depending on whether the COMSOL Multiphysics eigenmodes are used or the KM-method, the loading should be applied in a slightly different way, which is caused by the ordering of the degrees-of-freedom. It was shown that the COMSOL Multiphysics results matched the Matlab-COMSOL method and the KM-method. A simple static $0\,\mathrm{Hz}$ check was performed to verify the results.

Now that a stochastic point load could be applied correctly, the next step of incremental complexity could be taken. First, two point loads were used, since this served as a step between a single stochastic point load and a stocastic distributed load. The methods were verified for a load without correlation, a cross-correlation of 1 and of -1, meaning the loads are in phase and opposite phases respectively. Next, a distributed stochastic loading was used. COMSOL Multiphysics is not able to apply such a load. The KM-method agreed with the Matlab-COMSOL eigenmodes method. Also, the A-matrix method was implemented and verified with the previous two methods. The A-matrix method is needed to obtain the response of a non-proportionally damped system.

After the methods are verified for a solid in a vacuum, the solid can be placed in an infinite fluid domain. This is where the work of De Berg [3] ended. He found large discrepancies between his implantation of the A-matrix method and the COMSOL Mutliphysics response PSD. According to the author, the cause was likely scaling in the fluid part of the mass matrix. Multiple scaling factors were applied, although none were able to agree with the COMSOL Multiphysics response PSD. Furthermore, it was found that De Berg [3] used all right eigenmodes to construct the left eigenmodes. This is only feasible for a very small system, which he conveniently used. However, not all right eigenmodes were used to obtain the left eigenmodes. Also, the COMSOL Multiphysics model used by De Berg [3] raised questions about validity. Therefore, a new COMSOL Multiphysics model was constructed, to account for the infinite fluid domain.

First, the boundary conditions were discussed, where it was found that a spherical wave radiation boundary condition was most suitable for an eigenfrequency study. The fluid domain size was determined to be $1.34\,\mathrm{m}$. A mesh sensitivity study was performed, where it was found that a coarse mesh would still be able to perform a eigenfrequency analysis correctly, greatly reducing the computational costs. After the simulation was setup properly, a reference study was made in COMSOL Multiphysics that can be used as a baseline.

The first method to obtain a correct response PSD was to implement the A-matrix method, using the newly constructed COMSOL Multiphysics model that properly takes into account an infinite fluid domain. The stiffness, mass and damping matrix will be imported in Matlab, were the system matrix A will be constructed. The eigenfrequencies and the right eigenmodes will be obtained from the system matrix. By taking the transpose of the system matrix, the left eigenmodes are found. These eigenmodes will be used to compute the response PSD. Also, the KM-method will be used as reference to see the effect of the damping matrix.

The second method to obtain the correct response PSD is to reconstruct the state-space eigenmodes. Since COMSOL Multiphysics only provides the displacement part of the eigenmodes. By multiplying the displacement part of the eigenmodes with the eigenfrequency, the velocity part has to be obtained. This was demonstrated with a simple 3 degree-of-freedom system.

Now that two methods are defined, a stochastic point load can be applied. The results can be found in chapter 4.

4

Results

This chapter discusses the results of a 2D beam surrounded by water, introduced in section 3.5, excited by a stochastic point load.

First, the system matrix eigenmodes method, introduced in section 3.6, is implemented. The results will be presented in section 4.1. Next, the state-space eigenmode reconstruction (SSR) method, introduced in section 3.7, is implemented. The results of the method will be presented in section 4.2. A discussion will take place in section 4.3.

4.1. Method 1: System matrix eigenmodes results

This section discusses the results of the A-matrix method and the KM-method to model the response of a stochastically excited beam. The beam will be excited by a stochastic point load in subsection 4.1.1.

4.1.1. Stochastic point load

In this subsection, the response of a beam surrounded by a fluid, excited by a stochastic point load, is discussed. A point load of $1\,\mathrm{N}^2/\mathrm{Hz}$ is applied at $[0.9, 0.025]\,\mathrm{m}$ in the negative y-direction. The response is measured at the same coordinate. A schematic of the beam in the fluid can be found in Figure 3.20. The response PSD can be found in Figure 4.1.

The response of the COMSOL Multiphysics model and the KM-method show similarities in multiple ways. Up to $330\,\mathrm{Hz}$, the response PSD of both method agrees, although the peaks of the COMSOL Multiphysics response appear smaller than those of the KM-method. The difference is caused by the frequency step size over which the response is evaluated. After $330\,\mathrm{Hz}$, the KM-method shows a valley and a peak, which are not captured by the COMSOL Multiphysics PSD. This can be explained by looking at Table 4.1. In the second column, the eigenfrequencies found by COMSOL Multiphysics are shown. In total, eight eigenfrequencies in the range of $1\,\mathrm{Hz}$ to $1000\,\mathrm{Hz}$ are found. The eigenfrequencies found by the KM-method are shown in the third column. In total, 15 eigenfrequencies are found in the same range. Both Matlab and COMSOL Multiphysics use the ARPACK algorithm developed by Lehoucq et al. [24] to compute the eigenfrequencies and eigenmodes. Why COMSOL Multiphysics and Matlab find a different amount of eigenfrequencies while using the same algorithm could be caused by a different implementation, but this cannot be confirmed.

Between $334\,\mathrm{Hz}$ to $378\,\mathrm{Hz}$, the KM-method finds three eigenfrequencies, explaining the valley and peak of the PSD shown in Figure 4.1. Between $560\,\mathrm{Hz}$ to $600\,\mathrm{Hz}$, COMSOL Multiphysics produces a valley followed by a peak, while the KM-method finds a larger valley and a peak, which is followed by a smaller peak. Around $777\,\mathrm{Hz}$, a small peak is captured by the KM-method which is not captured by the COMSOL Multiphysics response. Again, looking at the eigenfrequencies found by both methods, the KM-method finds two eigenfrequencies around $777\,\mathrm{Hz}$, while COMSOL Multiphysics does not.

The A-matrix method response does not show agreement with the COMSOL Multiphysics response. Also, the method does not produce peaks around eigenfrequencies, although a downward trend can

be seen across the frequency. The eigenfrequencies and eigenmodes found by the KM-method and the A-matrix method are discussed in subsection 4.1.2 and subsection 4.1.3, respectively.

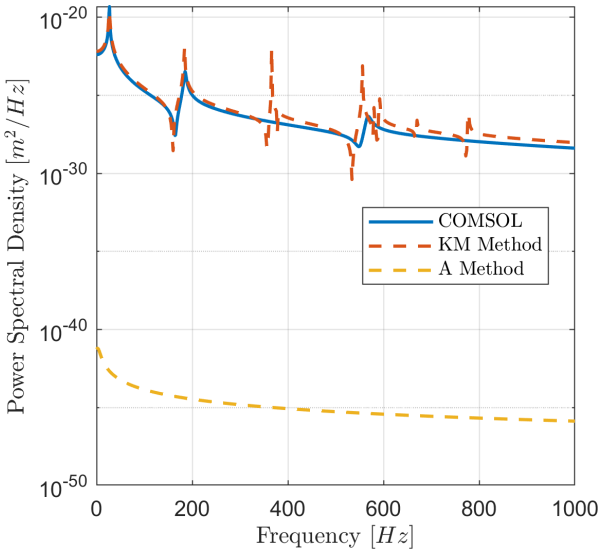

Figure 4.1: Power spectral density of the response of a 2D beam, excited by a stochastic point load using COMSOL Multiphysics Multiphysics, the KM-method and the A-matrix method.

4.1.2. KM-method eigenmodes analysis

This subsection discusses the eigenmodes found by the KM-method. All eigenmodes produced by the KM-method can be found in section D.1. The eigenmodes have been scaled to increase deformation to allow for easier visual analysis.

To compare the COMSOL Multiphysics eigenmodes of Figure 3.23 with the KM eigenmodes, a selection of six eigenmodes is made in Figure 4.2. The selection is based on the eigenfrequencies that are found by both the COMSOL Multiphysics method and the KM-method. COMSOL Multiphysics modes 1 and 2 are compared with the KM-method modes 1 and 2, since the eigenfrequency at which the modes were found agrees. The eigenmode shapes of both methods agree, which is expected since both methods found the modes at the same eigenfrequency. COMSOL Multiphysics mode 3 is represented by the KM-method mode 6. The shape agrees mostly, although the first halve-wave flexure is not well captured by the KM-method. COMSOL Multiphysics mode 4 and 5 are represented by KM-method eigenmodes 7 and 8, but the imaginary part of the eigenfrequency is not found by the KM-method. Still, the modes show similarities, although the COMSOL Multiphysics eigenmodes do not show a strong upward bend that is captured by the KM-method. COMSOL Multiphysics mode 6 is not found by the KM-method. In terms of eigenfrequency, KM-method mode 12 is closest to COMSOL Multiphysics eigenmodes 7 and 8. The shape of KM-method mode 12 shows similarities to COMSOL Multiphysics mode 8.

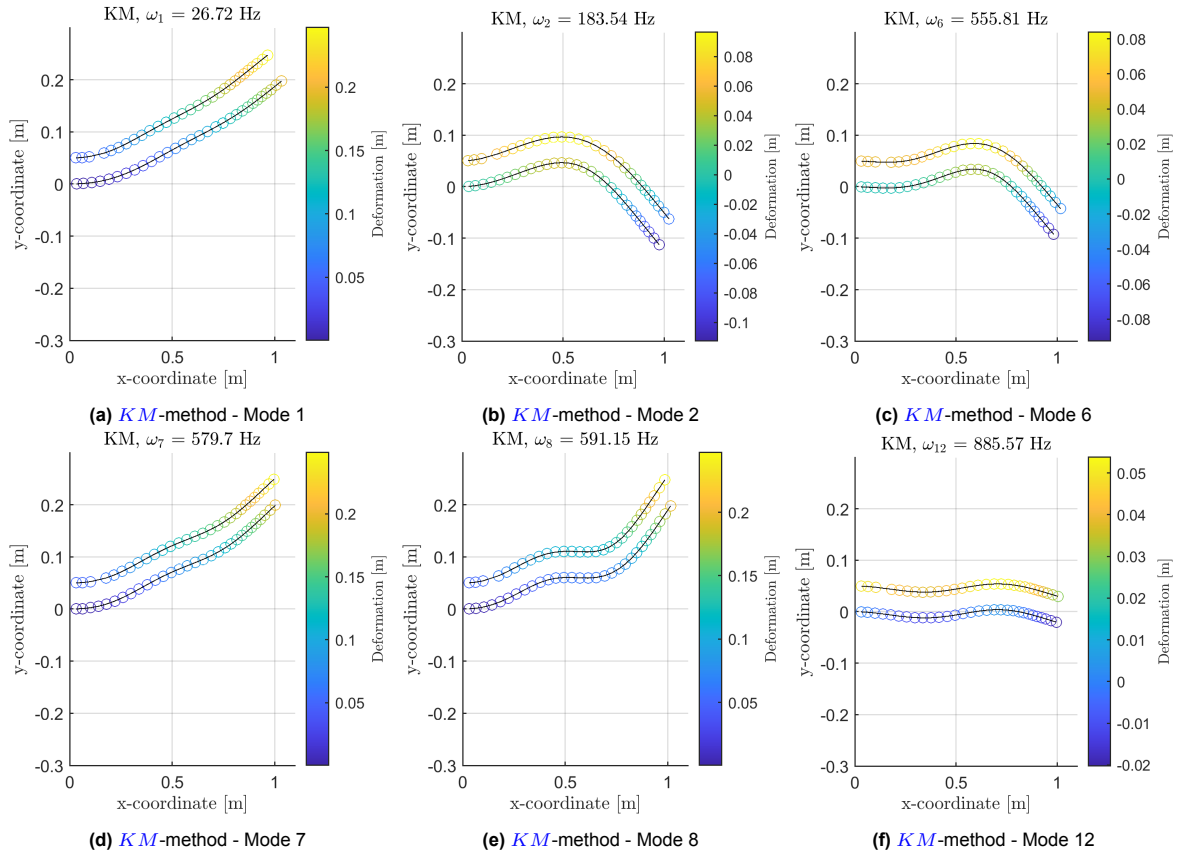

(a) KM-method - Mode 1 **(b)** KM-method - Mode 2 **(c)** KM-method - Mode 6

(d) KM-method - Mode 7 **(e)** KM-method - Mode 8 **(f)** KM-method - Mode 12

Figure 4.2: Selection of the eigenmodes found by the KM-method.

Now that the KM-method response PSD, eigenfrequencies and eigenmodes are discussed, the results of the A-matrix method can be presented in the next section.

4.1.3. A-matrix method eigenfrequencies and eigenmodes analysis

Solving for the eigenfrequencies and eigenmodes using the A-matrix method resulted in problems, since the eigenfrequency computation became prone to errors. The system matrix was close to singular and the order difference between elements was large. To illustrate this, a logarithmic plot is constructed of the absolute values in the system matrix, and can be found in Figure 4.3. To show how the system matrix is constructed, Equation 2.29 is repeated.

The order difference in the system matrix is large. The smallest can be regarded as floating point errors. The largest elements are larger than 10^{40} and are produced in the lower left quadrant, which is calculated as $-M^{-1}K$. The lower right quadrant, computed as $-M^{-1}C$, produces small values. In this particular system of a cantilever beam surrounded by a fluid, the damping is orders of magnitude lower than the stiffness.

$$A = \begin{bmatrix} 0 & I \\ -M^{-1}K & -M^{-1}C \end{bmatrix} \tag{2.29}$$

The eigenfrequencies produced by the A-matrix method can be found in Table 4.1. In the fourth column, the eigenfrequencies of A^T are shown. The eigenfrequencies of A are shown in the fifth column. The eigenfrequencies found in the system matrix and its transpose should be the same, as was shown in Equation 2.30 and Equation 2.31. However, this is not the case, indicating that something is going wrong with the input matrices of the system matrix.

The input matrices could be altered at different stages to prevent them from being used in this self-made A-matrix method. It is believed that the stiffness, damping and mass matrix extracted from COMSOL

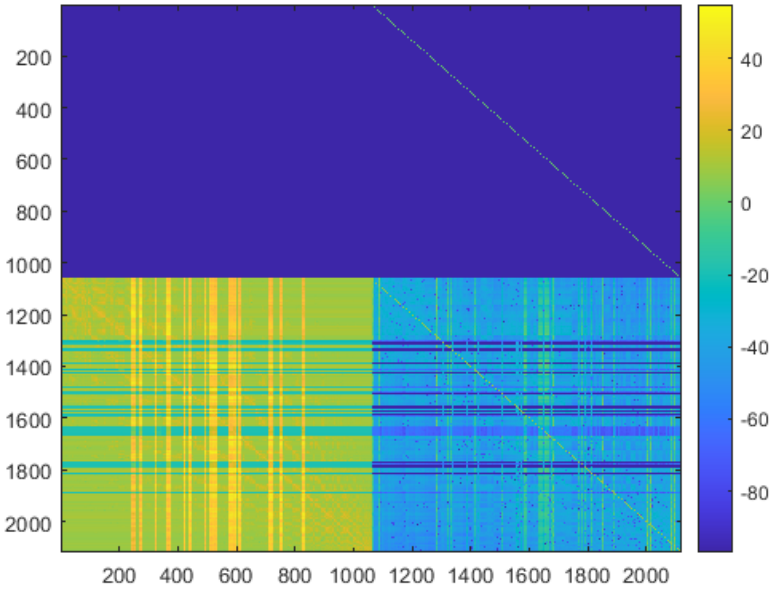

Figure 4.3: Log plot of the system matrix A.

Multiphysics are not used in the same that COMSOL Multiphysics uses internally to compute the eigenfrequencies and the eigenmodes. COMSOL Multiphysics matrices are likely to be scaled internally to increase numerical stability. When COMSOL Multiphysics is asked to produce the damping, stiffness, and mass matrix, this scaling is removed. In COMSOL Multiphysics, the user can request to turn off scaling. The exact scaling this is, is not well understood. However, when the unscaled input matrices are extracted from COMSOL Multiphysics and put into the A-matrix method, the eigenfrequencies of the system matrix and the transpose of the system matrix are still not the same. The method to extract non-scaled matrices is described in section A.3.

The mode shape is discussed next. The eigenfrequency of COMSOL Multiphysics modes 2, 6 7 and 8 are close to the right eigenfrequencies of modes 3, 8, 12 and 13 of the A-matrix method, respectively. These modes shapes can be found in Figure 4.4. The complete set of right eigenmodes can be found in section D.2. COMSOL Multiphysics eigenmode 2 and A-matrix method eigenmode 3 show no resemblances. However, COMSOL Multiphysics eigenmode 6 and A-matrix method eigenmode 8 show some agreement. Both capture roughly the same shape, although the bends in the COMSOL Multiphysics eigenmode are more spread over the beam, while the bends of the A-matrix method eigenmodes are closer to the fixed edge. COMSOL Multiphysics eigenmodes 12 and 13 show no resemblances to the A-matrix method eigenmodes 12 and 13.

The complete set of left eigenmodes can be found in section D.3. The first three left eigenmodes can be found in Figure 4.5. Due to the flawed input matrices, A^T produces eigenmodes that lose meaning to the original beam structure. The first and second left eigenmodes can no longer be represented on the original domain size.

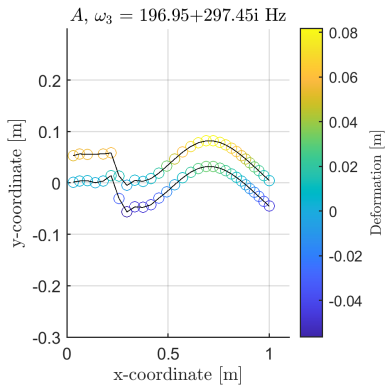

(a) A-matrix method - right mode 3

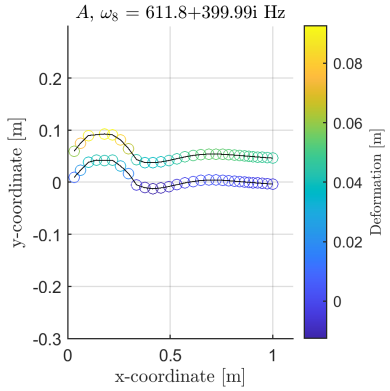

(b) A-matrix method - right mode 8

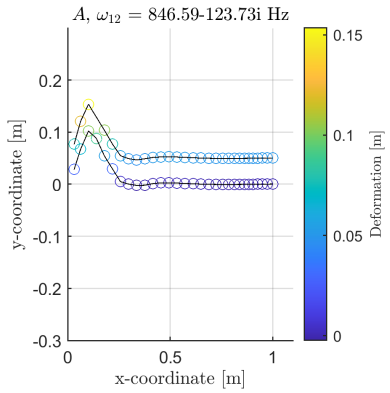

(c) A-matrix method - right mode 12

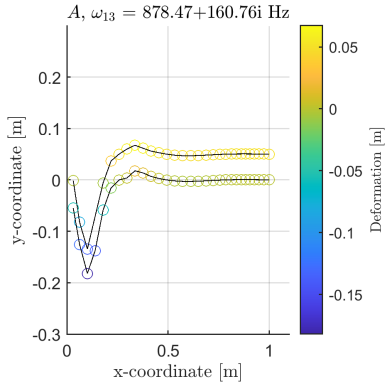

(d) A-matrix method - right mode 13

Figure 4.4: Selection of right eigenmodes of the system matrix A belonging to eigenfrequencies found by both the A-matrix method and COMSOL Multiphysics.

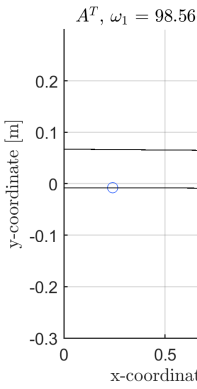

(a) A-matrix method - left mode 1

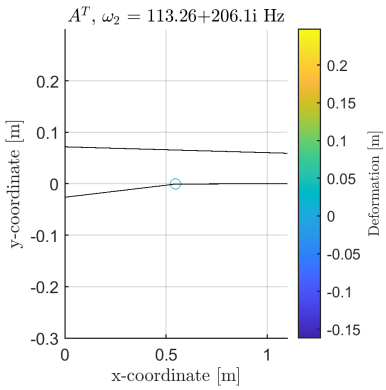

(b) A-matrix method - left mode 2

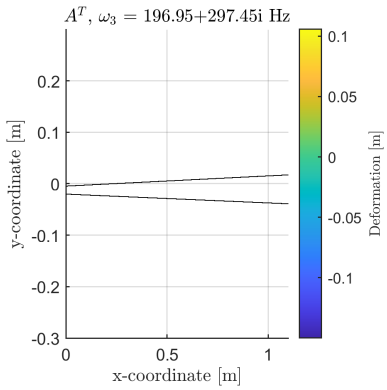

(c) A-matrix method - left mode 3

Figure 4.5: Selection of left eigenmodes of the system matrix A^T. No physical interpretation can be given to the modes.

	COMSOL Multiphysics (Hz)	KM matrix (Hz)	A^T (Hz)	A (Hz)
Mode 1	$26.73 + 0.078\text{i}$	26.72	$-114.2 - 394.24\text{i}$	$98.56 + 2.53\text{i}$
Mode 2	$184.75 + 1.38\text{i}$	183.53	$-73.17 - 263.34\text{i}$	$113.26 + 206.1\text{i}$
Mode 3	$565.10 + 5.23\text{i}$	334.32i	$-70.55 - 262.79\text{i}$	$196.95 + 297.45\text{i}$
Mode 4	$581.76 + 335.97\text{i}$	365.94	$-54.85 - 390.1\text{i}$	$251.43 - 351.92\text{i}$
Mode 5	$584.90 + 391.73\text{i}$	378.19	$-44.4 - 332.52\text{i}$	$263.25 + 369.81\text{i}$
Mode 6	$601.79 + 513.95\text{i}$	555.80	$-38.52 - 200.16\text{i}$	$320.03 + 407.47\text{i}$
Mode 7	$857.58 + 307.17\text{i}$	579.69	$-36.85 - 152.5\text{i}$	$323.17 + 414.56\text{i}$
Mode 8	$860.78 + 290.25\text{i}$	591.14	$-34.53 - 153.24\text{i}$	$611.8 + 399.99\text{i}$
Mode 9	-	668.78	$-13.39 - 67.42\text{i}$	$707.56 + 263.07\text{i}$
Mode 10	-	776.95	$-11.75 - 63.57\text{i}$	$762.21 + 168.15\text{i}$
Mode 11	-	778.25	$-2.59 - 148.97\text{i}$	$824.64 - 288.05\text{i}$
Mode 12	-	885.57	$-0.05 - 16.71\text{i}$	$846.59 - 123.73\text{i}$
Mode 13	-	957.97	-0.36i	$878.47 + 160.76\text{i}$
Mode 14	-	971.10	$5.69 + 56.46\text{i}$	$878.95 + 183.22\text{i}$
Mode 15	-	971.41	$839.53 - 586.52\text{i}$	$880.44 - 195.61\text{i}$

Table 4.1: Comparison of COMSOL Multiphysics eigenfrequencies, KM-method eigenfrequencies and the right and left eigenfrequencies obtained using the A-matrix method.

4.2. Method 2: State-space eigenmodes reconstruction results

In this section, the SSR-method results are discussed. The foundation of the method is discussed in section 3.7. First, the PSD response is discussed in subsection 4.2.1. Next, the eigenmodes are subsection 4.2.2.

4.2.1. Stochastic point load

The results of a cantilever beam of $1\,\text{m} \times 0.05\,\text{m}$, surrounded by an infinite fluid domain, excited by a stochastic point load of $1\,\text{N}^2/\text{Hz}$ at $[0.9, 0.025]$ m are presented in this subsection. The response is measured at the same location as where the force is applied. The PSD can be found in Figure 4.6. The COMSOL Multiphysics response PSD and the SSR-method response PSD show little resemblance. The order of the magnitude of the SSR response is much larger than that of the COMSOL Multiphysics response. Furthermore, the COMSOL Multiphysics response PSD and the SSR response PSD both show a downward trend when frequency increases.

The response function of a non-proportionally damped system, defined in Equation 2.35, was replaced by the proportionally damped system response function, which is repeated below in Equation 2.23. For now, ζ was set to zero. The resulting response PSD can be found in Figure 4.7. The resulting response PSD shows more similarities to the COMSOL Multiphysics response PSD compared to Figure 4.7. The first peak around $40\,\text{Hz}$ is captured well. Next, SSR response PSD shows a peak, followed by a valley. This is opposite of the COMSOL Multiphysics PSD, although the peak is captured at the same frequency. The final valley and peak are captured by the SSR response function too. The overall shape of the SSR response PSD is similar to the COMSOL Multiphysics response PSD, showing the same downward trend. However, the SSR response PSD seems to be shifted upwards by a constant.

$$G_k(\omega) = \frac{1}{-\omega^2 + 2i\zeta_k\omega\omega_k + \omega_k^2} \tag{2.23}$$

4.2.2. Eigenmode analysis

In this subsection, eigenmodes of the SSR-method are discussed. The right eigenmodes are given in Figure 4.8. These are identical to the eigenmodes provided by COMSOL Multiphysics directly in Figure 3.23, verifying that COMSOL Multiphysics only displays the right eigenmodes while it also computes and stores the left eigenmodes. The left eigenmodes are shown in Figure 4.9. Physical interpretation cannot be given to the left eigenmodes, which are used to map the excitation force to the modal domain.

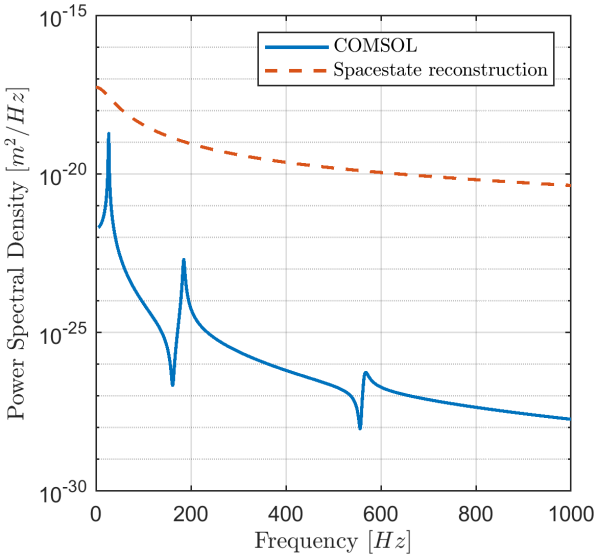

Figure 4.6: Response PSD of a beam surrounded by an infinite fluid domain, excited by a stochastic point load of $1\,\mathrm{N}^2/\mathrm{Hz}$. The COMSOL Multiphysics PSD is given in blue, the State-space reconstruction method PSD is given in red.

4.3. Discussion

The results of the A-matrix method, and the KM-method were shown in section 4.1 and the SSR results were down in section 4.2.

The KM-method showed reasonable agreement to the COMSOL Multiphysics response PSD. This could mean that the simplification that is used by only using the stiffness matrix K and mass M is acceptable in this scenario. It is thought that COMSOL Multiphysics writes the proportional part of the damping due to the radiation boundary condition into the mass matrix M. This would explain the negative and imaginary elements in the mass matrix, as shown in Figure 3.17. In addition, the mass matrix would no longer be suitable to be used in the system matrix A. How COMSOL Multiphysics writes the damping into the mass matrix exactly is not understood.

The SSR-method showed no agreement with the COMSOL Multiphysics response PSD. However, when a proportionally damped response function was used, the response PSD showed more agreement with the COMSOL Multiphysics response PSD. This could be another hint that the proportionally damped approximation used by the KM-method is reasonable.

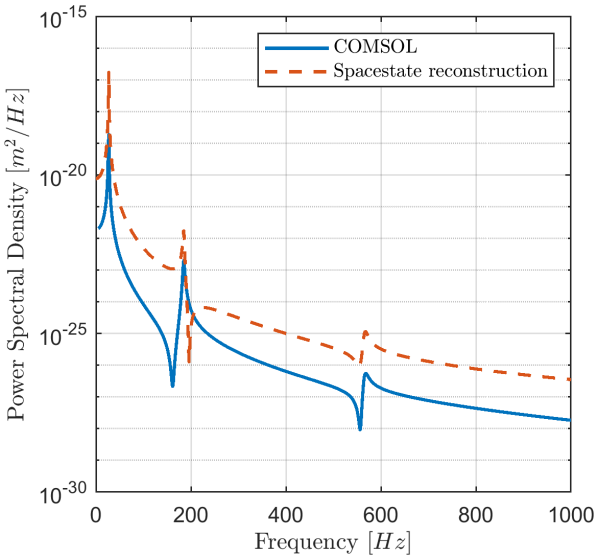

Figure 4.7: Response PSD of a beam surrounded by an infinite fluid domain, excited by a stochastic point load of $1\,\mathrm{N}^2/\mathrm{Hz}$. The COMSOL Multiphysics PSD is given in blue, the State-space reconstruction method PSD is given in red. The proportionally damped response function is used.

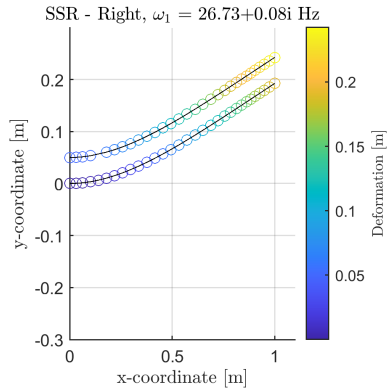

(a) SSR - Right Eigenmode 1

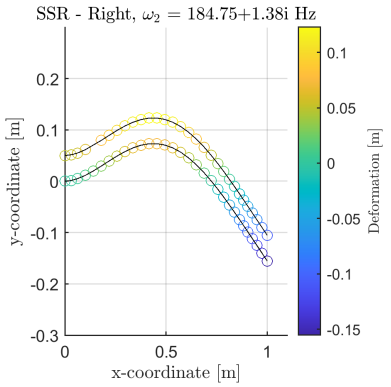

(b) SSR - Right Eigenmode 2

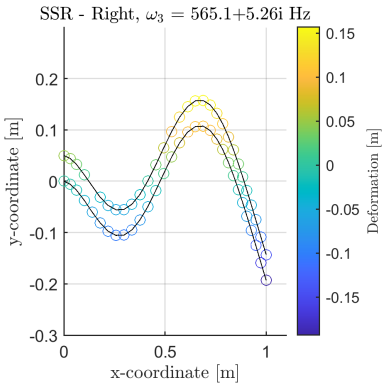

(c) SSR - Right Eigenmode 3

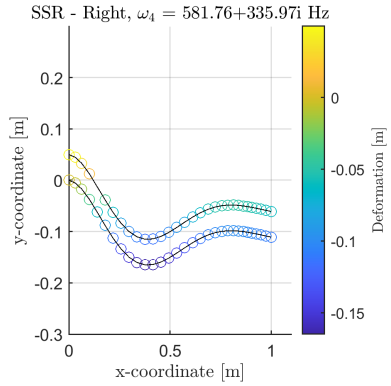

(d) SSR - Right Eigenmode 4

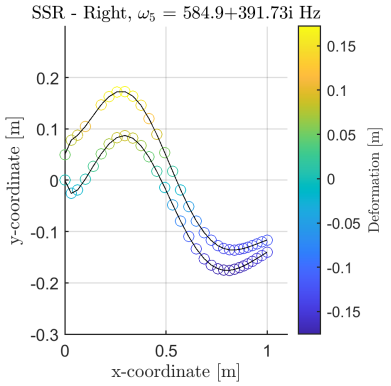

(e) SSR - Right Eigenmode 5

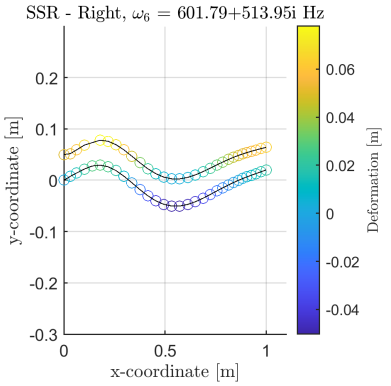

(f) SSR - Right Eigenmode 6

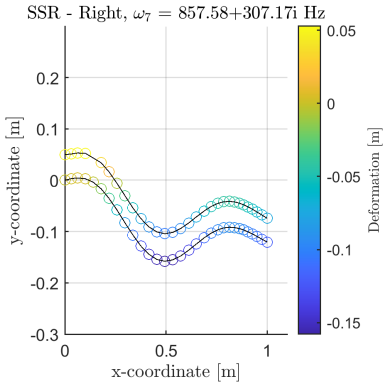

(g) SSR - Right Eigenmode 7

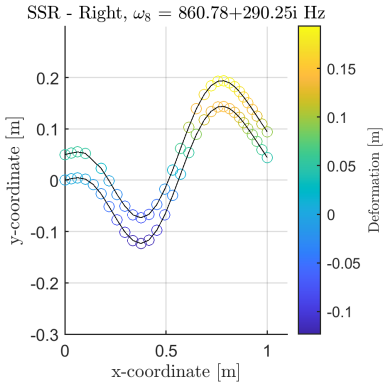

(h) SSR - Right Eigenmode 8

Figure 4.8: Right COMSOL Multiphysics eigenmodes used in the State-space reconstruction method.

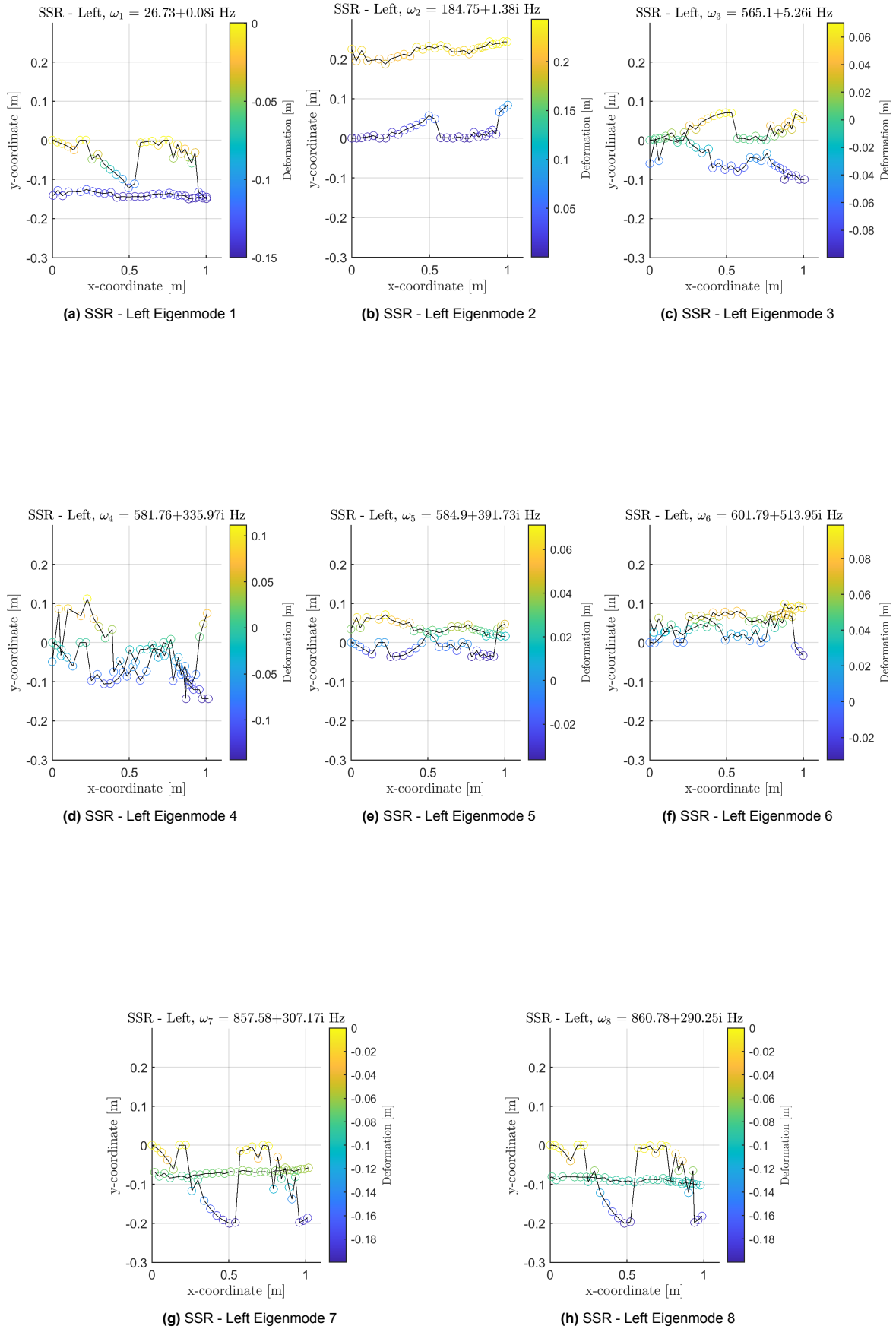

(a) SSR - Left Eigenmode 1

(b) SSR - Left Eigenmode 2

(c) SSR - Left Eigenmode 3

(d) SSR - Left Eigenmode 4

(e) SSR - Left Eigenmode 5

(f) SSR - Left Eigenmode 6

(g) SSR - Left Eigenmode 7

(h) SSR - Left Eigenmode 8

Figure 4.9: Left COMSOL Multiphysics eigenmodes used in the State-space reconstruction method.

5

Conclusion and recommendations

5.1. Conclusion

The goal of this study was to develop a method to model the vibroaucoustic response of a marine propeller, excited by a turbulent flow. In the frequency range of interest, a modal analysis is most suitable, since a relatively small amount of eigenmodes describe the system completely.

The software package COMSOL Multiphysics currently does not offer the possibility to apply a distributed stochastic excitation. This is the type of excitation needed to represent loading due to a turbulent flow. Turbulent excitation can be described through a cross-spectral density matrix. In order to apply such loads, alternative methods based on COMSOL Multiphysics outputs were implemented:

1. A-matrix method: Construct state-space system matrix A based on the stiffness (K), mass (M) and damping (C) matrices from COMSOL Multiphysics.
2. KM-method: Generalized eigenvalue problem using the stiffness (K) and the mass (M) matrices obtained from COMSOL Multiphysics. This is simplification of the A-matrix method.
3. State-space reconstruction method: From COMSOL Multiphysics, the left and right eigenmodes are obtained, but these only contain the displacement part of the eigenmodes. To use the COMSOL Multiphysics eigenmodes in Equation 2.34, the eigenmodes have to be in state-space. By multiplying the displacement part of the eigenmodes with the eigenfrequency, the velocity of the eigenmodes is obtained. Stacking the displacement part of the eigenmodes on top of the velocity part of the eigenmodes results in state-space eigenmodes.

These methods should give, in theory, identical results to all cases to which they apply, although the second method cannot be applied to systems where damping matrix C cannot be written in terms of matrix M and K.

These methods were used in problems of varying complexity to verify their implementation. In Table 5.1, model features (i.e. a type of geometry, loading or environment) for which correct results could be obtained using all methods are indicated in green. Model features indicated with red were not performed. Orange means that only the approximate method (KM-method) was successful. The most complex study case for which results were successfully verified was a cantilever plate in vacuum, excited by a distributed stochastic load.

Increasing complexity →			
Geometry	Cantilever beam	Cantilever plate	Cantilever complex
Loading	Deterministic point	Stochastic point	Distributed stochastic
Environment	Vacuum	Water	

Table 5.1: Model features of incremental complexity. Green indicates that the model feature was successful, Red indicates that the model feature was not implemented. Orange indicates that only the approximate method (KM-method) was successful.

A two-dimensional beam excited by a stochastic point load, surrounded by water, was used as a test case to compare the A-matrix method and the State-space reconstruction method to COMSOL Multiphysics. The methods did not agree with COMSOL Multiphysics. Potential reasons were identified:

1. Unclear which scaling is applied in K, M and C. It is unclear why negative and complex values are observed in M. They suggest that damping may be included partially in these matrices. Using scaling inconsistently leads to incorrect results. The matrices could be used incorrectly. COMSOL Multiphysics may apply certain scaling to obtain a symmetric/hermitian matrix or for numeric stability.
2. Unclear structure of matrices. The mass matrix M contains complex and negative components. Therefore, the mass matrix M (and perhaps the stiffness matrix K and damping matrix C) are not suited to be implemented in the system matrix A.

The KM-method provided a reasonable approximation of the expected results on the two-dimensional cantilever beam, excited by a stochastic load, and surround by water. Likely, COMSOL Multiphysics incorporates part of the damping due to the radiation boundary condition in the stiffness and mass matrix. If part of the terms associated with damping due to the radiation boundary conditions are indeed incorporated into the K and M matrices this could also explain the occurrence of negative and complex values observed in these matrices.

Therefore, in this scenario, the KM-method is a reasonable approximation. In section 5.2, recommendations are presented for future work.

5.2. Recommendations

In the end a method to produce the same PSD response as COMSOL Multiphysics based on eigenmodes for a structure submerged in fluid was not successfully implemented. In this section, recommendations that can be used in future work to complete this task are discussed.

A better understanding of the COMSOL Multiphysics mass, stiffness and damping matrices is needed in case a fluid domain is present. It was demonstrated that for a cantilever plate in vacuum, the eigenfrequencies and eigenmodes could be obtained by either: (1) using COMSOL Multiphysics, (2) using the KM-method, or (3) rewriting the input matrices into system matrix A. However, when a fluid domain was included, the system matrix A did not lead to the expected eigenmodes and that sets of left and right eigenfrequencies did not match. Agreement between the eigenfrequencies obtained from A and A^T is a fundamental property that should be observed. Therefore, a study should be performed on a small system to obtain system matrices that can be verified easily. These small system input matrices can then be compared to the COMSOL Multiphysics input matrices.

Alternatively, another FEM software package could be used to obtain the stiffness, mass and damping matrix. These can be used as input for the A-matrix method, and can also be used to verify the COMSOL Multiphysics input matrices.

Furthermore, the KM-method should be tested on a more complex geometry, with material damping. This could be a test case to see if the simplification still holds.

Obtaining the vibratory response of a marine propeller due to a stochastic load is only a part of the objective in which this study took place. Looking back at Figure 1.1, two large research fields are not included in this study, which are needed to develop a model to predict the vibroacoustic response of a marine propeller. The two missing research fields which should be better understood are:

1. The load as a result of the turbulent flow
2. The acoustic radiation of marine propellers as a result of the structural response

Using a model that predicts the vibroacoustic response of a marine propeller, material variation studies can be performed. This would answer the last research question of this study.

The last recommendation is to obtain experimental data from a non-cavitating propeller. This would allow for validation of the obtained eigenmodes. Ideally, the eigenmodes of a cantilever plate in water and of a more complex geometry, such as a propeller, would then be obtained. Different loads could be

applied to solids, and the radiated sound could be measured at different locations. However, performing such an experiment is challenging.

References

[1] Syed Haider Abbas, Jae-Kyeong Jang, Dong-Ho Kim, and Jung-Ryul Lee. “Underwater vibration analysis method for rotating propeller blades using laser Doppler vibrometer”. In: *Optics and Lasers in Engineering* 132 (2020), pp. 106–133.

[2] Sondipon Adhikari. “Damping modelling using generalized proportional damping”. In: *Journal of Sound and Vibration* 293.1-2 (2006), pp. 156–170.

[3] Ravi de Berg. “Noise from stochastically excited structures: Modelling the noise from marine propellers excited by a turbulent boundary layer”. MA thesis. Utrecht University, 2022.

[4] Arthur Berkhoff. “Comsol matrix export for fluid-structure problems with external computation of eigenmodes”. 2022.

[5] Hannah B Blair, Nathan D Merchant, Ari S Friedlaender, David N Wiley, and Susan E Parks. “Evidence for ship noise impacts on humpback whale foraging behaviour”. In: *Biology letters* 12.8 (2016), p. 20160005.

[6] William K. Blake. *Mechanics of flow-induced sound and vibration, Volume 2: Complex flow-structure interactions*. Academic press, 2017.

[7] Robert D. Blevins and R. Plunkett. “Formulas for natural frequency and mode shape”. In: *Journal of Applied Mechanics* 47.2 (1980), p. 461.

[8] L.C. Burrill and W.L. Hughes. “Underwater propeller vibration tests and propeller blade vibrations”. In: *The North East Coast Institution of Engineers and Shipbuilders, Bolbec Hall, Newcastle upon Tyne, UK, Institution Transactions, Volume 65* (1949).

[9] John Carlton. *Marine propellers and propulsion*. Butterworth-Heinemann, 2018.

[10] David M. Chase. “Modeling the wavevector-frequency spectrum of turbulent boundary layer wall pressure”. In: *Journal of sound and Vibration* 70.1 (1980), pp. 29–67.

[11] E. Ciappi, F. Magionesi, Sergio De Rosa, and Francesco Franco. “Hydrodynamic and hydroelastic analyses of a plate excited by the turbulent boundary layer”. In: *Journal of Fluids and Structures* 25.2 (2009), pp. 321–342.

[12] COMSOL. “COMSOL Multiphysics Acoustics Module”. In: *COMSOL User’s Guide* (2023).

[13] G. M. Corcos. “Resolution of pressure in turbulence”. In: *The Journal of the Acoustical Society of America* 35.2 (1963), pp. 192–199.

[14] G. M. Corcos. “The structure of the turbulent pressure field in boundary-layer flows”. In: *Journal of Fluid Mechanics* 18.3 (1964), pp. 353–378.

[15] Sergio De Rosa and Francesco Franco. “Exact and numerical responses of a plate under a turbulent boundary layer excitation”. In: *Journal of Fluids and Structures* 24.2 (2008), pp. 212–230.

[16] I. Elishakoff. *Probabilistic Methods in the Theory of Structures*. New York: Wiley, 1983.

[17] Christine Erbe, Sarah A Marley, Renée P. Schoeman, Joshua N. Smith, Leah E. Trigg, and Clare Beth Embling. “The effects of ship noise on marine mammals—a review”. In: *Frontiers in Marine Science* 6 (2019), p. 606.

[18] J. M. Everink. “Numerically solving the wave equation using the finite element method”. B.S. thesis. Utrecht University, 2018.

[19] Frank J. Fahy. *Sound and structural vibration: radiation, transmission and response*. Elsevier, 2007.

[20] Gerrit Heilmann. “A Consistent Helmholtz Framework for the Accurate Prediction of Linear and Nonlinear Thermoacoustic Stability in Gas Turbine Combustors”. PhD thesis. Technische Universität München, 2023.

[21] John A. Hildebrand. “Anthropogenic and natural sources of ambient noise in the ocean”. In: *Marine Ecology Progress Series* 395 (2009), pp. 5–20.

[22] Lawrence E. Kinsler, Austin R Frey, Alan B. Coppens, and James V. Sanders. *Fundamentals of acoustics*. John wiley & sons, 2000.

[23] RC. Leaper and MR. Renilson. “A review of practical methods for reducing underwater noise pollution from large commercial vessels”. In: *International Journal of Maritime Engineering* 154.A2 (2012).

[24] Richard B Lehoucq, Danny C Sorensen, and Chao Yang. *ARPACK users’ guide: solution of large-scale eigenvalue problems with implicitly restarted Arnoldi methods*. SIAM, 1998.

[25] F. Magionesi, G. Dubbioso, and R. Muscari. “Fluid–structure interaction of a marine rudder at incidence in the wake of a propeller”. In: *Physics of Fluids* 36.6 (2024).

[26] Francesca Magionesi. “Flow induced structural noise on a sonar dome of a ship”. In: *INTER-NOISE and NOISE-CON Congress and Conference Proceedings*. Vol. 253. 4. Institute of Noise Control Engineering. 2016, pp. 4273–4284.

[27] Leonard Meirovitch. *Fundamentals of vibrations*. Waveland Press, 2010.

[28] Nathan D. Merchant, Rosalyn L. Putland, Michel André, Eric Baudin, Mario Felli, Hans Slabbekoorn, and René Dekeling. “A decade of underwater noise research in support of the European Marine Strategy Framework Directive”. In: *Ocean & Coastal Management* 228 (2022), p. 106299.

[29] Ron B. Mitson and Hans P. Knudsen. “Causes and effects of underwater noise on fish abundance estimation”. In: *Aquatic Living Resources* 16.3 (2003), pp. 255–263.

[30] Andreï Sergeevich Monin and Akiva M. Yaglom. *Statistical fluid mechanics, volume II: mechanics of turbulence*. Vol. 2. Courier Corporation, 2013.

[31] Roger Payne and Douglas Webb. “Orientation by means of long range acoustic signaling in baleen whales”. In: *Annals of the New York Academy of Sciences* 188.1 (1971), pp. 110–141.

[32] William Rees Sears. “A systematic presentation of the theory of thin airfoils in non-uniform motion”. PhD thesis. California Institute of Technology, 1938.

[33] Theodore Theodorsen. *General theory of aerodynamic instability and the mechanism of flutter*. Tech. rep. 1979.

[34] Konstantinos Tsigklifis, Marcus Wong, Steven De Candia, Paul Dylejko, Paul Croaker, and Alex Skvortsov. “Reduced order modelling of vibroelastic response of a hydrofoil in homogeneous isotropic turbulence”. In: *Proceedings of Acoustics*. Vol. 21. 23. 2021, p. 2022.

[35] Yorick de Valk. “Internal Communication”. 2020.

[36] Jonathan Whiteley. *Finite element methods*. Oxford: Springer, 2014.

[37] Andrew J. Wright. “International Workshop on Shipping Noise and Marine Mammals”. In: *Oceanos—Foundation for the Sea, Hamburg, Germany, Tech. Rep. Final Report* (2008).

A

Livelink Code Examples

A.1. Eigenmode command

When the eigenmodes are imported from COMSOL Multiphysics, this is done by the following commands

```
% Get eigenmode deformation in x,y,z
eigenmodes = mpheval(model, {'u', 'v', 'w'},'dataset','dset1');
eigenmodes_x = (eigenmodes.d1);
eigenmodes_y = (eigenmodes.d2);
eigenmodes_z = (eigenmodes.d3);
```

A.2. Obtaining the mass matrix while using a spherical wave radiation boundary condition

During this research, it was discovered that COMSOL Multiphysics 6.3 contains a bug that prevented the user from obtaining the mass matrix from a geometry that involved a spherical wave radiation boundary condition, that has to be used to obtain correct eigenfrequencies. Therefore, a different method had to be developed in order to obtain the mass matrix. Rather than using an eigenfrequency study, an eigenvalue study had to be used, from which the mass matrix could be obtained using the following command:

```
% Obatin Mass Matrix
MassMatrix = mphmatrix(model,'sol1','out',{'E'},'eigname','lambda','extractafter','end','
    eigref',1000*(-2*pi*1i));
```

```
%Compute eigenfrequencies [rad/s] and eigenmodes
nmbrofeig = 10;     %Number of eigenfrequencies to compute
freq = 300;         %[Hz], search around this frequency

[PHI,OMEGA] = eigs(K-sqrt(eps),M,nmbrofeig,freq*2*pi);  % APB, see Meirovitch, p. 610.

%Sort and convert eigenfrequencies [Hz]
[w,k] = sort(sqrt(diag(OMEGA))/(2*pi));
```

A.3. Non-scaled input matrices

Another method was developed by Berkhoff [4] to scale the mass matrix. First, all scaling is turned off in COMSOL Multiphysics, after which the stiffness, damping and mass matrices are imported to Matlab. Here, the constrained nodes are filtered, in the same way was was shown in Equation 3.15. After this, the elements of the stiffness and mass matrix are scaled with the following code:

Here, K represents the stiffness matrix, and the degree of freedom coordinates are indicated with dof_i where x, y and z represent the spatial coordinates, and a the degrees of freedom in the fluid domain. The subscript a is used since this is the acoustic domain. The density of the fluid is indicated as rho_{fluid}.

Three different types of scaling are used in the code. First, in line 2, the coupled stiffness matrix is scaled with the density of the fluid. The degrees of freedom in the stiffness matrix representing the fluid domain are scaled with the density squared. As was described earlier, the part of the mass matrix representing the plate sums to the analytical mass three times. Therefore, no scaling is applied to these elements. The degrees of freedom representing the fluid are scaled with the density squared.

However, this method does not include scaling of the damping matrix. The example that is provided with the code is of a beam in an infinite fluid domain. A PML is used to represent the infinite domain, although COMSOL Multiphysics advises against the use of a PML with an eigenfrequency study. Furthermore, the eigenfrequencies and eigenvalues are computed with:

```
1 % Scale the coupling matrix with the desired fluid density
2 K([dof_x,dof_y,dof_z],dofs_a) = K([dof_x,dof_y,dof_z],dofs_a) / rho_fluid;
3 K(dofs_a,dofs_a) = K(dofs_a,dofs_a) / rho_fluid^2;
4 % Scale the mass matrix with the desired fluid density
5 M(dofs_a,dofs_a) = M(dofs_a,dofs_a) / rho_fluid^2;
```

Although an infinite fluid domain is assumed, the damping matrix is not taken into account when computing the eigenfrequencies and eigenmodes.

B

FEM example

B.1. Finite Element Method

In order to solve the system for the eigenfrequencies and eigenmodes, the Finite Element Method (FEM) will be used in COMSOL Multiphysics. This method discretizes partial differential equations on finite domains, such that they can be solved.

In general, the Finite Element method consists of six steps [36]:

1. Derivation of the weak formulation for the specified boundary value problem
2. Definition of the finite element mesh
3. With the nodes and elements defined in the mesh, searching for suitable basis functions
4. Using the linear sum of the basis functions to derive the finite element solution
5. Using the algebraic equations to assemble the system matrices
6. Solving the system matrices

The workings of the method will be demonstrated by means of an example. This will be based on the work of Everink [18], and the full derivation can be found there as well. The wave equation is rewritten to

$$\frac{\partial^2 u}{\partial t^2} - c^2 \Delta u = 0 \quad for \quad c > 0 \tag{B.1}$$

Instead of the pressure p, a generic function u is used. Furthermore, in order to simplify it, the equation is used on a two-dimensional domain $D \subset \mathbb{R}^2$. The following boundary and initial conditions are used:

$$\begin{aligned} u(x,y,t) &= 0 \quad \text{for all} \quad (x,y) \in \partial D \\ u(x,y,0) &= u_0(x,y) \quad \text{for all} \quad (x,y) \in D \\ \nabla u(x,y,0) &= u_1(x,y) \quad \text{for all} \quad (x,y) \in D \end{aligned} \tag{B.2}$$

First, the weak form of the wave equation needs to be derived. This can be achieved by multiplying the equation with a test function $v(x,y)$, which has the property that it is zero at the boundary, as is the wave equation in this case. Next, an integration is performed over the whole domain D. Using Green's first identity, the following form of the wave equation can be derived:

$$a(u(x,y,t), v(x,y)) = \int_D \frac{\partial^2 u}{\partial t^2}(x,y,t) v(x,y) dA + c^2 \int_D \nabla u(x,y,t) \cdot \nabla v(x,y) dA = 0 \tag{B.3}$$

More information on the requirements of test functions can be found in Whiteley [36]. For instance, these functions have to be square integrable, which means that the above integral is finite. This requirement is also known as the L_2-norm. Next, a function $u(x, y, t)$ has to be found, such that it holds that $a(u(x, y, t), v(x, y)) = 0$ for all test functions $v(x, y)$. Of course, Equation B.2 should still hold. The equations are still in continuous form, and the space that contains u and v are infinite-dimensional. Since the goal is to discretize the function such that it can be solved numerically, a subspace that is spanned by the global basis function $\phi_i(x, y)$ has to be found. A finite element formulation is obtained where the solution is expressed as:

$$U(x, y, t) = \sum_{i=1}^{n} U_i(t)\phi(x, y) \tag{B.4}$$

And the finite element test function can be expressed as

$$V(x, y) = \sum_{i=0}^{n} V_i\phi_i(x, y) \tag{B.5}$$

Substituting this back into Equation B.3 results in

$$a(U(x, y, t), V(x, y)) = 0 \tag{B.6}$$

The grid on which these equations will be solved is called the mesh. The mesh is a discretized domain. Many types of elements can be used, each resulting in advantages and disadvantages. In this case, for simplicity's sake, a linear element is used. The mesh consists of N Elements E_j and n nodes $\overrightarrow{x_{j,i}}$. Three nodes,$\overrightarrow{x_{j,1}}$, $\overrightarrow{x_{j,2}}$, $\overrightarrow{x_{j,3}}$ are used per element, resulting in a triangular element. Using a transformation $\tau_i(X, Y)$, the elements can be mapped to cover the complete domain. Before the global basis functions can be defined, the local basis functions on the elements are defined. These are functions that are 1 on one of the nodes, and 0 on the other two nodes. They are defined as:

$$\begin{aligned} \phi_{l,1}(x, y) &= 1 - x - y \\ \phi_{l,2}(x, y) &= x \\ \phi_{l,3}(x, y) &= y \end{aligned} \tag{B.7}$$

A graphical representation can be found in Figure B.1.

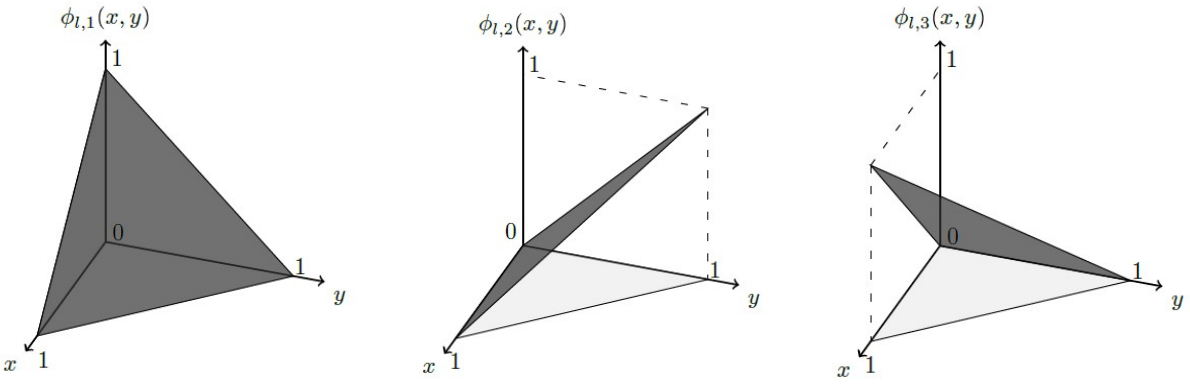

(a) Local basis function $\phi_{l,1}(x, y)$ **(b)** Local basis function $\phi_{l,2}(x, y)$ **(c)** Local basis function $\phi_{l,3}(x, y)$

Figure B.1: Two-dimensional local basis functions [18]

For each node $\overrightarrow{x_i}$, a single global basis function can be defined. In the case that the node $\overrightarrow{x_i}$ is a corner point of the element E_j, the global basis function can be defined as:

$$\phi_i(x,y) = \phi_{l,k}(\tau_j^{-1}(x,y)) \tag{B.8}$$

Where k indicates the k^{th} corner point of element E_j. The function is zero for all elements for which the node is not a corner point. Substituting Equation B.4 in the FEM formulation, the result for all nodes that are not on the boundary is

$$\begin{aligned} &\sum_{i=1}^{n} \ddot{U}_i(t) T_{i,j} + c^2 \sum_{i=1}^{n} U_i(t) S_{i,j} = 0 \\ &\text{with} \quad T_{i,j} = \int_D \phi_i(x,y)\phi_j(x,y)dA \\ &\text{and} \quad S_{i,j} = \int_D \nabla\phi_i(x,y) \cdot \nabla\phi_j(x,y)dA \end{aligned} \tag{B.9}$$

If this is combined with $\ddot{U}_j(t) = 0$ for all the nodes that are on the boundary, the following ordinary differential equation can be obtained:

$$T\ddot{U}(t) + c^2 SU(t) = 0 \tag{B.10}$$

The coefficients can now be obtained. A second order approximation for the second derivative with respect to time can be used:

$$\ddot{U}(t) \approx \frac{U(t+dt) - 2U(t) + U(t-dt)}{dt^2} \tag{B.11}$$

Although the method used by COMSOL Multiphysics involves much more complex schemes and element shapes, the underlying principle remains the same.

C

Acoustics

An infinite fluid surrounding the cantilever plate introduces damping since the pressure waves produced by the vibration, and hence energy, can leave the domain. Although outside the scope of this study, it is still good practice to discuss the propagation of pressure wave shortly. This section is based on documentation from COMSOL [12].

The wave equation, which describes the propagation of pressure waves, is defined as:

$$\frac{1}{c^2}\frac{\partial^2 p}{\partial t^2} - \nabla \cdot (\nabla p) = 0 \tag{C.1}$$

The fluid compressibility is related to the speed of sound c. The bulk modulus is defined as ρc^2. The time-harmonic wave is a special case, where the pressure changes in time with:

$$p(\overrightarrow{x}, t) = p(\overrightarrow{x})e^{i\omega t} \tag{C.2}$$

The angular frequency is defined as $\omega = 2\pi f$ in radians per second. The frequency is denoted with f. Acoustic waves reduce the wave equation to the Helmholtz equation, which is defined as:

$$\nabla \cdot (\nabla p) + \frac{\omega^2}{c^2} p = 0 \tag{C.3}$$

The wavenumber k is defined as the ratio ω/c. The Helmholtz equation can be used to solve for the eigenmodes and eigenfrequencies. The full derivation of the wave and Helmholtz equations can be found in Appendix C. An example where FEM is applied to the wave equation can be found in Appendix B.

D

Mode Shapes

D.1. KM-method eigenmodes

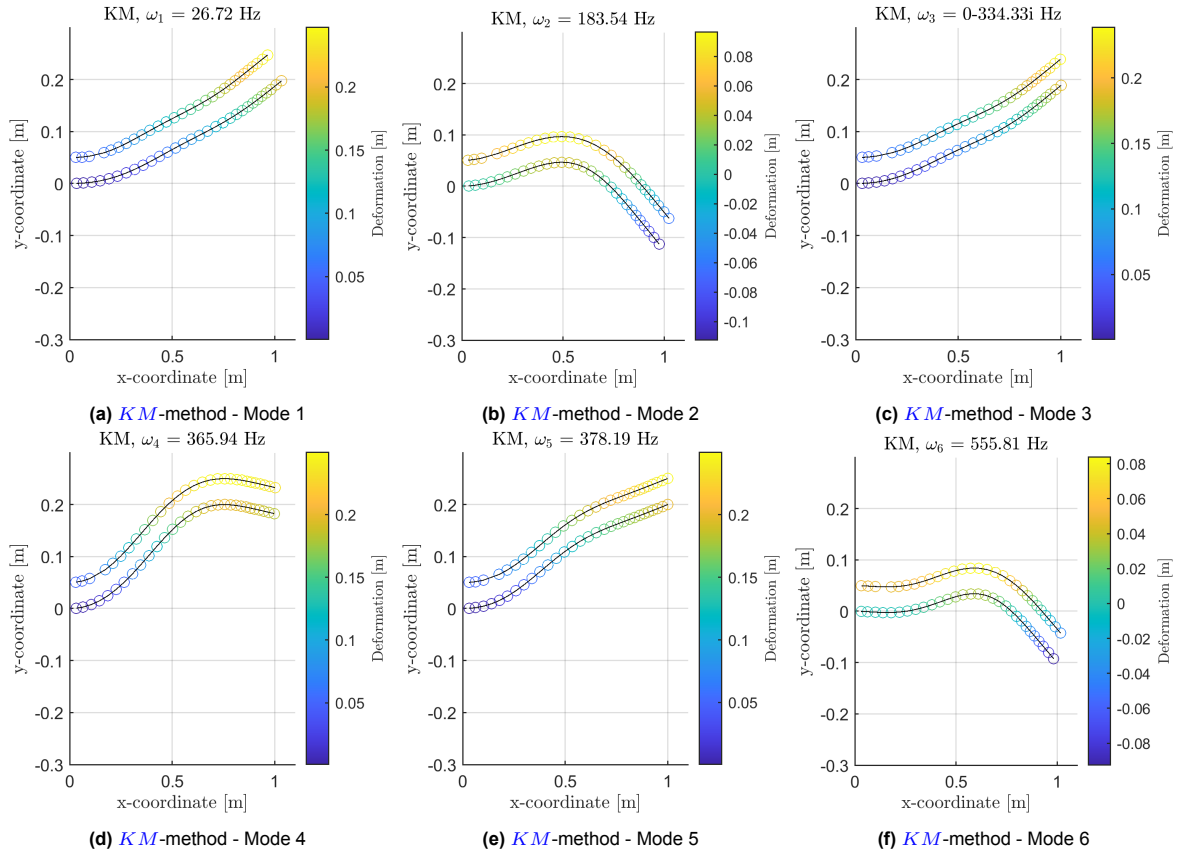

(a) KM-method - Mode 1 **(b)** KM-method - Mode 2 **(c)** KM-method - Mode 3

(d) KM-method - Mode 4 **(e)** KM-method - Mode 5 **(f)** KM-method - Mode 6

Figure D.1: Eigenmodes of a 2D cantilever beam up to $1000\,\mathrm{Hz}$ using the KM-method.

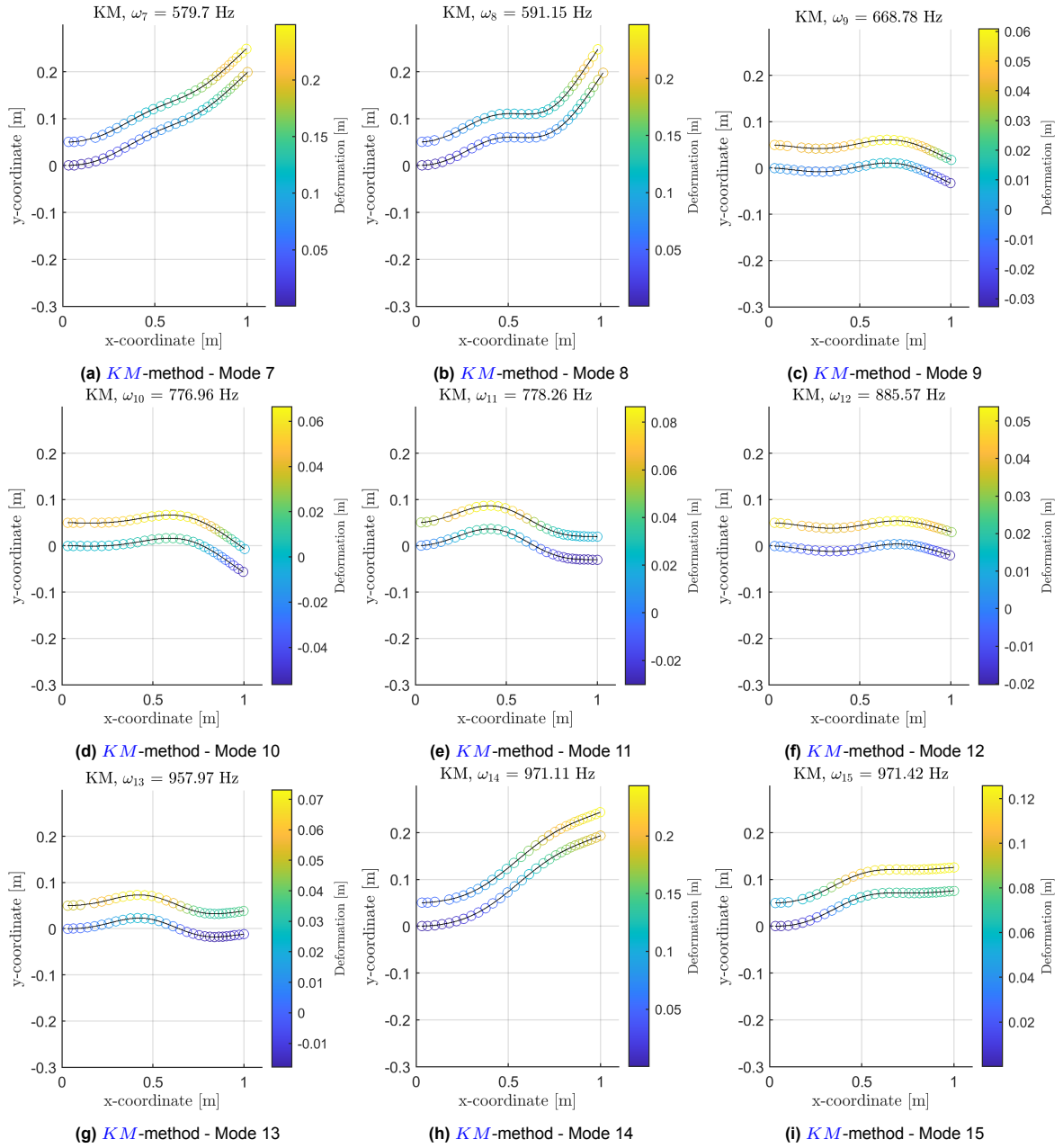

(a) KM-method - Mode 7 **(b)** KM-method - Mode 8 **(c)** KM-method - Mode 9

(d) KM-method - Mode 10 **(e)** KM-method - Mode 11 **(f)** KM-method - Mode 12

(g) KM-method - Mode 13 **(h)** KM-method - Mode 14 **(i)** KM-method - Mode 15

Figure D.2: Eigenmodes of a 2D cantilever beam up to $1000\,\mathrm{Hz}$ using the KM-method.

D.2. A method right eigenmodes

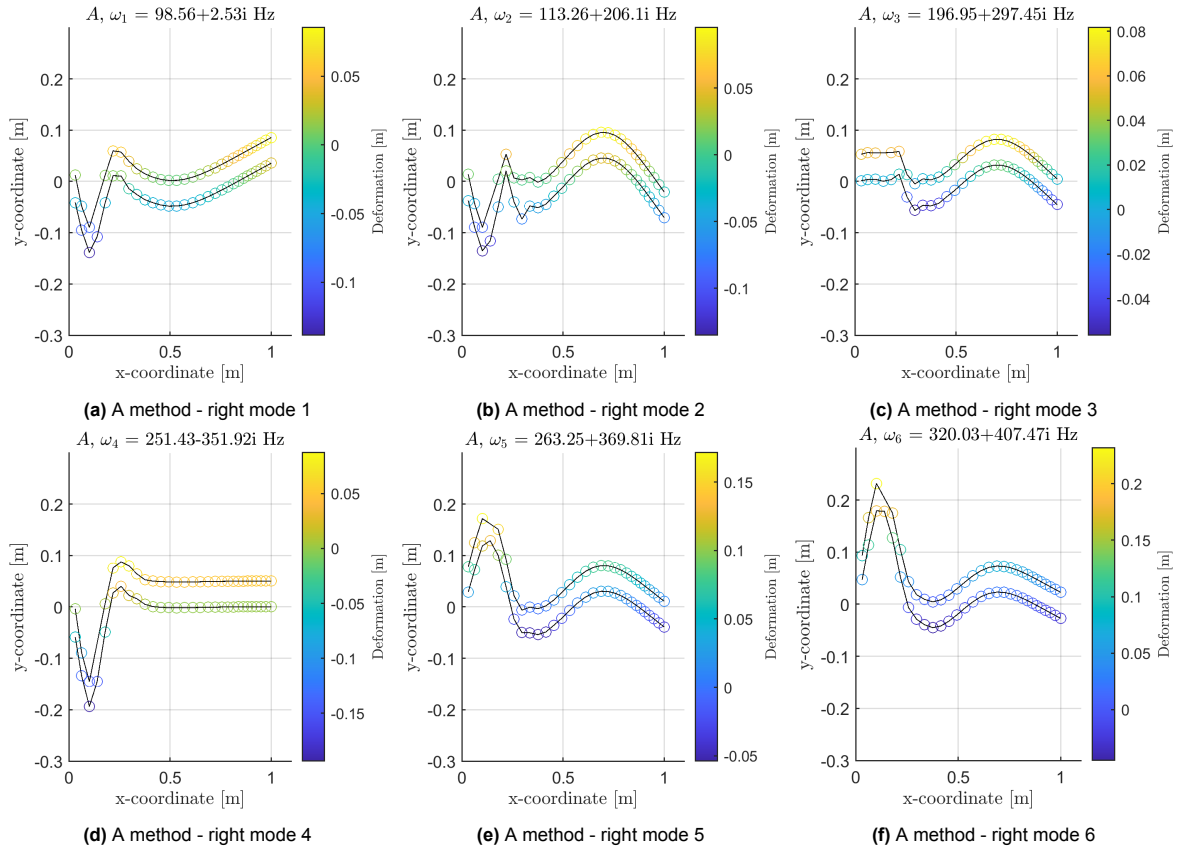

(a) A method - right mode 1 **(b)** A method - right mode 2 **(c)** A method - right mode 3

(d) A method - right mode 4 **(e)** A method - right mode 5 **(f)** A method - right mode 6

Figure D.3: Right eigenmodes of a 2D cantilever beam up to $1000\,\mathrm{Hz}$ using the system matrix A.

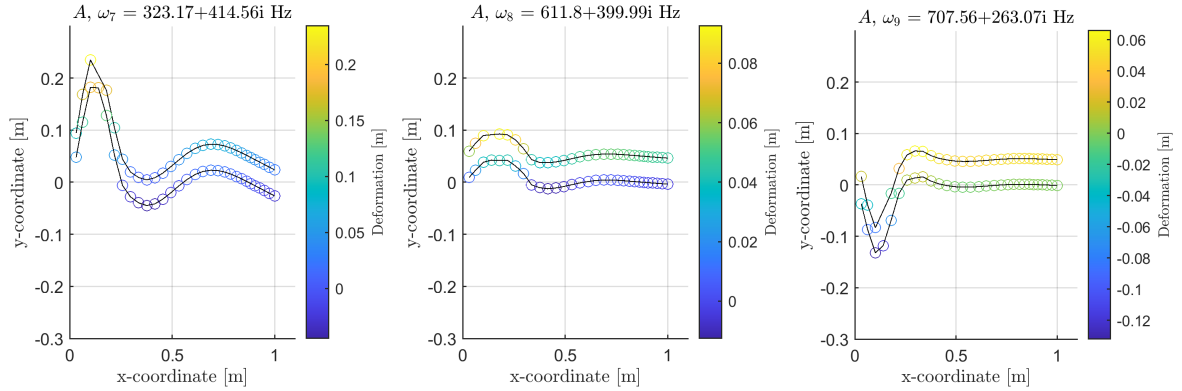

(a) A method - right mode 7 **(b)** A method - right mode 8 **(c)** A method - right mode 9

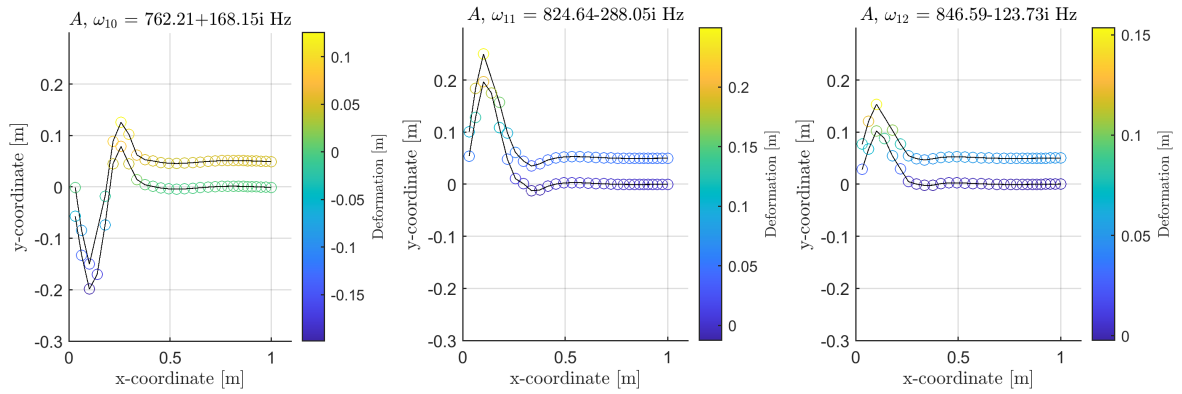

(d) A method - right mode 10 **(e)** A method - right mode 11 **(f)** A method - right mode 12

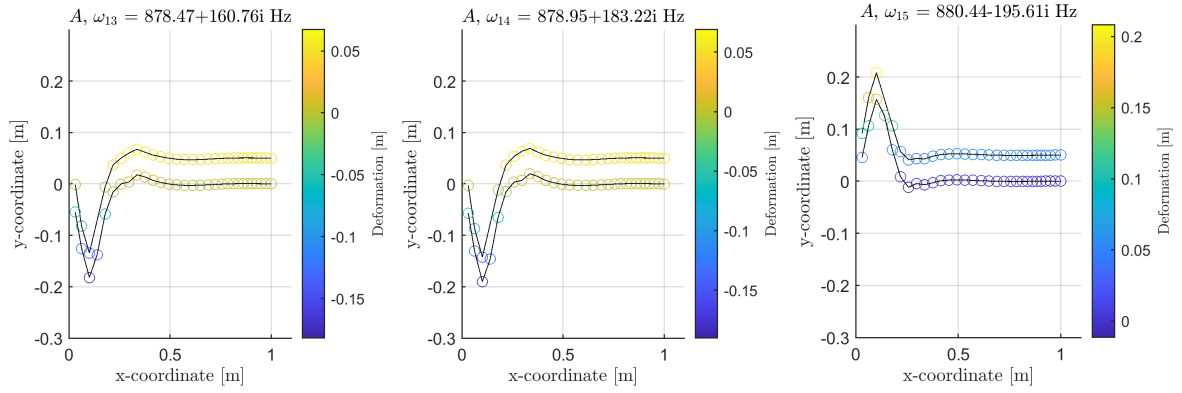

(g) A method - right mode 13 **(h)** A method - right mode 14 **(i)** A method - right mode 15

Figure D.4: Eigenmodes of a 2D cantilever beam up to $1000\,\mathrm{Hz}$ using the system matrix A.

D.3. A method left eigenmodes

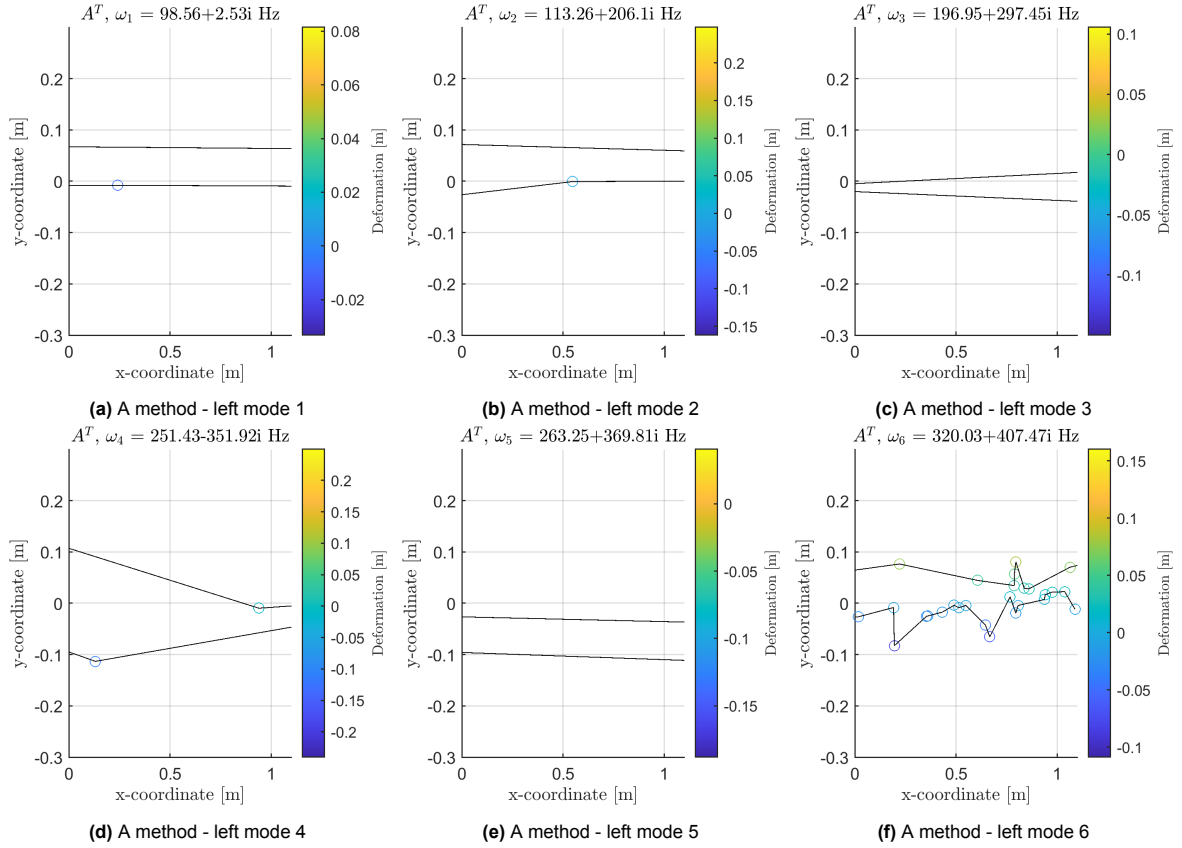

(a) A method - left mode 1

(b) A method - left mode 2

(c) A method - left mode 3

(d) A method - left mode 4

(e) A method - left mode 5

(f) A method - left mode 6

Figure D.5: Left eigenmodes of a 2D cantilever beam up to $1000\,\mathrm{Hz}$ using the system matrix A^T.

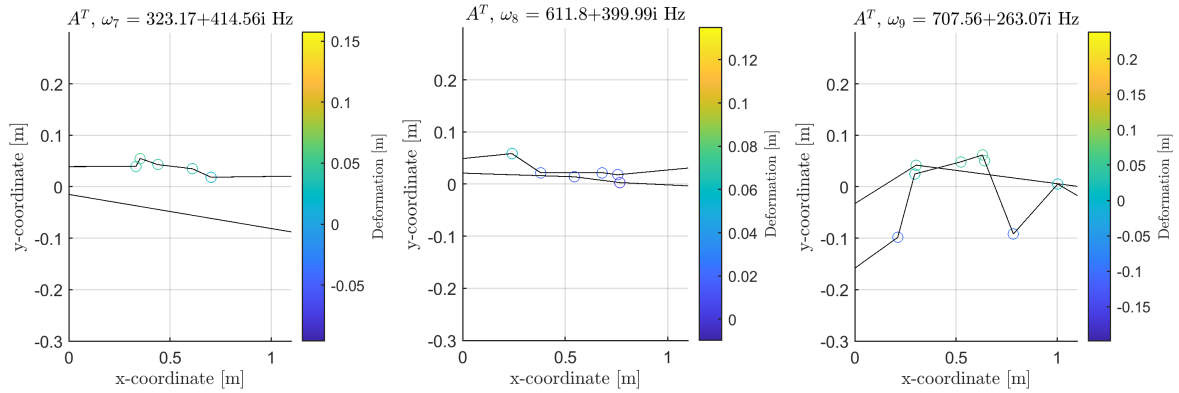

(a) A method - left mode 7 **(b)** A method - left mode 8 **(c)** A method - left mode 9

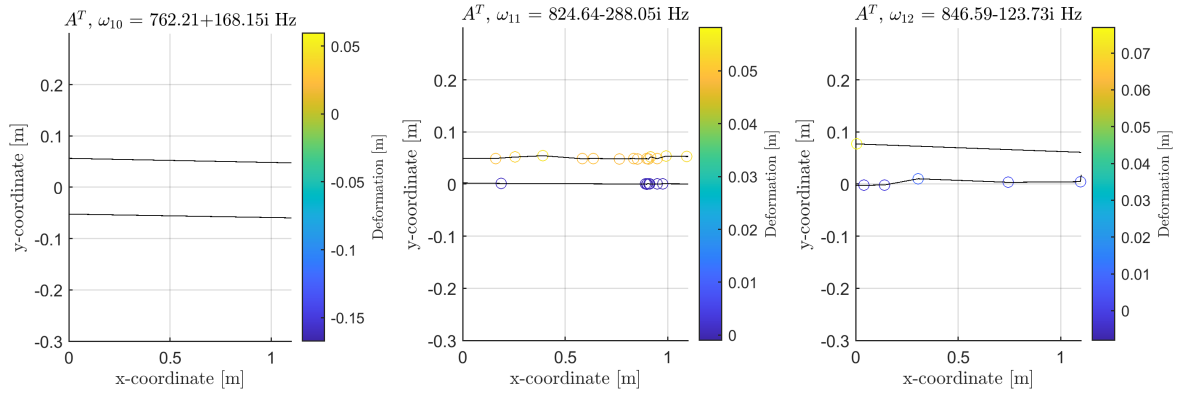

(d) A method - left mode 10 **(e)** A method - left mode 11 **(f)** A method - left mode 12

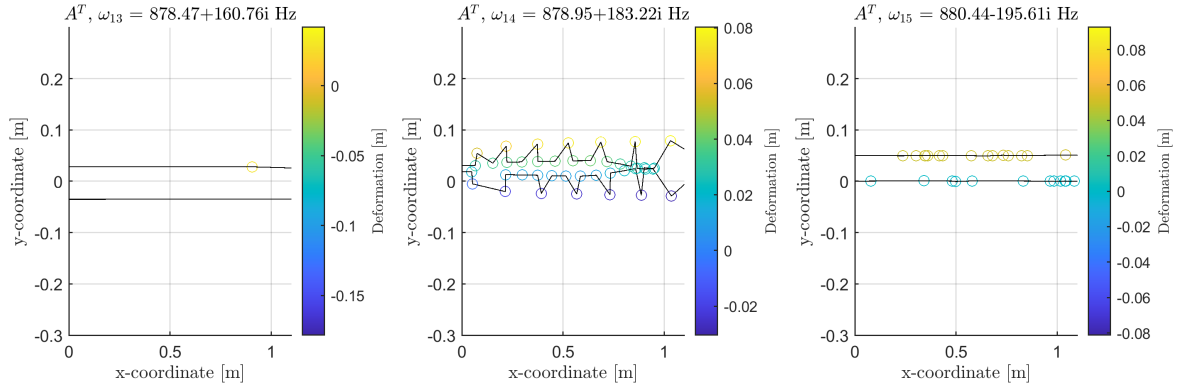

(g) A method - left mode 13 **(h)** A method - left mode 14 **(i)** A method - left mode 15

Figure D.6: Eigenmodes of a 2D cantilever beam up to $1000\,\mathrm{Hz}$ using the system matrix A^T.

D.4. State-space reconstruction right eigenmodes

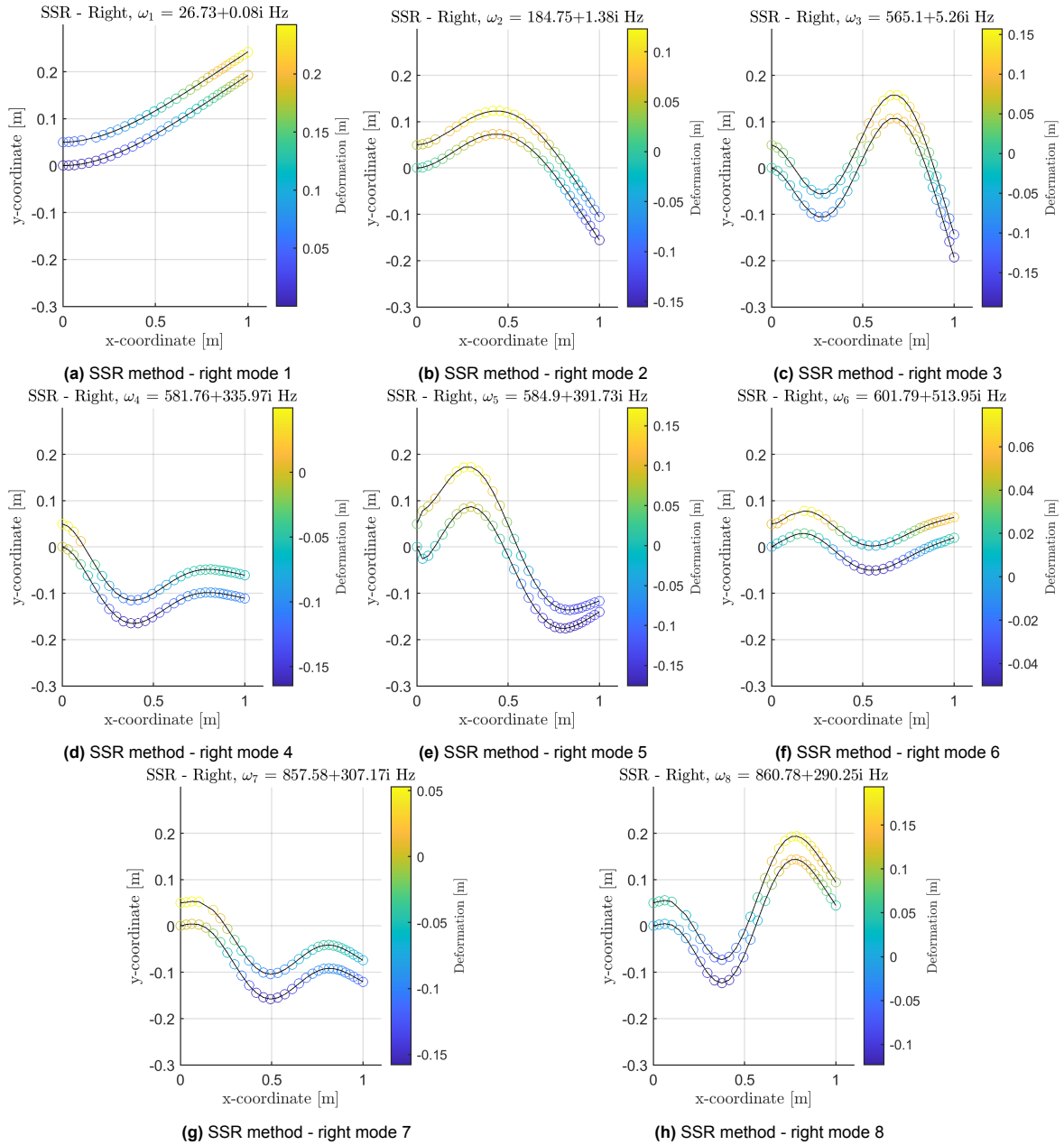

(a) SSR method - right mode 1 **(b)** SSR method - right mode 2 **(c)** SSR method - right mode 3

(d) SSR method - right mode 4 **(e)** SSR method - right mode 5 **(f)** SSR method - right mode 6

(g) SSR method - right mode 7 **(h)** SSR method - right mode 8

Figure D.7: Right eigenmodes of a 2D cantilever beam up to $1000\,\mathrm{Hz}$ using the SSR method.

D.5. State-space reconstruction left eigenmodes

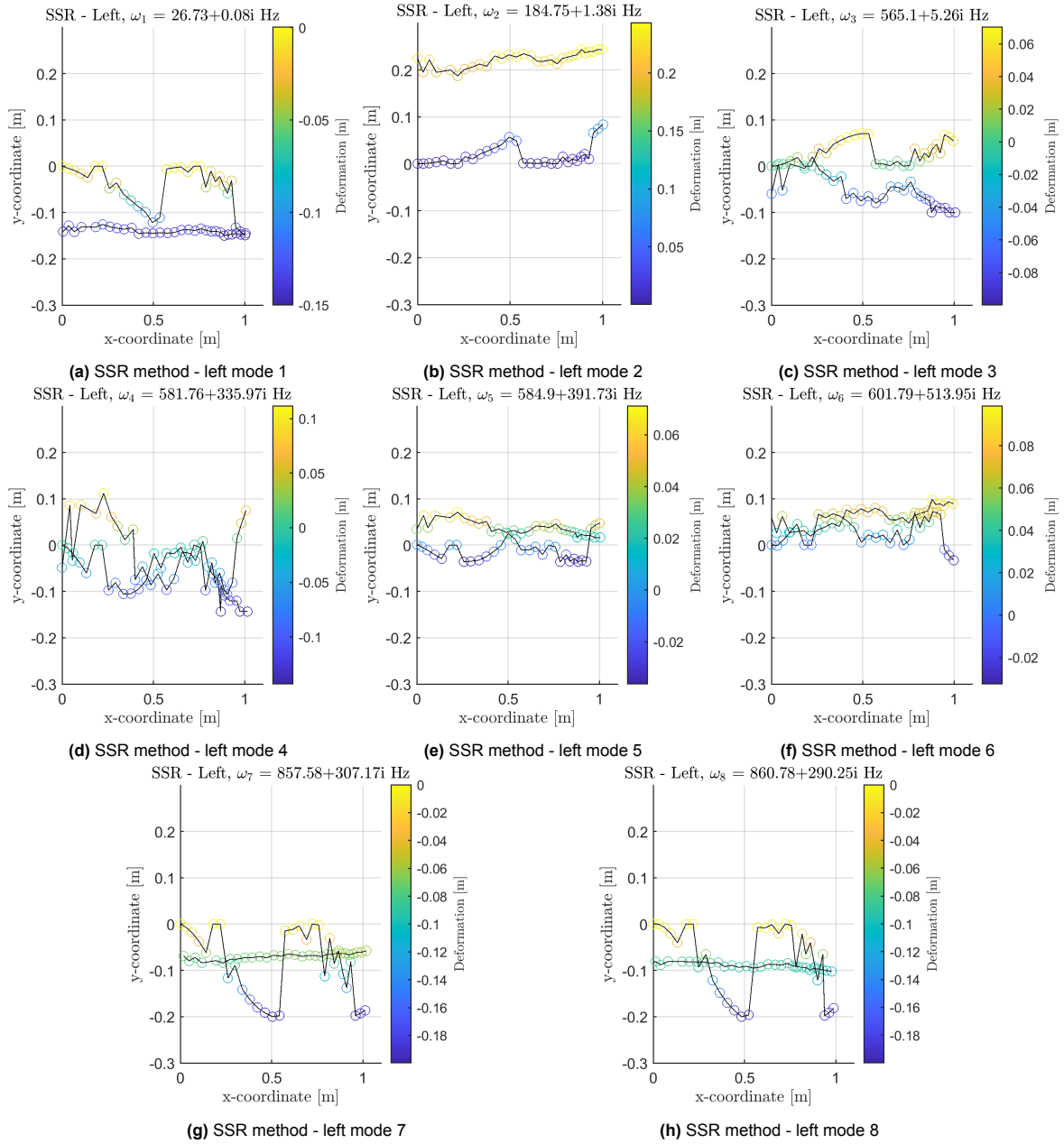

(a) SSR method - left mode 1 **(b)** SSR method - left mode 2 **(c)** SSR method - left mode 3

(d) SSR method - left mode 4 **(e)** SSR method - left mode 5 **(f)** SSR method - left mode 6

(g) SSR method - left mode 7 **(h)** SSR method - left mode 8

Figure D.8: Left eigenmodes of a 2D cantilever beam up to $1000\,\mathrm{Hz}$ using the SSR method.